2010-12-15

Optimum Design of Renewable Energy Systems by using Deterministic and Probabilistic Approaches

Yi Hu
University of Miami, yi.hu@miami.edu

UNIVERSITY OF MIAMI

OPTIMUM DESIGN ON RENEWABLE ENERGY SYSTEMS BY USING DETERMINISTIC AND PROBABILISTIC APPROACHES

By

Yi Hu

A DISSERTATION

Submitted to the Faculty
of the University of Miami
in partial fulfillment of the requirements for
the degree of Doctor of Philosophy

Coral Gables, Florida

December 2010

UNIVERSITY OF MIAMI

A dissertation submitted in partial fulfillment of
the requirements for the degree of
Doctor of Philosophy

OPTIMUM DESIGN ON RENEWABLE ENERGY SYSTEMS BY USING DETERMINISTIC AND PROBABILISTIC APPROACHES

Yi Hu

Approved:

_____
Singiresu S. Rao, Ph.D.
Professor and Chair
Department of Mechanical
& Aerospace Engineering

_____
Terri A. Scandura, Ph.D.
Dean of the Graduate School

_____
Michael R. Swain, Ph.D.
Associate Professor
Department of Mechanical
& Aerospace Engineering

_____
Jizhou Song, Ph.D.
Assistant Professor
Department of Mechanical
& Aerospace Engineering

_____
Ramasubramanian Krishnan, Ph.D.
Professor
Department of Marketing

HU, YI (Ph.D., Mechanical Engineering)

Optimum Design of Renewable Energy Systems (December 2010)
by using Deterministic and Probabilistic Approaches

Abstract of a dissertation at the University of Miami.

Dissertation supervised by Professor Singiresu S. Rao
No. of pages in text: (177)

This work consists of the study for optimum design of the renewable energy systems. Different renewable energy systems including two solar energy systems, one wind turbine system and one fuel cell system have been optimized by using different optimization or robust techniques.

The multi-objective optimum designs of flat plate and compound parabolic concentrator solar collector systems by using deterministic and probabilistic approaches are considered. Three objectives are considered in the optimization problem formulation: maximization of the annual average incident solar energy, maximization of the lowest month incident solar energy and minimization of the cost. The game theory methodology is used for the solution of the three objective constrained optimization problems to find a best compromise solution. Sensitivity analyses with respect to different parameters are conducted, which are expected to help designers in better understanding and aid in creating optimized solar collectors based on specified requirements.

The robust design of horizontal axis wind turbines, including both parameter and tolerance designs, is presented. This work considers multiple design parameters

(variables), multiple objectives, and multiple constraints simultaneously by using the traditional Taguchi method and its extensions; it provides a simple way of designing robust horizontal axis wind turbine systems under realistic conditions. The performance of these turbines is predicted using the axial momentum theory and the blade element momentum theory. In the parameter design stage, the energy output of the turbine is maximized using the Taguchi method and a novel extended penalty-based Taguchi method which is proposed to solve constrained parameter design problems. The results of the unconstrained and constrained parameter design problems, in terms of the objective function and constrains are compared. Using an appropriate set of tolerance setting of the parameters, the tolerance design problem is formulated so as to yield an economical design while ensuring a minimal variability of performance of the wind turbine. The resulting objective function is formulated as a multi-objective function and solved by traditional Taguchi method.

In the optimum design of fuel cells, a three-dimensional, single-phase, multi-component mathematical model has been used for a liquid-fed direct methanol fuel cell. The genetic algorithm coupled with sequential quadratic programming optimization technique is applied based on the numerical model for seeking global optimum solution. The maximization of the power density and minimization of the cost are considered subsequently. The polarization, power density and methanol crossover curves are presented and explained to help designers better understand the significance of optimum design behind the optimization results.

This work is expected to help designer improve the performance and quality as well as reduce the cost for renewable energy systems.

ACKNOWLEDGEMENTS

I would like to extend my sincere gratitude and appreciation to my Ph.D dissertation advisor and chairman of the committee, Dr. Singiresu S. Rao for his patient guidance, practical advice, multiple revisions, and consistent encouragement throughout the work. I am very proud and lucky to have him as my academic advisor.

My thanks also goes to Dr. Michael R. Swain and Dr. Jizhou Song of Department of Mechanical & Aerospace Engineering, and Dr. Ram Krishnan of the Department of Marketing, University of Miami, for accepting the appointment to dissertation committee, as well as their helpful suggestions and advice.

I must extend sincere gratitude to Dr. Hongtan Liu and Dr. Xiangyang Zhou in the Department of Mechanical & Aerospace Engineering who helped me in the renewable energy research and Dr. Ram Krishnan in the Department of Marketing who helped me in learning design of experiments and other related knowledges.

I would like to thank the Department of Mechanical & Aerospace Engingeering of providing the full financial support for more than three years.

My special thanks goes to Dr. Kwang-Tzu Yang, Viola D. Hank Professor of Engineering in the Department of Aerospace and Mechanical Engineering, University of Notre Dame, for his consistent encouragement and suggestion in the recent years.

I would like to thank all the other faculty and stuff members as well as friends in the Department of Mechanical & Aerospace Engineering particularly Dr. Saif Matar, Dr. Bertrand Dano, Dr. Yiqing Shen, Dr. Xiujun Fang, Dr. Zhiqiang Zhou, and Ms. Aparna Aravelli for their assistance when I met various academic difficulties.

I also want to thank the dissertation editor, Ms. Doreen Yamamoto, in the graduate school of University of Miami, for her assistance in the final revising and formatting of this work.

Finally, my deepest sense of gratitude to my family members including my parents, my parents in law, my wife Ting, and my new born son James, for their constant love, understanding and support.

Yi Hu

December 2010

CONTENTS

LIST OF TABLES vii
LIST OF FIGURES ix
CHAPTER 1 Introduction 1
1.1 Current Status of Renewable Energy 1
1.2 Solar Collectors 5
1.3 Wind Turbines 10
1.4 Fuel Cells 12
1.5 Summary of Present Work 15
CHAPTER 2 Optimum Design of Flat-plate Solar Collector System 17
2.1 Introduction and Literature Review 17
2.2 Solar Insolation Analysis 21
2.3 Formulation of Single-objective Optimization Problem 25
2.3.1 Determinist form 25
2.3.2 Probabilistic form 26
2.3.3 Maximization of annual average incident solar energy 29
2.3.4 Maximization of average incident solar energy for the lowest month 32
2.3.5 Minimization of cost 33
2.3.6 Uncertainty of parameters 34
2.4 Formulation of the multi-objective optimization problem 36
2.4.1 Game theory approach 37
2.4.2 Computational procedure 40
2.5 Illustrative examples and numerical results 42
2.5.1 Deterministic optimization 42
2.5.2 Probabilistic optimization 48
2.6 Conclusions 66
CHAPTER 3 Optimium Design of Compound Parabolic Concentrator (CPC) Solar Collector System 68
3.1 Introduction and Literature Review 68
3.2 Deterministic Single-objective Optimization of CPC solar collector system 72
3.2.1 Maximization of annual average incident solar energy 72
3.2.2 Maximization of average incident solar energy for the lowest month 75
3.2.3 Minimization of cost 76

3.2.4 Numerical Example 77
3.2.5 Sensitivity Analyses 79
3.3 Optimization of CPC solar collector system Under probabilistic uncertainty 84
3.3.1 Numerical example of single-objective optimization problems under probabilistic uncertainty 84
3.3.2 Numerical example of multi-objective optimization problems under probabilistic uncertainty 89
3.3.3 Numerical example with a constraint on the CPC ratio 91
3.4 Conclusions 93
CHAPTER 4 Optimum Design of Horizontal Axis Wind Turbine System 96
4.1 Introduction and Literature Review 96
4.2 Aerodynamic theory 99
4.2.1 Axial momentum theory 99
4.2.2 Blade element momentum theory 103
4.2.3 Solution procedure and computer codes 105
4.3 Wind Speed Distribution 106
4.3.1 Wind speed variation with height 106
4.3.2 Probability density function 107
4.3.3 Average power in the wind 108
4.3.4 Optimum wind speed 108
4.4 Taguchi Method of Design 109
4.5 Numerical Example of Robust Design of Wind Turbine Using Taguchi Method 111
4.5.1 Parameter design 111
4.5.2 Tolerance design 129
4.6 Conclusions 137
CHAPTER 5 Optimum Design of Direct Methanol Fuel Cell (DMFC) System 139
5.1 Introduction and Literature Review 139
5.2 DMFC model 141
5.2.1 Assumptions made 143
5.2.2 Governing equations 144
5.2.3 Electrochemical kinetics 145
5.2.4 Solution procedure 146
5.2.5 Cost model 147
5.3 Optimization problem 148

5.3.1 Optimization method 149
5.3.2 Maximization of the power output 150
5.3.3 Maximization of power output with a minimum operating voltage constraint 150
5.3.4 Minimization of cost 151
5.4 Numerical Results 151
5.5 Conclusions 161
CHAPTER 6 Conclusions and Future Work 163
6.1 Conclusions 163
6.2 Future work 167
References 169

LIST OF TABLES

Table 1-1 Renewable energy status in the recent years (2005 ~ 2008) 3
Table 1-2 List of Solar Collectors 6
Table 1-3 Growth in Wind turbine size in the past thirty years 11
Table 2-1 Correction factors for different climate types (Hottel, 1976) 22
Table 2-2 Recommended Average Days of Months 35
Table 2-3 Initial Design and deterministic single objective optimization results 43
Table 2-4(a) Initial design and deterministic multi-objective optimization result 43
Table 2-4(b) Initial design and deterministic multi-objective optimization results (weights of each single objective functions) 44
Table 2-4(c) Initial design and determinist multi-objective optimization results (objective function values) 44
Table 2-5 Monthly average temperature of Miami (Weather Channel, 2010) 51
Table 2-6 Effect of Variability (C.V.) on Multi-objective Optimization (Probability of constraint satisfaction: 95%) 58
Table 2-7 Variation of Constraint Satisfaction Probability on Multi-objective Optimization (Coefficient of variation of uncertain parameters: 0.01) 59
Table 3-1(a) Initial design and single-objective optimization results (design variables) 78
Table 3-1(b) Initial design and single-objective optimization results (objective functions and other outputs) 78
Table 3-2(a) Multi-objective optimization results (design variables) 90
Table 3-2(b) Multi-objective optimization results (objective functions and other outputs) 91
Table 3-3(a) Initial design and single-objective optimization results (design variables) 92
Table 3-3(b) Initial design and single-objective optimization results (objective functions and other outputs) 92
Table 3-4(a) Multi-objective optimization results with an additional constraint that CPC ratio should be at least 1.2 (design variables) 93
Table 3-4(a) Multi-objective optimization results with an additional constraint that CPC ratio should be at least 1.2 (objective functions and other outputs) 93
Table 4-1 Friction Coefficient α of Various Terrains (Patel, 2006) 107
Table 4-2 Design variables and their levels 113
Table 4-3 Noise factors and levels 114
Table 4-4 Specific values chosen for the design parameters (Inner Array) and values of noise factor (Outer Array) 116

Table 4-5 Results of the 27 experiments of parameter design 117
Table 4-6 Results of analysis of variance (ANOVA) for S/N ratios 119
Table 4-7 Comparison of Initial design and optimum design 121
Table 4-8 Results of parameter design using penalized Taguchi method 123
Table 4-9 Comparison of Initial design and Optimum results by Traditional and Penalized Taguchi Methods 125
Table 4-10 Refinement of design levels and results by penalized Taguchi method 127
Table 4-11 Control factors and levels in tolerance design 132
Table 4-12 Specific values chosen for the tolerance (Inner Array) and values of noise factor (Outer Array) 134
Table 4-13 Results of all 27 runs of tolerance design 135
Table 4-14 Optimum mean and tolerance values of design variables 137
Table 5-1 Physical parameters and basic operation conditions 152
Table 5-2 Cost parameters 153
Table 5-3 Results of optimization 154

LIST OF FIGURES

Figure 1-1 World share of renewable energy supply (2009) 4
Figure 1-2 Pictorial View of flat-plate solar collector 8
Figure 1-3 A typical flat plate photovoltaic module or panel 8
Figure 1-4 Geometric cross section of a symmetrical compound parabolic collector 9
Figure 1-5 Wind turbine configurations 10
Figure 1-6 Diagram of a fuel cell 14
Figure 2-1 Multi-row flat plate collector in a given area 17
Figure 2-2 Zenith angle, slope, surface azimuth angle and solar azimuth angle for a tilted surface 22
Figure 2-3 Cooperative and non-cooperative game solutions 39
Figure 2-4 Sensitivity analysis with respect to the design valuable H 46
Figure 2-5 Sensitivity analysis with respect to the design valuable L 46
Figure 2-6 Sensitivity analysis with respect to the design valuable D 47
Figure 2-7 Sensitivity analysis with respect to the design valuable β 47
Figure 2-8 Sensitivity analysis with respect to the design valuable K 48
Figure 2-9 Probabilistic single objective optimization; Minimization of $\boldsymbol{f1 + \sigma f1}$; Variation of design variables 60
Figure 2-10 Probabilistic single objective optimization; Minimization of $\boldsymbol{f1 + \sigma f1}$; Variation of objective functions 61
Figure 2-11 Probabilistic single objective optimization; Minimization of $\boldsymbol{f3 + \sigma f3}$; Variation of design variables 62
Figure 2-12 Probabilistic single objective optimization; Minimization of $\boldsymbol{f3 + \sigma f3}$; Variation of objective functions 63
Figure 2-13 Probabilistic multi-objective optimization (Game theory); Variation of design variables 64
Figure 2-14 Probabilistic multi-objective optimization (Game theory); Variation of objective functions 65
Figure 3-1 Geometric cross section of a truncated compound parabolic solar collector 70
Figure 3-2 Multi-row compound parabolic collector in a given area 71
Figure 3-3 Sensitivity Analysis with respect to P and S_2 83
Figure 3-4 Sensitivity Analysis with respect to probability of constraint satisfactions 89
Figure 4-1 Axial flow model 100
Figure 4-2 A blade element 103

Figure 4-3 Blade geometry for analysis of a horizontal axis wind turbine 104
Figure 4-4 Three different levels of shape profiles 114
Figure 4-5 Response graphs for the S/N ratio (Parameter design) 118
Figure 4-6 Response graph for S/N ratio (Parameter design using Penalized Taguchi Method) 124
Figure 4-8 Sample tolerance-cost curve 132
Figure 4-9 Relative cost for different tolerance levels 133
Figure 4-10 Response graphs for the S/N ratio (Tolerance design) 136
Figure 5-1 Schematic of the modeling domain 143
Figure 5-2 Polarization curves for the optimum designs 155
Figure 5-3 Power density vs. current density curves of the optimum designs 157
Figure 5-4 Power destiny vs. voltage curves for the optimum designs 157
Figure 5-5 Methanol crossover vs. current density curves for the optimum designs 159
Figure 5-6 Methanol crossover vs. voltage curves for optimum designs 160

CHAPTER 1
Introduction

1.1 Current Status of Renewable Energy

Energy is available in two different alternatives, the non-renewable energy and the renewable energy. The non-renewable energies including coal, petroleum, oil and natural gas are natural resources which need thousands of years to form and cannot be re-grown, regenerated or reused immediately. Nuclear energy, as a special type of energy, is still remaining controversial on the feature of environmental friendly and the risk of nuclear accidents and failures (Sovacool, 2010). Renewable energy is the energy that derived from natural processes and can always be replenished. Solar, wind, ocean, hydropower, biomass, geothermal, biofuels, tide and hydrogen are all considered as renewable energies. Climate change concerns, coupled with high energy prices, as well as the increasing energy demand for the developing world's economy, many countries have shown an increased interest in the utilization of renewable energies.

Renewable energies are categorized into traditional and modern renewable energies. The former mainly includes large hydropower energy and traditional biomass energy which usually refers to wood fuels, agricultural by-products and solid waste burned for cooking and heating purpose; the latter generally contains solar energy, wind energy, small hydropower energy, geothermal energy, ocean energy, modern biomass energy and

hydrogen energy. As shown in Fig. 1-1, in 2009, fossil fuel and nuclear energy contribute 78% and 3% respectively to the world energy consumption and only about 19% of the global energy consumption was supplied from renewable energy, with 13% from traditional biomass heating and 3% coming from large hydroelectricity. All of the modern renewable energies only accounted for the rest 3%, but they are growing very fast. Compared to the traditional renewable energies, modern renewable energies not only contain the common renewability feature but also have other multiple benefits such as no greenhouse emission, no air pollution and low noise pollution. The total solar energy absorbed by Earth's atmosphere, oceans and land masses is approximately 3,850,000 exajoules (1 EJ = 10^{18} J) a year. It is estimated that 30 minutes of solar radiation falling on earth is equal to the world energy demand for one year (Kalogirou, 2004). Wind energy is created by the uneven heat from the sun. The amount of wind energy is 2,250 exajoules a year (Archer and Jacobson, 2005), even though this number is much less than the total energy of solar, it is still the second largest amount of energy resource in the world. Compared to the total worldwide energy consumption in 2008 which is 474 exajoules, either of the two energies would be sufficient to supply all of our energy demands.

Table 1-1 presents the renewable energy status in the recent years from 2005 to 2009. It is clearly that modern renewable energies grows much faster than traditional renewable energies, particularly two most promising renewable energy sources—photovoltaic solar power and wind power—which have an average yearly increase rate of 57% and 28%. (REN21, 2007, 2009, 2010).

Table 1-1 Renewable energy status in the recent years (2005 ~ 2008)

Selected Indicators	Year / Unit	2005	2006	2007	2008	2009	Average yearly increase
Wind power	GW	59	74	94	121	159	28%
Small hydro power	GW	66	73	78	85	90	8%
Biomass power	GW	44	45	50	52	54	5%
Grid-connected solar PV	GW	3.5	5.1	7.5	13	21	57%
Geothermal	GW	9.3	9.5	9.7	10	11	4%
Ocean wave power	GW	0.3	0.3	0.3	0.3	0.3	0%
Modern renewable power	GW	182	207	240	281	335	17%
Large hydro power	GW	748	813	830	860	890	4%
Total renewable power	GW	930	1020	1070	1141	1225	7%
Solar collector for heating	GWth	87	105	126	145	180	20%
Geothermal heating	GWth	28	33	41	50	60	21%
Modern renewable heating	GWth	115	138	167	195	240	20%
Biomass heating	GWth	221	235	242	250	270	5%
Total renewable thermal	GWth	336	373	409	445	510	11%
Bio-ethanol production	Billion liters	34	39	53	69	76	23%
Bio-diesel production	Billion liters	3.9	6	10	15	17	46%
Total Biofuel production	Billion liters	37.9	45	63	84	93	26%

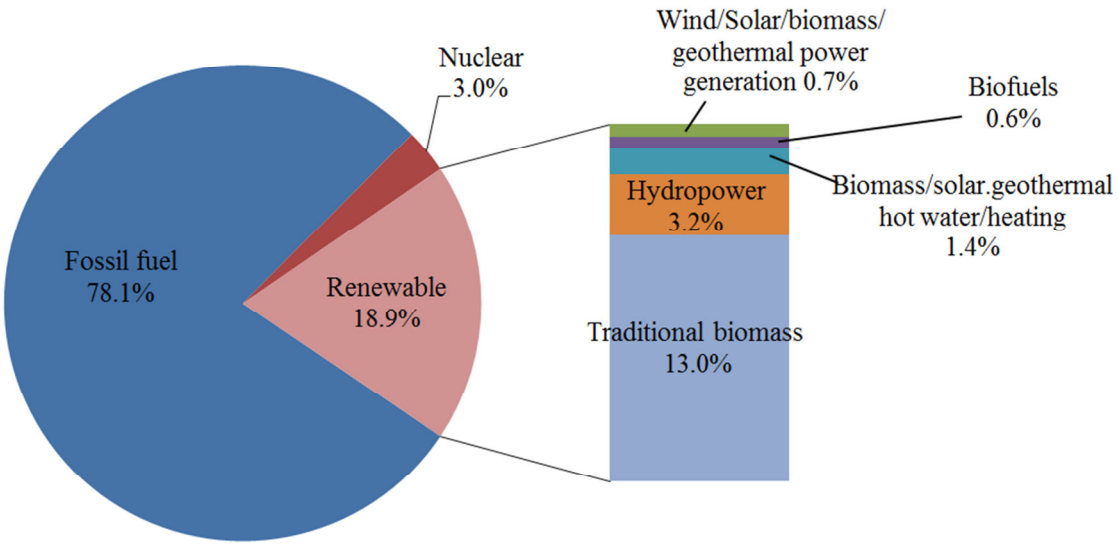

Figure 1-1 World share of renewable energy supply (2009)

Although the cost of many renewable energies have been declining significantly in the recent years, it is still much higher compared to conventional fuels. Typical power generation costs from conventional fuels are in the range of 3~8 U.S. cents per kilowatt-hour (kWh). In contrast, cost of wind energy is in the range of 5~12 U.S. cents per kWh, cost of solar photovoltaic modules is as high as 20~80 U.S. cents per kWh. On the one hand, many countries and states have implemented incentives including government tax subsidies, partial copayment schemes and various rebates over purchase of renewable energies to encourage consumers to shift to renewable energy sources. On the other hand, engineers should make great effort to optimize the renewable product, make it cheaper and more efficient.

Besides the high cost concern, solar and wind energy are challenged for their uncontrollable variability and intermittent availability compared to traditional internal combustion engines and conventional batteries. For example, solar energy is only

available during the daytime and the intensity of the solar radiation changes all the time even for a sunny day. Wind energy needs a wind speed of at least 3 m/s to start to generate electricity and if the wind speed is too high, the turbines will have to be shut down to avoid damage. As a result, these two renewable energies are also called intermittent energy sources. These shortcomings can be overcome by hydrogen energy system, more specifically, hydrogen based fuel cells are considered a leading contender to replace internal combustion engines and conventional batteries.

1.2 Solar Collectors

Solar technology has been developed since the 7th century B.C. In the ancient times, people magnified glass to concentrate sun's ray in order to make fires for various purpose. In 1767, Swiss scientist Horace De Saussure built the world's first solar collector which was used for cooking food later in the South Africa expedition in the 1830s. In 1839, the French scientist Edmond Becquerel discovers the photovoltaic effect using an experiment method. In the following century, many scientist and researchers reported many different types of solar collectors and cells, but most of them cannot continuously power electronics. In 1954, Daryl Chapin, Calvin Fuller and Gerald Pearson developed the first silicon photovoltaic cell at Bell Lab (USA) that was capable of converting enough of the sun's energy into electrical power to run equipment for daily use. The efficiency of this photovoltaic cell was about 4%. Now the efficiency of solar cells has significantly been improved to over 40%. In 2009, researchers at the Fraunhofer Institute of Solar Energy

Systems have set a new record of 41.1% for converting sunlight into electricity (Guter et al., 2009).

The basic theory of any solar system is that the solar collectors absorb the incoming solar radiation and transfer the heat to a fluid (solar thermal collectors) or convert into electricity directly by using semiconductors (photovoltaic solar collectors). In general, there are two types of solar collectors: non-concentrating and concentrating. Non-concentrating solar collectors usually have the same intercepting area and absorbing area while concentrating solar collectors usually have concave reflecting surfaces to intercept and focus the sun's beam radiation to smaller receiving areas in order to get higher radiation flux. Various types of solar collectors are listed in Table 1-2 (Kalogirou, 2003).

Table 1-2 List of Solar Collectors

Motion	Collector type	Absorber type	Concentration ratio	Indicative temperature range (°C)
Stationary	Flat plate collector	Flat	1	30-80
	Evacuate tube collector	Flat	1	50-200
	Compound parabolic collector	Tubular	1-5	60-240
Single-axis tracking	Linear Fresnel reflector	Tubular	10-40	60-250
	Parabolic trough collector	Tubular	15-45	60-300
	Cylindrical trough collector	Tubular	10-50	60-300
Double-axis tracking	Parabolic dish reflector	Point	100-1000	100-500
	Heliostat field collector	Point	100-1500	150-2000

In this work, two different types of stationary solar collector systems—flat-plate solar collectors and compound parabolic solar collectors—are selected as the objectives for optimization in the following chapters. Here is a belief introduction of the two types of solar collectors.

Flat-plate collectors were first developed by Hottel and Whillier in 1950s (Whillier, 1953). As shown in Fig. 1-2, when solar radiation passes through a transparent cover and impinges on the blackened absorber surface of high absorptivity, a large portion of this energy is absorbed by the plate and then carry away by the liquid fluids inside the tubes for storage or use. The underside of the absorber plate and the side of casing are well insulated to reduce conduction losses. The liquid tubes can be welded to the absorbing plate, or they can be an integral part of the plate. The liquid tubes are connected at both ends by large diameter header tubes.

The flat plate solar collectors are the most economical and popular among the various types of solar collector systems since they are permanently fixed in positions, involve simple construction, and require little maintenance. They are used in many different thermal applications, such as air conditioning, industrial processes, domestic water heating, space-heating. Moreover, the most common design of photovoltaic panels is the flat-plate photovoltaic modules. Figure 1-3 presents one typical flat-plate module design of photovoltaic panel. It uses a substrate of metal, glass or plastic to provide structural support in the back, an encapsulate material to protect the cells and a transparent cover of plastic or glass.

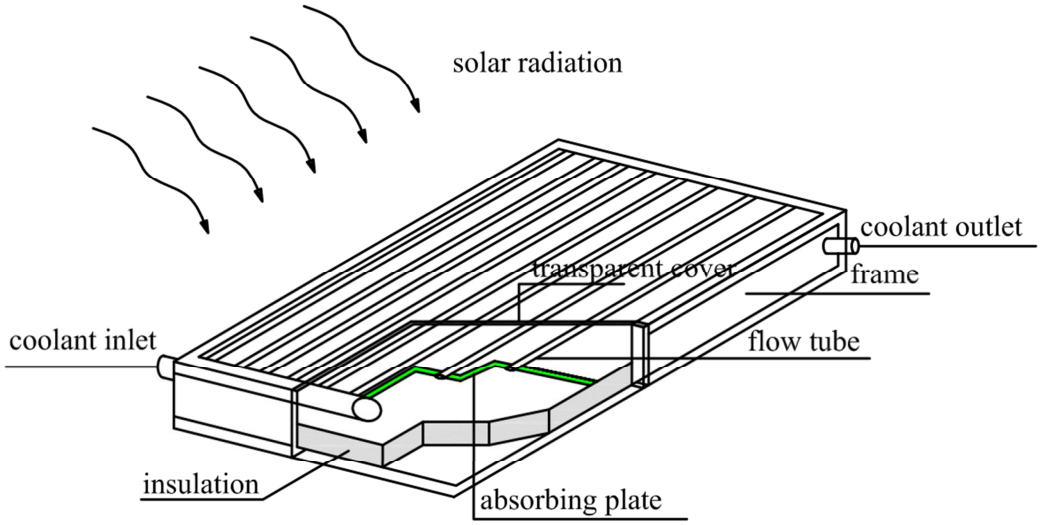

Figure 1-2 Pictorial View of flat-plate solar collector

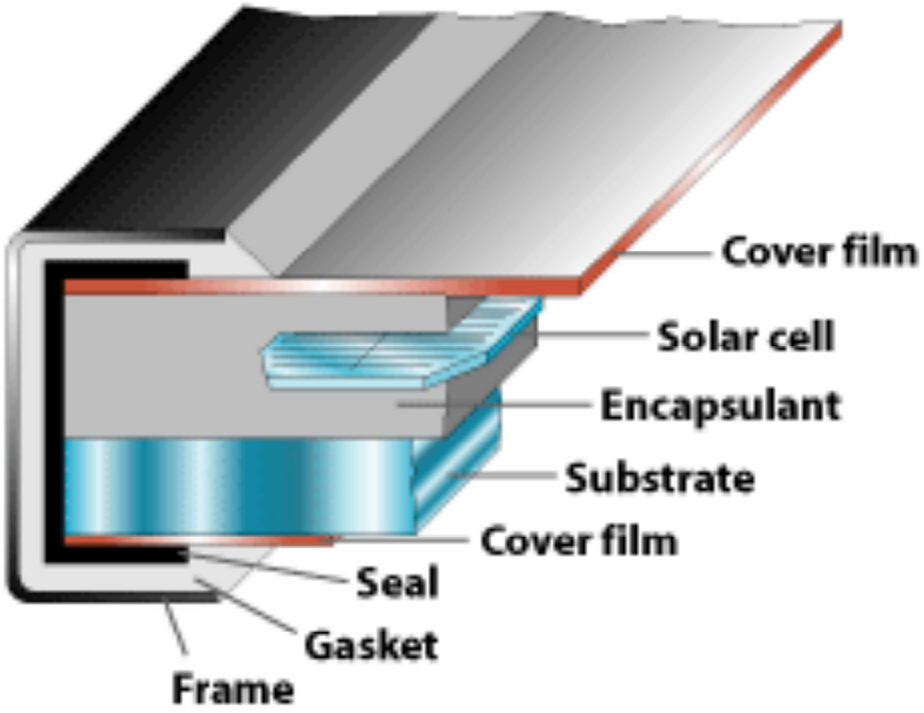

Figure 1-3 A typical flat plate photovoltaic module or panel

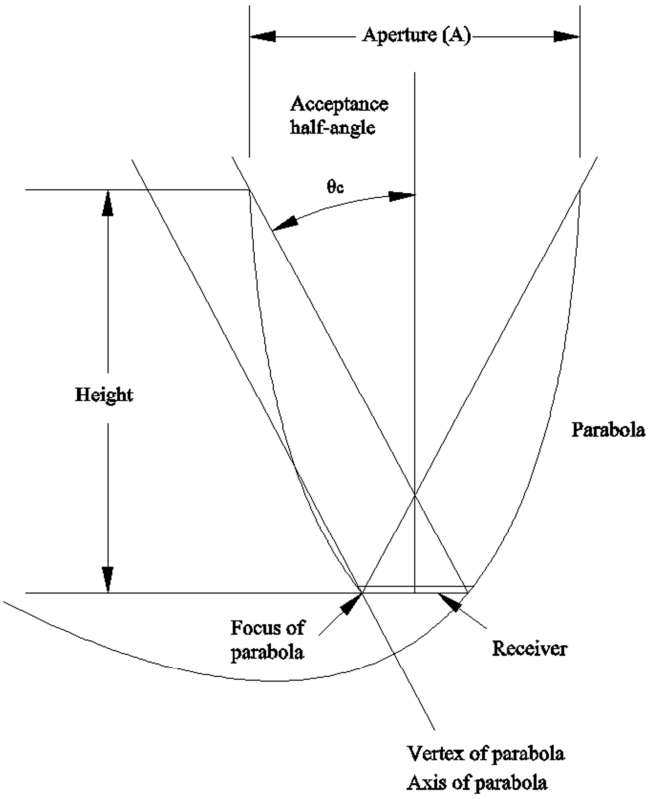

Figure 1-4 Geometric cross section of a symmetrical compound parabolic collector

Compound parabolic collectors (CPC), first proposed by Winston and Hinterberger (1975), have the capability of reflecting to the absorber all the incident radiation within wide limits. Figure 1-4 shows a geometric cross section of a symmetrical compound parabolic collector. By using multiple internal reflections, any radiation that is entering the aperture, within the collector acceptance angle, finds its way to the absorber surface located at the bottom of the collector. The absorber can take a variety of configurations. It can be flat as shown in Fig. 1-4 or cylindrical. Since it has both merit of flat plate solar collector and concentrating collector, it is an excellent substitute to the corresponding flat plate solar collectors. CPC could reach considerably higher temperatures and offer superior yearly energy delivery compared to flat plate solar collectors for thermal purpose.

1.3 Wind Turbines

People start to use wind energy as early as 200 B.C. in the sail boats and sail-type windmills. The first practical windmillers were built in Sistan, a region between Afghanistan and Iran from the 7th century (Al-Hassan and Hill, 1986). They are used for grinding corns, drawing up water, grist milling and sugarcane industries (Hill, 1991). In the 14th century, Dutch windmills were established to pump water to the drain area of the Rhine River. The first automatically operated wind turbine for electricity production was built in Cleveland, Ohio (USA) by Charles F. Brush in 1888 (Righter, 1996). It was 18 meters tall with a diameter of 17 meters, weight of 36 tons and had a 12 kW turbine.

Nowadays, wind energy conversion devices can be broadly categorized into two types as shown Fig. 1-5, the horizontal-axis wind turbines (HAWT) and the vertical-axis wind turbines (VAWT).

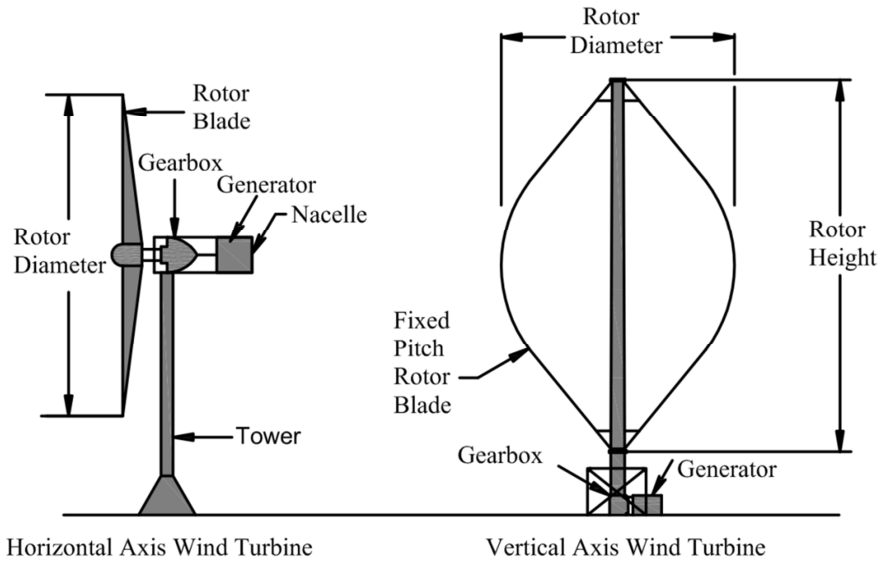

Figure 1-5 Wind turbine configurations

HAWTs need to have a main rotor shaft and electrical generator at the top of a tower, and the turbine are pointed into the wind while VAWTs set the main rotor shaft vertically and do not need to be pointed into the wind. Although VAWT has its advantages like easy install and simple control, it cannot produce as much energy as a HAWT at a given site with the same height. Today the majority of commercial turbines and all grid-connected commercial wind turbines are HAWTs. All the design and optimization in this thesis are referring to HAWT.

The design a wind turbine system essentially involves determining the diameter of the rotor, number of blades, blade size, material and profile, chord length, setting of pitch angles, height of the tower, the type of transmission system and gear box.

Since power is a function of the swept rotor area, which is a function of the diameter squared, the rotor has been designed larger and larger. It is evident shown in Table 1-3 that the size of the wind turbines is growing dramatically in past thirty years. The hub height, which is equal to the height of tower, is also increase with the increase of rotor diameter.

Table 1-3 Growth in Wind turbine size in the past thirty years

Product	1981	1985	1990	1995	2000	2005	2008
Rotor diameter (m)	15	20	40	50	80	124	126
Hub height (m)	24	43	54	80	104	114	135
Capacity (kW)	55	100	225	600	2000	5000	6000

The determination of the number of blades depends on many factors including aerodynamic efficiency, cost, reliability and noise. In general, two-blade and three-blade design are dominating in today's commercial HAWTs' market while fewer or more blade design is not that popular. The choice of two-blade or three-blade design depends on certain factors. The two-blade design has less nacelle weight and is much simpler to install. The three-blade design can increase the power coefficient by 5~10%, offer smoother power output and more balanced gyroscopic force, and has less chances of failure but it also involves 33.3% more weight and cost due to an extra blade. Wood and canvas sails were originally used on early windmills due to their low price, availability, and easy of manufacture. Nowadays, smaller blades can be made from light metals such as aluminum. Carbon fiber has recently been identified as a cost effective material with relatively higher stiffness in large HAWTs. The design of other parameters like control system, transmission system and gear box varies one case by another, but all the designers seek for optimum designs which is high-efficiency with relatively low cost.

1.4 Fuel Cells

A fuel cell is an energy conversion device that produces electricity directly from a fuel by electrochemical combination of the fuel with an oxidant. The fuel cell operating principle is discovered by William R. Grove (UK) in 1839 (Grove, 1839). But this discovery has not been further researched for a century until another English man Francis T. Bacon, who started working on practical fuel cells in 1937 and developed the first hydrogen-oxygen fuel cell by the end of 1950. At the beginning, all of the fuel cells are applied in

space shuttle, like Gemini and Apollo space program. This situation last until the early 1990s, fuel cells started to be applied in some other field, like submarine and automobile as well as small electronics. But the fuel cells have not been fully commercialized even today due to relatively higher cost.

In general, there are five major types of fuel cells, differentiate by the electrolyte used in the cells and they are: proton exchange membrane fuel cell (PEMFC), alkaline fuel cell (AFC), phosphoric acid fuel cell (PAFC), molten carbonate fuel cell (MCFC), and solid oxide fuel cell (SOFC). Although they are different types of fuel cells, they all work in the same general manner. As shown in Fig. 6, any type of fuel cells is made up of three segments which are sandwiched together, the anode, the electrolyte and the cathode. Two different chemical reactions occur at the interface of the three different components. The fuel at the anode side is oxidized and this reaction divides the fuel into a positivity charged ion and a negatively charged electron. The freed electrons travel through a wire to create the electricity. The ions pass through the specifically designed electrolyte and arrive at cathode side. Once reaching the cathode, the ions are reunited with the electrons and the two react with a third chemical, usually oxygen to create water or / and carbon dioxide. Therefore the net result of the two reactions is that fuels are consumed, water or / and carbon dioxide is created, and electricity is generated which can be used to power electrical devices.

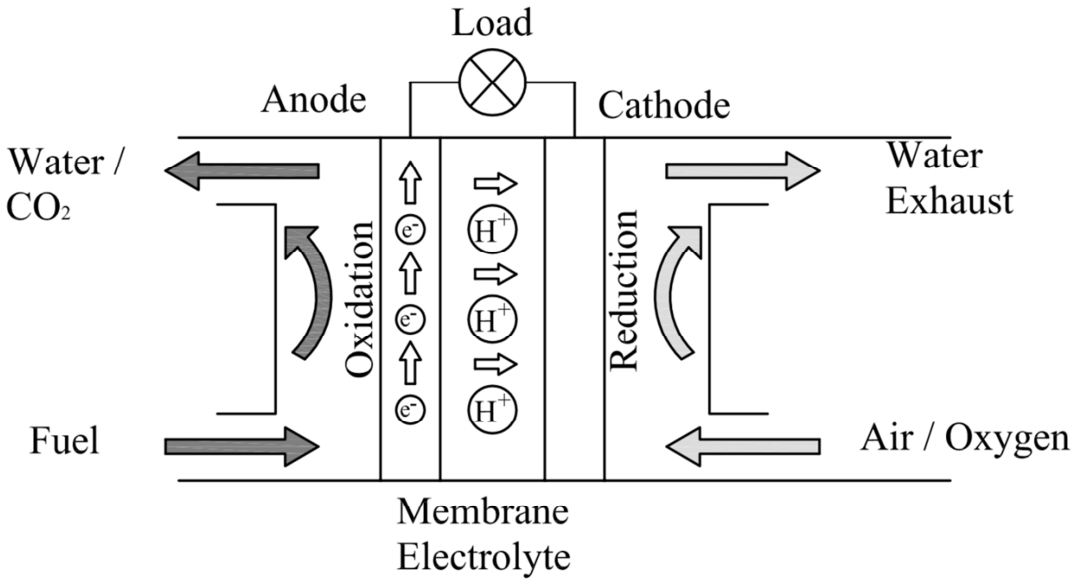

Figure 1-6 Diagram of a fuel cell

A typical fuel cell produce an open circuit voltage around 0.6~0.8 V and the voltage decreases with the increase of current because of three losses including activation loss, ohmic loss and mass transport loss. Fuel cells can be combined in series and / or parallel, namely fuel cell stack, in order for seeking higher voltage and / or current respectively in different applications.

Direct methanol fuel cell (DMFC) is a subcategory of proton exchange membrane fuel cells (PEMFCs) in which methanol is used as the fuel. Since methanol is supplied to the fuel cell in liquid form, it is easy to store, deliver and recharge compared to hydrogen. This type of fuel cell was invented by Dr. Surya Prakash and Dr. George A. Olah in 1990. However many researchers later noticed that DMFC was limited in reaction speed and power production. This makes this type of fuel cell ill-suited for large power application, but ideal for small consumer goods such as mobile phones, digital cameras, laptops and some small vehicles such as forklifts and tuggers. Besides the disadvantage of low power

output, DMFC is also challenged for the high cost concern since it needs high loading platinum as a catalyst for both half reactions.

1.5 Summary of Present Work

The major concern of all types of renewable energies are the relatively higher cost compared to fossil fuels. The present work is expected to help designers to seek optimum designs of improving the performance and reducing the cost by using different optimization approaches. The design of some typical renewable energy systems including flat-plate solar collector, compound parabolic concentrator solar collector, horizontal axis wind turbine and direct methanol fuel cell system are chosen as optimum objectives. The following chapters of this dissertation are organized as follows.

Chapter 2 and 3 present multi-objective optimum designs of flat plate and compound parabolic concentrator solar collector systems. Sequential Quadratic Programming combined with the game theory under determinist and probabilistic optimization technique is applied in the examples. The game theory methodology is used for the solution of the three objective constrained optimization problems including maximization of the annual average incident solar energy, maximization of the lowest month incident solar energy and minimization of the cost to find the best compromise solution. Most design variables and some other parameters are treated as probabilistic variables following normal distribution in order to make the optimization problem more realistic. The sensitivity analyses based on optimum design presented in this work are expected to help designers in creating optimized solar collectors based on any specified requirements.

In Chapter 4, the robust design of horizontal axis wind turbines, including both parameter and tolerance designs, is presented. This work considers multiple design parameters (variables), multiple objectives, and multiple constraints simultaneously by using the traditional Taguchi method and its extensions; it provides a simple way of designing robust horizontal axis wind turbine systems under realistic conditions.

In chapter 5, a three-dimensional DMFC model is established and two optimization problems have been formulated. Most geometrical parameters and operating parameters are treated as design variables, while power output and cost are two different objective functions subject to multiple constraints. A hybrid method base on the genetic algorithm (GA) is applied for seeking the global optimization point.

In Chapter 6, the conclusions and suggestions for further research are summarized.

CHAPTER 2

Optimum Design of Flat-plate Solar Collector System

2.1 Introduction and Literature Review

The design of a flat-plate solar collector embraces many relationships among the collector parameters, field parameters and solar radiation data at any given location. Figure 2-1 shows multi-row flat-plate solar collectors in a given area. Increasing the number of solar collector rows and height of the collector will definitely increase the total collector area; however, it also increases the shading area (darker area shown in Figure 2-1), which will reduce the radiation energy received from the sun.

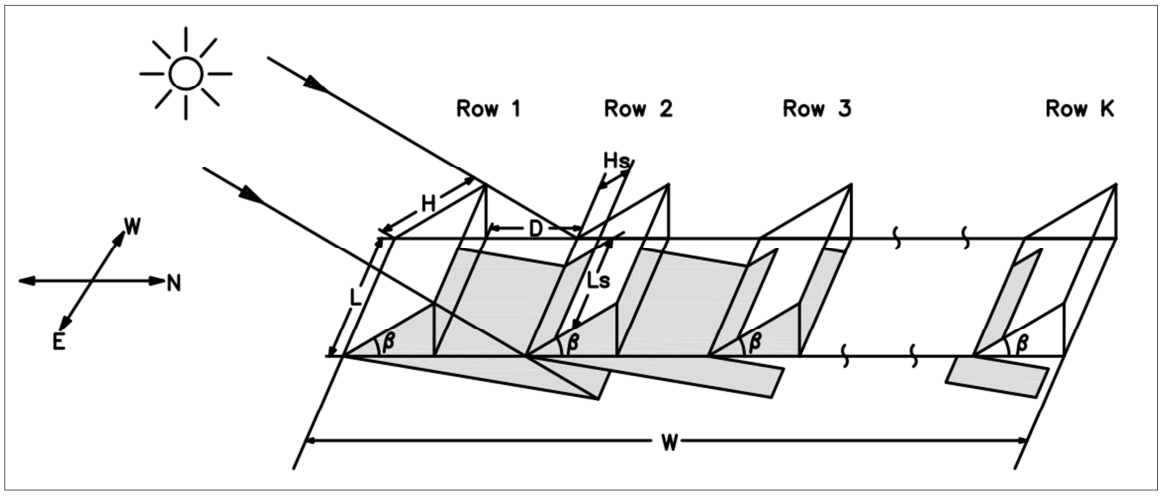

Figure 2-1 Multi-row flat plate collector in a given area

Appelbaum and Bany (1979) and Bany and Appelbaum (1987) introduced the effect of shading in the analysis and design of a large-area flat-plate solar collector system. Gopinathan (1991) developed a method for the evaluation of the effect of shading on concentric cylindrical parabolic collectors. Other researchers (Groumpos and Kouzam 1987, Reise and Kovach 1995, Carlsson, *et al.* 1998) presented different models including the effect of shading on different systems, including buildings. Weinstock and Appelbaum (2004, 2007) extended the model and formulated different optimization objectives including maximum incident energy on the collector plane, minimum field area for given incident energy, maximum energy per unit collector area and minimum cost and during a single objective optimization study. Because all objectives are important in a practical situation, the present work considers all the objectives simultaneously. The solution technique developed in this work is based on the concepts of game theory, which was first developed by Von Neumann and advanced by Von Neumann and Morgenstern (1947). Many researchers (Rao and Hati 1979, 1986, Hati and Rao 2001, Marston 2001, Miyamoto *et al.* 2008, Di Barba 2008) extended the application of game theory to solve problems from different areas of engineering with multiple objectives. Rao and Hati used game theory in the two-criteria design of beams (1986), and function generating mechanisms (1979), and Hati and Rao applied game theory for an air pollution control system related to environmental problems (2001). Marston (2001) used a game theory approach for the solution of several types of engineering design problems. Di Barba (2006) applied game theory to optimize the design of electromechanics. Miyamoto *et al.* (2008) utilized game theory to select a specific Pareto optimal solution among many optimum designs in an electromagnetic apparatus design.

Similar to many design problems, the solar collector design problem involves conflicting objectives in the form of maximization of average incident solar energy and minimization of cost. In the context of game theory, two players are associated with these two objectives. However, for achieving a true optimum and robust design of solar collectors, we need to consider another objective. It is possible that the annual average incident solar energy is maximized so that the collector gets too much energy in the summer; however its performance may be deficient in the winter due to the seasonal position of sun which results in low average temperatures. Thus in order to make the problem more realistic, a third objective, namely the maximization of the average incident solar energy for the lowest month (probably in winter) is introduced. More objective functions could be introduced into the formulation of the optimization problem, if necessary. It is to be noted that in the presence of multiple objectives, these will be no single design which will be optimum for all the objectives simultaneously. There will only be compromise solutions, known as Pareto-optimal solutions. Since there are multiple Pareto-optimal Solutions for any multi-objective problem, additional information or criterion needs to be used to find a specific Pareto-optimal (or compromise) solution. In this work, the final compromise solution (specific Pareto-optimal solution) is found using additional information based on supercriterion.

In practice, most of the parameters influencing in any design problem are uncertain. For example, Datskov *et al.* (2005) considered the effect of uncertainty by employing eight design or control variables—temperature, pressure, thickness of anode, cathode, catalyst layer and membrane, diffusivity of methanol, concentration of methanol—on DMFC (directs methanol fuel cell) since uncertainty is always associated with chemical reaction

process of fuel cells. Zhao *et al.* (2006) successfully estimated and optimized the wind farm capacity using probabilistic uncertainty analysis because no one can predict the wind velocity accurately. In the solar energy system design problem, the incident solar radiation measured in terms of the solar constant at any location varies from instant to instant. Only for convenience and simplicity, an average value of solar radiation is defined not only for each day but also for a typical day of the month/year. Available statistical analyses of solar radiation measurements acknowledge this variability / uncertainty. Kulkarni et al. (2007) incorporated uncertainty of solar radiation in the optimal design of a solar water heating system. Instead of getting a final optimum point, an optimum curve corresponding to different levels of solar radiation was determined. Different methods like Monte Carlo technique (Crawford and Rao, 1989, Conti and Raiti, 2007) and fuzzy approach (Kaushika et. al, 2005) has been introduced to solve probabilistic optimization problems. In the present work, probabilistic optimization problems have been transferred into equivalent deterministic problems by applying the chance constrained programming technique.

In the design and manufacture (or construction) of solar collectors, design parameters such as the width and length of a flat plate solar collector, distance between any two rows of solar collectors and the inclined angle of solar flat plate collectors are to be specified using tolerances, such as $\bar{x} \pm \Delta x$ where $\bar{x}$ is the mean value and Δx is the tolerance ($\Delta x = 3\sigma_x$ if the manufacturing / construction process follows normal distribution) of a design parameter. In order to make the optimization problem more realistic, the present work treats many of the design variables as well as the solar constant, altitude and typical

day of each month as probabilistic variables following normal distribution in the probabilistic approach. The results are compared with the deterministic approach.

As mentioned above, most design parameters are subject to variations due to random uncertainties, and manufacturing / installation errors; a sensitivity analysis based on the result of optimal design of deterministic approach is conducted and expected to identify the most (and least) influential parameters of the design. The result of the sensitivity analysis can help in identifying the parameters that need to be controlled tightly. Another sensitivity analysis with respect to the changes in the standard deviation of the design variables and the satisfaction level of the probabilistic constraints is conducted based on the result of optimal design of probabilistic approach. The work of sensitivity analyses are expected to help in a more realistic analysis and design of flat plate solar collectors. The optimization strategy presented and the results are expected to help designers to create optimized solar collectors depending on the specific requirements of the customers.

2.2 Solar Insolation Analysis

Since the atmospheric condition and air mass always change, the scattering and absorbing radiation also vary with time; thus it is difficult to accurately estimate the amount of solar radiation. It is therefore necessary to define a standard "clear" sky and calculate the hourly radiation that would be received on a horizontal surface under these standard conditions at a given location. Hottel (1976) provided a method of estimating the beam radiation transmitted through clear atmosphere, which takes into account the zenith angle and altitude for a standard atmosphere and for the four climate types (Figure 2-2). Accordingly, the atmospheric transmittance for beam radiation τ_b is given by:

$$\tau_b = a_0 + a_1 \exp(\frac{-k}{\cos\theta_z}) \qquad (2.1)$$

where the constants a_0, a_1 and k for the standard atmosphere with 23 km visibility are found from the values a_0^*, a_1^* and k^* corresponding to altitudes less than 2.5 km:

$$a_0^* = 0.4237 - 0.00821(6 - A)^2 \tag{2.2}$$

$$a_1^* = 0.5055 + 0.00595(6.5 - A)^2 \tag{2.3}$$

$$k^* = 0.2711 + 0.01858(2.5 - A)^2 \tag{2.4}$$

where A is the altitude at a given location in kilometers

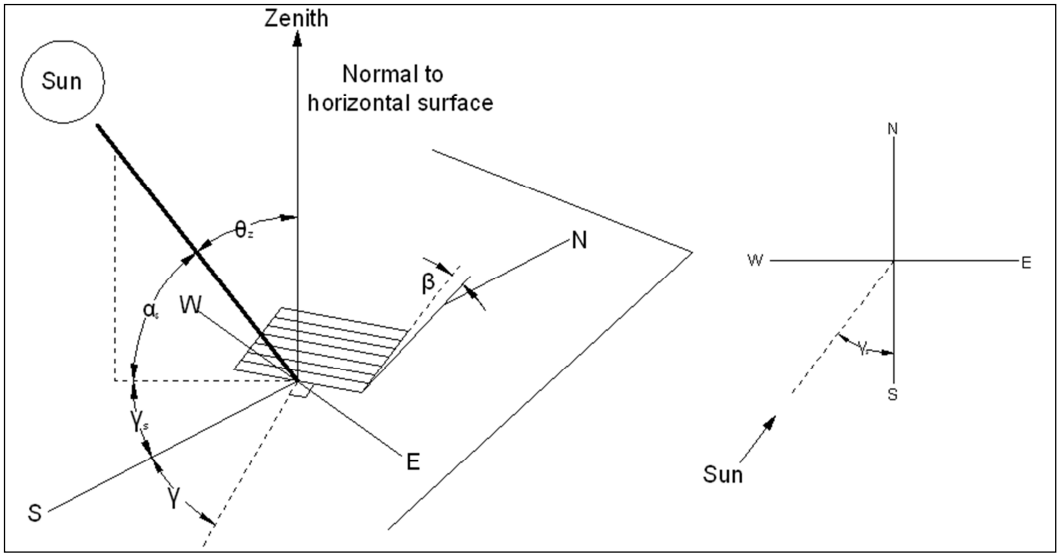

Figure 2-2 Zenith angle, slope, surface azimuth angle and solar azimuth angle for a tilted surface

Table 2-1 Correction factors for different climate types (Hottel, 1976)

Climate Type	r_0	r_1	r_k
Tropical	0.95	0.98	1.02
Midlatitude summer	0.97	0.99	1.02
Subarctic summer	0.99	0.99	1.01
Midlatitude winter	1.03	1.01	1

For different climate types, Table 2-1 gives the correction factors $r_0 = a_0 / a_0^*$, $r_1 = a_1 / a_1^*$ and $r_k = k / k^*$. Thus the transmittance of the standard atmosphere for beam radiation can be determined for any zenith angle and any altitude up to 5 km. The clear-sky beam radiation is given by:

$$G_{cnb} = G_{on}\tau_b$$

where $G_{on} = G_{sc}(1 + 0.033\cos\frac{360n}{365})$ (2.5)

and G_{sc} is the solar constant (a value of 1367 W/m^2 (Iqbal, 1983) is used for G_{sc} in this work). The clear-sky horizontal beam radiation can be determined as

$$G_b = G_{on}\tau_b \cos\theta_z \tag{2.6}$$

Liu and Jordan (1960) developed an empirical relationship between the transmission coefficient for beam and diffuse radiation for clear days:

$$\tau_d = 0.271 - 0.294\tau_b \tag{2.7}$$

$$G_d = G_{on}\tau_d \cos\theta_z \tag{2.8}$$

The shaded and un-shaded irradiation per unit area is:

$$S = H\,L[q_b + q_d + (K-1)(q_b^{sh} + q_d^{sh})] \tag{2.9}$$

where the yearly beam irradiation per unit area of an unshade collector (first row), q_b, is given by:

$$q_b = \sum_{n=1}^{12}\sum_{T=1}^{24} G_b \cos\theta \Delta T \tag{2.10}$$

The yearly diffuse irradiation per unit area of an unshade collector (first row), q_d, is given by:

$$q_d = \sum_{n=1}^{12}\sum_{T=1}^{24} G_{dh}\Delta T \tag{2.11}$$

The average yearly beam irradiation per unit area of a shaded collector ((K-1) rows); q_b^{sh}, is given by:

$$q_b^{sh} = \sum_{n=1}^{12}\sum_{T=1}^{24} G_b \cos\theta(1-a_s)\Delta T \tag{2.12}$$

and the average yearly diffuse irradiation per unit area of a shade collector ((K-1) rows); q_d^{sh}, is given by:

$$q_d^{sh} = F_d^{sh}\sum_{n=1}^{12}\sum_{T=1}^{24} G_{dh}\Delta T \tag{2.13}$$

where G_b is the direct beam irradiance on the collector perpendicular to solar rays and G_{dh} is the horizontal diffuse irradiance. The angle between the solar beam and the normal to the collector (θ) is given by:

$$\cos\theta = \cos\beta\sin\alpha + \sin\beta\cos\alpha\cos\gamma \tag{2.14}$$

The shape factors for un-shaded and shaded solar collectors are given by:

$$F_d = \cos^2(\beta/2) \tag{2.15}$$

$$F_d^{sh} = \cos^2(\beta/2) - 1/2[(d^2+1)^{1/2} - d]\sin\beta \tag{2.16}$$

where d is the normalized distance between two rows given by

$$d = D/H\sin\beta \tag{2.17}$$

The relative shaded area a_s is given by

$$a_s = l_s\, h_s \tag{2.18}$$

with

$$l_s = 1 - \frac{d\sin\beta + \cos\beta}{l} \frac{|\sin\gamma|}{\cos\beta\tan\alpha + \sin\beta\cos\gamma} \text{ is the relative shadow length} \quad (2.19)$$

$$a_s \geq 0, \qquad |\gamma| \leq 90\,\text{deg}, \qquad 0 \leq l_s \leq 1$$

$$h_s = 1 - \frac{d\sin\beta + \cos\beta}{\cos\beta + [\sin\beta\cos\gamma / \tan\alpha]} \text{ is the relative shadow width} \quad (2.20)$$

$$a_s \geq 0, \qquad |\gamma| \leq 90\,\text{deg}, \qquad 0 \leq h_s \leq 1\text{, and}$$

$l = L / H \sin\beta$ is the normalized collector length.

2.3 Formulation of Single-objective Optimization Problem

2.3.1 Determinist form

The flat-plate solar collector optimal design problem consists of several design valuables, a set of linear or nonlinear equality or inequality constrains and an objective function. Mathematically, it can be stated in the following general form:

Minimize or maximize f($\vec{X}$) with respect to $\vec{X}$,

subject to: $$g_j(\vec{X}) = 0, \qquad j = 1,2,....m \quad (2.21)$$

$$h_j(\vec{X}) \leq 0, \qquad j = 1,2,....n \quad (2.22)$$

$$a_k \leq x_k \leq b_k, \qquad k = 1,2,....l \quad (2.23)$$

where x_k is the k^{th} component of the design vector $\vec{X}$, and a_k and b_k are the lower and upper bounds on the design variable x_k, respectively.

2.3.2 Probabilistic form

When some of the parameters involved in the objective function and / or constraints vary about their respective mean values, the optimization problem needs to be formulated as a stochastic programming problem. For simplicity, we assume that all the random variables are independent and follow normal distribution. A probabilistic nonlinear programming problem can be stated as:

Find $\vec{X}$ which minimizes $f(\vec{Y})$, subject to $P[g_j \le 0] \ge p_j, \; j = 1,2,...,m$ (2.24)

where $\vec{Y}$ is the vector of N random variables $y_1, y_2, ..., y_N$ that might include the decision variables $x_1, x_2, \ldots, x_l$. The case when $\vec{X}$ is deterministic can be obtained as a special case of the present formulation. Equations (2.24) denote that the probability of realizing $g_j(\vec{Y})$ less than or equal to zero must be greater than or equal to the specified minimum probability p_j. The problem stated in (2.24) can be converted into an equivalent deterministic programming problem by applying the chance constrained programming technique as indicated below.

1. Objective Function

The Taylor's series expansion of the objective function $f(\vec{Y})$ about the mean values of y_i, $\bar{y}_i$ is given by

$$f(\vec{Y}) = f(\bar{\vec{Y}}) + \sum_{i=1}^{N} \left(\left. \frac{\partial f}{\partial y_i} \right|_{\bar{\vec{Y}}} \right) (y_i - \bar{y}_i) + \text{ higher-order derivative terms} \qquad (2.25)$$

If the standard deviations of all y_i, σ_{yi}, are small, $f(\vec{Y})$ can be approximated by the first two terms of Eq.(25):

$$f(\vec{Y}) \cong f(\bar{\vec{Y}}) - \sum_{i=1}^{N} \left(\left. \frac{\partial f}{\partial y_i} \right|_{\bar{\vec{Y}}} \right) \bar{y}_i + \sum_{i=1}^{N} \left(\left. \frac{\partial f}{\partial y_i} \right|_{\bar{\vec{Y}}} \right) y_i \equiv \psi(\vec{Y}) \qquad (2.26)$$

If all y_i (i = 1, 2, … , N) follow normal distribution, $\psi(Y)$, a linear function of Y, also follows normal distribution. The mean and the variance of ψ are given by

$$\bar{\psi} = \psi(\bar{\vec{Y}}) \qquad (2.27)$$

$$Var(\psi) = \sigma_{\psi}^2 = \sum_{i=1}^{N} \left(\left. \frac{\partial f}{\partial y_i} \right|_{\bar{\vec{Y}}} \right)^2 \sigma_{y_i}^2 \qquad (2.28)$$

since all y_i are independent. For the purpose of optimization, a new objective function $F(\vec{Y})$ can be constructed as

$$F(\vec{Y}) = k_1 \bar{\psi} + k_2 \sigma_{\psi} \qquad (2.29)$$

where k_1 and k_2 indicate the relative importances of $\bar{\psi}$ and σ_{ψ} for minimization.

2. Constraints

If some parameters are random in nature, the constraints will also be probabilistic and one would like to have the probability of satisfying a given constraint to be greater than a certain value. This is precisely what is stated in Eq.(2.24). The inequality constraint of Eq. (2.24) can be written as

$$\int_{-\infty}^{0} f_{g_j}(g_j)dg_j \geq p_j \tag{2.30}$$

where $f_{gj}(g_j)$ is the probability density function of the random variable g_j whose range is assumed to be $-\infty$ to ∞. The constraint function $g_j(\vec{Y})$ can be expanded around the vector of mean values of the random variables, $\bar{Y}$, in Taylor's series as

$$g_j(\vec{Y}) \cong g_j(\bar{\vec{Y}}) + \sum_{i=1}^{N}\left(\frac{\partial g_j}{\partial y_i}\bigg|_{\bar{\vec{Y}}}\right)(y_i - \bar{y}_i) \tag{2.31}$$

From this equation, the mean value, $\bar{g}_j$, and the standard deviation, σ_{gj}, $of\ g_j$ can be obtained as

$$\bar{g}_j = g_j(\bar{\vec{Y}}) \tag{2.32}$$

$$\sigma_{gj} = \left\{\sum_{i=1}^{N}\left(\frac{\partial g_j}{\partial y_i}\bigg|_{\bar{\vec{Y}}}\right)^2 \sigma_{y_i}^2\right\}^{1/2} \tag{2.33}$$

By introducing the new variable

$$\theta = \frac{g_j - \bar{g}_j}{\sigma_{gj}} \tag{2.34}$$

and noting that

$$\int_{-\infty}^{\infty} \frac{1}{\sqrt{2\pi}} e^{-t^2/2} dt = 1 \tag{2.35}$$

Eq. (2.30) can be expressed as

$$\int_{-\infty}^{-(\bar{g}_j/\sigma_{g_j})} \frac{1}{\sqrt{2\pi}} e^{-\theta^2/2} d\theta \geq \int_{-\infty}^{(\phi_j(p_j))} \frac{1}{\sqrt{2\pi}} e^{-t^2/2} dt \tag{2.36}$$

where $\Phi_j(p_j)$ is the value of the standard normal variate corresponding to the probability p_j. Therefore Eq. (2.37) can be rewritten as Eq. (2.38):

$$-\frac{\bar{g}_j}{\sigma_{gj}} \geq \phi_j(p_j) \qquad \text{or} \qquad \bar{g}_j + \sigma_{gj}\, \phi_j(p_j) \leq 0 \tag{2.37}$$

$$\bar{g}_j + \phi_j(p_j) \left[\sum_{i=1}^{N} \left(\frac{\partial g_j}{\partial y_i} \bigg|_{\vec{Y}} \right)^2 \sigma_{y_i}^2 \right]^{1/2} \geq 0, \qquad j = 1,2,...,m \tag{2.38}$$

Thus the optimization problem of Eq. (2.24) can be stated in its equivalent deterministic form as: minimize $F(\vec{Y})$ given by Eq. (2.29) subject to the m constraints given by Eq. (2.38).

2.3.3 Maximization of annual average incident solar energy

The problem of optimization of the solar collector design is to obtain maximum incident energy on a given horizontal and fixed flat-plate collector of dimensions L × W (length ×

width). The solar collector system (Figure 1) includes K rows of solar collectors with distance D between two neighboring rows and each collector is of length L and height H and inclined at an angle β with respect to the horizontal line. The design vector of the problem is:

$$\vec{X} = \begin{Bmatrix} H \\ L \\ D \\ \beta \\ K \end{Bmatrix} \tag{2.39}$$

The random variable vector is:

$$\vec{Y} = \begin{Bmatrix} H \\ L \\ D \\ \beta \\ A \\ G_{sc} \\ N_d \end{Bmatrix} \tag{2.40}$$

where A is the altitude, G_{sc} is the solar constant and N_d is the typical day of each month. These variables vary with the location.

The average incident solar energy of the field (for maximization) is given by:

$$Q = H\,L[q_b + q_d + (K-1)(q_b^{sh} + q_d^{sh})] \tag{2.41}$$

and the objective function for minimization is taken as:

$$f_1(\vec{Y}) = -Q = -H\,L[q_b + q_d + (K-1)(q_b^{sh} + q_d^{sh})] \tag{2.42}$$

The expressions for computing $q_b, q_d, \ q_b^{sh}, \ q_d^{sh}$ are given in Appendix A. The constraints of the optimization problem can be stated as follows.

The total width (length) of the collectors must be less than or equal to the maximum width (length) of the available land:

$$K\,H\cos\beta + (K-1)\,D - W \le 0 \tag{2.43}$$

along with

$$L_{\min} \le L \le L_{\max} \tag{2.44}$$

The distance between two adjacent collector rows (spacing) must be larger than the minimum distance specified by the relevant standards:

$$D \ge D_{\min} \tag{2.45}$$

The height of the collector above the ground may have a limitation based on the installation and maintenance requirements:

$$H\sin\beta \le Y_{h\max} \tag{2.46}$$

The collector tilt angle is required to vary in the range of 0° to 90°:

$$0^\circ \le \beta \le 90^\circ \tag{2.47}$$

The number of rows should be less than a specified maximum number, K_{max}:

$$K \le K_{\max} \tag{2.48}$$

The dimensions of the solar collector are bounded as:

$$b_1 \leq \frac{W}{L} \leq b_2 \tag{2.49}$$

where b_1 and b_2 are constants.

The number of rows should be a positive integer:

$$K \in \{\text{Positive Integers}\} \tag{2.50}$$

The integer requirement constraint, Eq. 2.50, is handled using the following procedure:

Step1: Solve the optimization problem by treating all the design variables to be continuous. (i.e. by ignoring the constraint of Eq. (2.50)) Let the optimum solution give the number of rows , for example, as 72.2 (non integer).

Step2: Fix the number of rows at an integer value in the close neighborhood of the value found by the continuous variable optimization approach. If the optimal value of number of rows found in step1 is 72.2, we use the values of K=71, 72, 73 and 74, one at a time, successively and solve the corresponding continuous variable optimization problems (by fixing the value of K at a different integer each time).

Step3: Compare the optimum values of the objective functions obtained for different settings of the value of K. Choose the result corresponding to the best objective function and the corresponding integral number of rows used as the final (approximate) optimum solution of the problem with the constraint of Eqs. (2.50).

2.3.4 Maximization of average incident solar energy for the lowest month

In general, the incident solar energy is more in summer than in winter; however, consumers need more heat energy in winter. It is therefore necessary to consider the

maximization of incident solar energy for the lowest month as the objective function. The design variables and constraints will be same as in the case of the optimization problem formulated in section 2.2.3. The lowest incident solar energy month from the twelve month information can readily be found to evaluate the value of the objective function. Then the objective function for minimization is given by

$$f_2 = \text{- lowest incident monthly solar energy} \tag{2.51}$$

2.3.5 Minimization of cost

Another important objective function in the design of a solar collector is to minimize the cost. The design variables are same as those indicated in Eq. (2.39). The objective function (cost) to be minimized can be expressed as:

$$f_3 = Cost = s_1 L W + s_2 L H K \tag{2.52}$$

where s_1 is the unit cost of the land and s_2 is the unit cost of the collector. Note that additional cost components such as those associated with piping, heat exchanger, pump backup energy system as well as maintainess cost could be added to the objective function if necessary.

The following additional constraints are considered while minimizing f_3.

The daily average incident solar energy in any month should be at least 60% of the daily optimum value found in the case of the problem described in section 2.3.3:

$$Q - 60\% \times H L[q_b + q_d + (K-1)(q_b^{sh} + q_d^{sh})] \le 0 \tag{2.53}$$

The average incident solar energy for the lowest month should be at least 60% of the daily optimum value found in the case of the problem describe in section 2.3.4:

$$Q_{\min} - 60\% \times H\,L[q_b + q_d + (K-1)(q_b^{sh} + q_d^{sh})]_{\min} \leq 0 \qquad (2.54)$$

2.3.6 Uncertainty of parameters

As stated earlier, the design variables, H, L, D and β are random due to the manufacturing tolerances used during production / construction of flat plate solar collectors. The altitude varies with different cities. Even within a city, different locations may have different altitudes. For example, the solar panels installed near a beach and on the roof of a skyscraper will correspond to different altitudes. Thus it becomes necessary to treat the altitude as a random variable. The solar constant (G_{sc}) denotes the amount of Sun's incoming radiation per unit area, measured on the outer surface of Earth's atmosphere in a plane perpendicular to the rays. The solar constant includes all types of solar radiation, not just the visible light. In 1884, Langley attempted to estimate the solar constant from Mount Whitney in California. By taking readings at different times of the day, he attempted to remove the effects due to atmospheric absorption. However, the value he obtained, 2903 W/m², was found to be too large. Between 1902 and 1957, measurements by Abbot and others at various high-altitude sites found the value of the solar constant to lie between 1322 and 1465 W/m². Abbot proved that one of Langley's corrections was erroneously applied. His results estimated the value of the solar constant to lie between 1318 and 1548 W/m², a variation that appeared to be due to the Sun's and not the Earth's atmosphere. At present, the value of the solar constant, as measured by satellites, is found to be roughly 1367 watts per square meter (W/m²), although the value fluctuates by about

6.9% during the year (from 1412 W/m² in early January to 1321 W/m² in early July) due to the variations in the distance between Earth and Sun. In fact, the value of the solar constant was found to vary by few parts per thousand from day to day (Frohlich, 2006). Thus the solar constant is considered to be a random variable.

Instead of computing the incident solar energy for each day of the month and then finding the average, a typical day of each month is chosen in this work in order to reduce the computational effort during optimization. Klein (1977) used both numerical and experimental methods to find a typical day which would represent the average radiation of each month as indicated in Table 2-1.

Table 2-2 Recommended Average Days of Months

Jan.	Feb.	Mar.	Apr.	May	Jun.
17	16	16	15	15	11
Jul.	Aug.	Sep.	Oct.	Nov.	Dec.
17	16	15	15	14	10

In this work, the fifteenth day of each month (the mean value of the average days indicated in Table 1) as the typical day for calculating value of the incident solar energy per day in any month, with 1% ~ 5% of the mean value chosen as the standard deviation of the incident solar energy in the formulation of the probabilistic optimization problem.

The conversion of probabilistic objective and constraint functions to equivalent deterministic form requires the partial derivatives of f and g_j with respect to the random variables y_k (k = 1, 2, …, N) as indicated in Eqs. (2.29) and (2.38). These derivatives are computed numerically using a finite difference scheme in this work.

2.4 Formulation of the multi-objective optimization problem

The problem of multi-objective optimization of the solar collector design can be stated in the following form:

Minimize the objective functions (A maximization problem can be converted into a minimization problem, simply by changing the sign of the objective function):

$$f_1(\vec{X}), f_2(\vec{X}),..., f_k(\vec{X}) \tag{2.55}$$

with respect to the design vector

$$\vec{X} = \{x_1 \quad x_2 \quad ... \quad x_l\}^T \tag{2.56}$$

subject to the constrains

$$g_j(\vec{X}) = 0, j = 1,2,...m \tag{2.57}$$

$$h_j(\vec{X}) \le 0, j = 1,2,...n \tag{2.58}$$

$$a_k \le x_k \le b_k, k = 1,2,...,l \tag{2.59}$$

In this work, the multi-objective problem stated in Eqs.(2.55)-(2.59) is solved using a modified game theory approach. A game is defined by the actions of a set of players who act according to their own strategies to maximize their individual gains. If the players act independently without cooperating with each other, the game is called a non-cooperative game and the resulting solution is called a Nash Equilibrium Solution (NES) [Nash, 1953]. The Nash equilibrium is a solution concept of a game involving two or more

players, in which each player is assumed to know the equilibrium strategies of the other players, and no player has anything to gain by changing only his or her own strategy. If each player has chosen a strategy and no player can benefit by changing his or her strategy while the other players keep their unchanged, then the current set of strategy choices and the corresponding payoffs constitute a Nash equilibrium.

If the players cooperate with each other, all of them could reach an eventual outcome that is better than the NES. The measure of success of a cooperative play is embodied in the concept of pareto-optimality, which involves a single objective function formed by a convex combination of the various objective functions. The effect of a cooperative game is represented by a typical pareto-optimal solution (POS).

2.4.1 Game theory approach

The concept of game theory can be illustrated with reference to a two objective, two design variable optimization problem whose graphical representation is shown in Figure 2-3. Let $f_1(x_1, x_2)$ and $f_2(x_1, x_2)$ represent two scalar objectives and x_1 and x_2 two scalar design variables. It is assumed that one player is associated with each objective. The first player wants to select a design variable x_1, which will minimize his/her objective f_1 and similarly the second player seeks a variable x_2, which will minimize his/her own objective f_2. If f_1 and f_2 are continuous, then the contours of constant values of f_1 and f_2 appear as shown in Figure 3. The dotted lines passing through O_1 and O_2 represent the loci of rational (minimizing) choices for the first and second players for fixed values of x_2 and x_1, respectively. The intersection of these two lines, if it exists, is a candidate for the two objective minimization problem assuming that the players do not cooperate with each

other (non- cooperative game). In Figure 2-3, the point N (x_1^*, x_2^*) represents such a point. This point, known as a Nash equilibrium solution, represents a stable equilibrium condition in the sense that no player can deviate unilaterally from this point for further improvement of his own objective. This point has the characteristic that

$$f_1(x_1^*, x_2^*) \le f_1(x_1, x_2^*) \tag{2.60}$$

and

$$f_1(x_1^*, x_2^*) \le f_1(x_1^*, x_2) \tag{2.61}$$

where x_1 may be to the left or right of x_1^* in Eq. (2.60) and x_2 may lie above or below x_2^* in Eq. (2.61). Extension of the idea to a k-player non-cooperative game gives the mathematical definition of a Nash equilibrium solution as [Rao and Hati, 1979, 1986]

$$\begin{aligned} &f_1(x_1^*, x_2^*, ..., x_k^*) \le f_1(x_1, x_2^*, ..., x_k^*) \\ &f_2(x_1^*, x_2^*, ..., x_k^*) \le f_1(x_1^*, x_2, ..., x_k^*) \\ &\quad . \\ &\quad . \\ &\quad . \\ &f_k(x_1^*, x_2^*, ..., x_k^*) \le f_k(x_1^*, x_2^*, ..., x) \end{aligned} \tag{2.62}$$

So far it has been assumed that there exists only one Nash equilibrium point, i.e. the dotted lines in Figure 2-3 intersect only at one point. An interesting situation occurs when the two lines intersect at more than one point. In this case, since the values of f_1 and f_2 are different at different Nash equilibrium points, any player can have the advantage of declaring his/her move first thereby forcing the other player(s) to play at the equilibrium point of his/her own choice.

In a cooperative game, the two players agree to cooperate with each other and hence any point in the shaded region S of Figure 2-3 will provide both of them with a better solution than their respective Nash equilibrium solutions. Since the region S does not provide a unique solution, the concept of Pareto-optimal (non-inferior) solutions can be introduced to eliminate many solutions from the region S. It can be seen that all points in the region S can be eliminated except those on the continuous line $O_1ACQDBO_2$ which represents the loci of tangent points between the contours of f_1 and f_2. Every point on this line has the property that it is not dominated by any other point in its neighborhood, i.e.

$$f_1(Q) \leq f_1(P) \tag{2.63}$$

and

$$f_2(Q) \leq f_2(P) \tag{2.64}$$

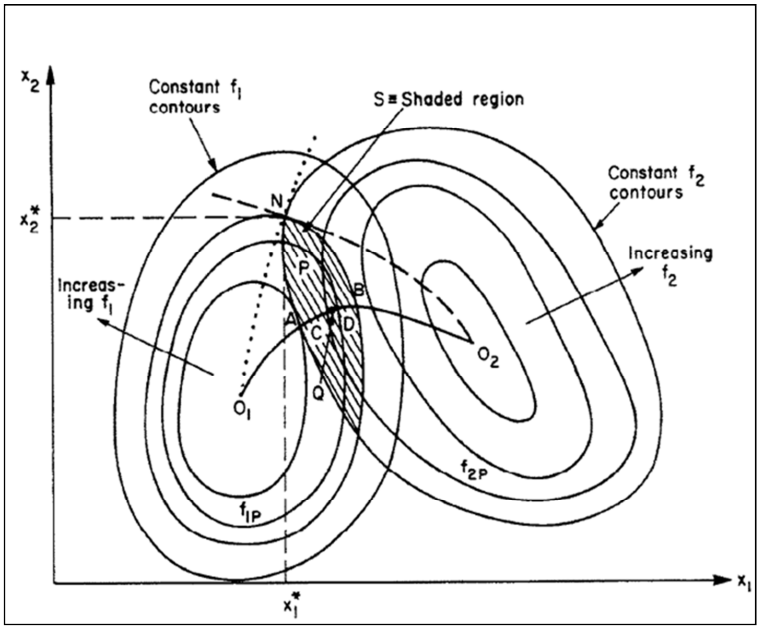

Figure 2-3 Cooperative and non-cooperative game solutions

where Q is a point lying on the line O_1O_2 and P is a neighboring point. Thus all points of S that do not lie on the line O_1O_2 need not be considered during cooperative play. The set of all points lying on AB is known as a Pareto-optimal set and is denoted by S_p. Since S_p represents the solution set to be considered in a cooperative game, the main task in a multi-criteria optimization problem is to determine the solution set S_p.

After determining the Pareto-optimal set, one has to pick up a particular element from the set by adopting a systematic procedure. If it is possible to convert all the criteria involved in the problem to some common units, then the problem will be greatly simplified. If this is not possible, further rules of negotiation in the form of a supercriterion or bargaining model should be specified before selecting a particular element from the set S_p. A procedure for finding the set S_p, and an element of S_p, based on a supercriterion, similar to the one considered by Rao and Freiheit [1991], is presented in the following section.

2.4.2 Computational procedure

The cooperative game theory approach of solving the multi-criteria optimization problem (MCOP) can be described as follows. The k objective functions are assumed to correspond to k players, each player representing one objective function. When playing the game, each player tries to develop his/her own strategy. The players will start bargaining from their respective reference (a point in the feasible space) values and put a joint effort in maximizing a subjective criterion (supercriterion) formed by themselves. It is assumed that each player has considered his/her own criterion before starting the game to find the maximum possible benefit he/she could achieve. This will also help him/her guarantee against the worst value. This analysis is necessary since each player should

know the extreme values of his/her own and others so that none of them begin to bargain from a reference value which is unrealistic. The following computational procedure has been used to implement the cooperative game theory.

(1) Normalize the objectives so that no objective due to its magnitude will be favored. The following normalization procedure gives zero as optimum value and one as the worst value of ith objective function:

$$f_{ni}(X) = \frac{f_i(X) - f_i(X_i^*)}{F_{iu} - f_i(X_i^*)} \tag{2.65}$$

where F_{iu} is the worst value, and $f_i(X_i^*)$ is the optimum value of the ith objective.

(2) Formulate a supercriterion S as the product of deviations of all objective functions from their respective worst values:

$$S = \prod_{j=1}^{k} \{1 - f_{ni}(X)\} \tag{2.66}$$

(3) Formulate a Pareto optimal objective FC using a weighted sum method as:

$$FC = \sum_{i=1}^{n} c_i f_{ni}(X) \tag{2.67}$$

where the sum of the weights c_i is equal to one.

(4) Since FC has to be minimized and S has to be maximized, a new objective is constructed as (for minimization):

$$\text{OBJ} = \text{FC} - \text{S} \tag{2.68}$$

subject to all the constraints. The minimization of OBJ gives the compromise Pareto optimal solution of the multi-objective optimization problem.

2.5 Illustrative examples and numerical results

Numerical examples are considered to illustrate the game theory approach for the multi-objective optimum design of stationary flat plate collectors using both the deterministic and probabilistic approach. The following data are assumed:

L_{min} = 15m, L_{max} = 30m, H_{min} = 0.5m, H_{max} = 2m, W_{min} = 15m, W_{max} = 30m, $Y_{h\,max}$ = 2m, D_{min} = 0.8m, β_{min} = 50, β_{max} = 200, K_{min} = 50, K_{max} = 200, s_1 = 100 \$/m^2, s_2 = 100 \$/m^2.

The solar collector is assumed to be installed in a specific location, Miami (USA), where the latitude is 25.4°N and the altitude is 5m, and the solar collector is assumed to face the equator (south). The starting design vector is chosen as:

$$\vec{X}_0 = \begin{Bmatrix} H \\ L \\ D \\ \beta \\ K \end{Bmatrix} = \begin{Bmatrix} 1.5 \\ 27 \\ 0.9 \\ 40 \\ 80 \end{Bmatrix}$$

2.5.1 Deterministic optimization

1. Deterministic optimization result

For comparison, the single-objective and multi-objective optimization problem are solved using a deterministic approach. The initial design and the results of deterministic optimization are shown in Table 2-3 and 2-4(a) – (c). It can be seen that the height of the

collector (H) reached its upper bound in all single as well as multi-objective optimizations. The length of the collector (L) attained its upper bound and the distance between the collector rows (D) attained its lower bound in the case of minimizations of f_1, f_2 and multi-objective optimization. The relative weights of the objective functions f_1, f_2 and f_3 at the compromise solution achieved by the game theory are 0.8, 0.1 and 0.1, respectively. This indicates that the first objective function (annual solar energy) dominates the compromise solution as per the supercriterion used. The multi-objective (compromise) solution corresponds to a value of f_1 that is 0.17% worse than the best value and 63.14% better than the worst possible value, a value of f_2 that is 1.52% worse than the best value and 60.34% better than the worst possible value, and a value of f_3 that is 62.38% worse than the best value and 12.00% better than the worst possible value.

Table 2-3 Initial Design and deterministic single objective optimization results

Parameter	H	L	D	β	K	f_1	f_2	f_3
Unit	m	m	m	Deg	#	10^6×W	10^6×W	10^6×$
Initial	1.8	27	0.9	40	80	-1.057	-0.8942	0.8786
Min f1	2	30	0.8	35.3602	83	-1.3689	-1.1004	1.0956
Min f2	2	30	0.8	53.4313	101	-1.3407	-1.1135	1.2049
Min f3	2	21.6629	0.8543	30	67	-0.8376	-0.6839	0.6625

Table 2-4(a) Initial design and deterministic multi-objective optimization result

Parameter	H	L	D	β	K
Unit	m	m	m	Deg	#
Initial design	1.8	27	0.9	40	80
Multi-objective optimization	2	30	0.8	30	79

Table 2-4(b) Initial design and deterministic multi-objective optimization results (weights of each single objective functions)

Weights of objectives	c_1	c_2	c_3
Initial Design	0.3333	0.3333	0.3334
Multi-objective optimization	0.8	0.1	0.1

Table 2-4(c) Initial design and determinist multi-objective optimization results (objective function values)

Item	f_1 w/o standard deviation	f_2 w/o standard deviation	f_3 w/o standard deviation	FC	S	Obj (FC-S)
Unit	10^6×W	10^6×W	10^6×$	-	-	-
Initial Design	-1.057	-0.8942	0.8786	0.4986	0.1216	0.377
Multi-objective optimum	-1.3665	-1.0966	1.0758	0.0837	0.2276	-0.1439

2. Sensitivity analysis with respect to the design valuables: Numerical results

The effect of the five inputs (design valuables) on the performance of the flat plate solar collector, in terms of the three objective functions considered, is investigated in this section. The multi-objective optimum design (shown in Table 2-4(c)) is considered as the reference design and each of the design variables is changed by ±20% (one at a time) about its corresponding optimum value while keeping the values of the remaining design variables at their respective optimum values. The values of the three objective functions - average incident solar energy, average incident solar energy for the lowest month and the cost - are computed at different settings of the perturbed design variable (in the range ±20%). The variations of the composite objective function (or supercriterion) with charges in the design variables are also found. The results are shown in Figures 4-8. As expected, the objectives f_1, f_2 and f_3 have conflicting nature. Figures 2-4, 2-5, 2-6 and 2-8

indicate that $f_1$and f_2 are positively correlated to the design valuables H, L, D and K but f_3 is negatively correlated to these variables. Figure 2-7 denotes that $f_1$and f_2 are negatively correlated to the design variables, H, L, D and K while f_3 is positively correlated to these variables. All these figures show that the supercriterion decreases for any change in the design variables, unless, possibly, there is a constraint violation at a perturbed value of any of the design variable(s). It can also be seen, from Figs 4-8, that the three objectives vary by different amounts for any specific variation in any of the design variables. The variations in the objective functions can be seen to be almost linear with respective to variations in any of the five design variables H, L, D, β and K. In particular, the design variables H, L and K have greater influence on the three objectives compared to the other two design variables, D and β. This indicates that the solar collector parameters - height, length and number of rows - have more influence than the installation factors - tilt angle and the distance between two adjacent solar collectors on these objective functions. Thus both the manufacturer and customer should concentrate on improving the quality of construction of the solar collector.

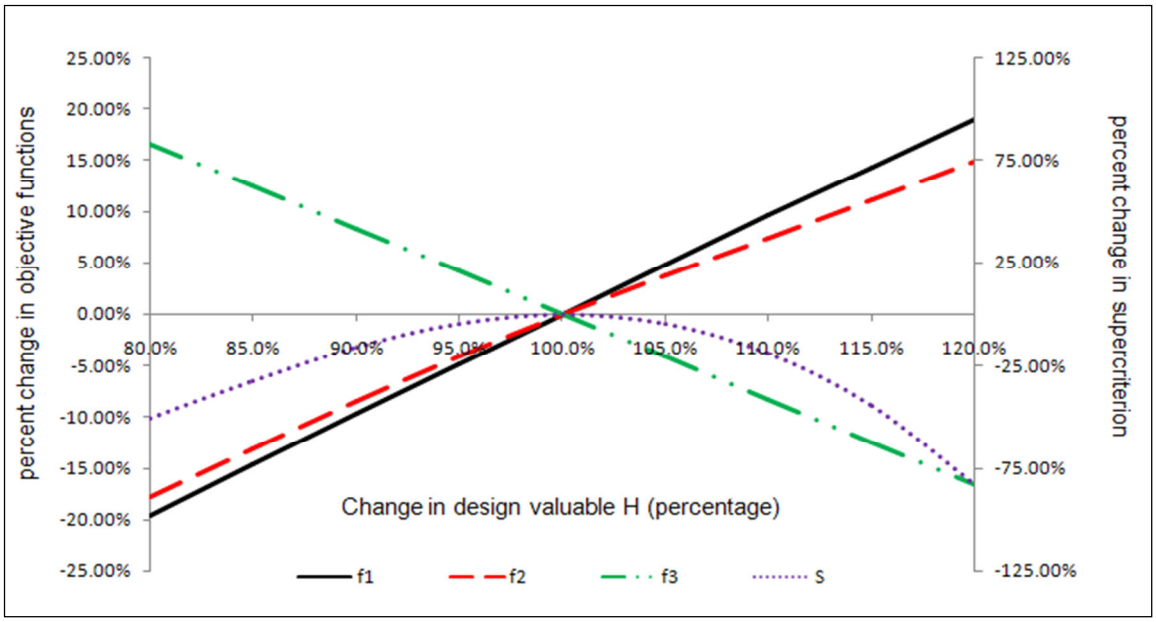

Figure 2-4 Sensitivity analysis with respect to the design valuable H

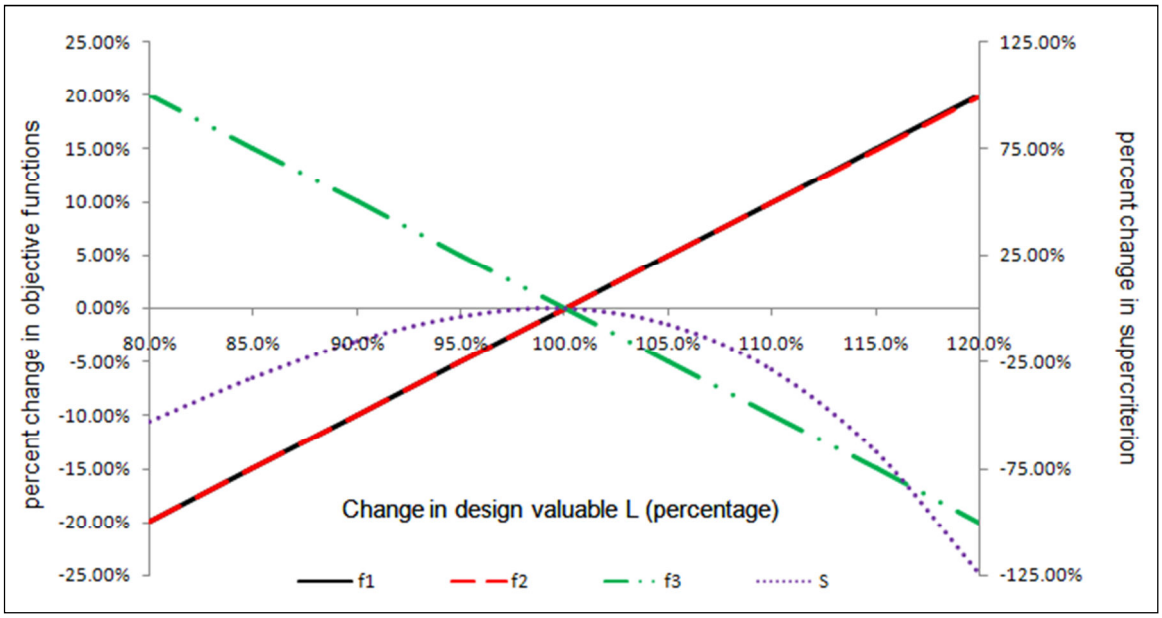

Figure 2-5 Sensitivity analysis with respect to the design valuable L

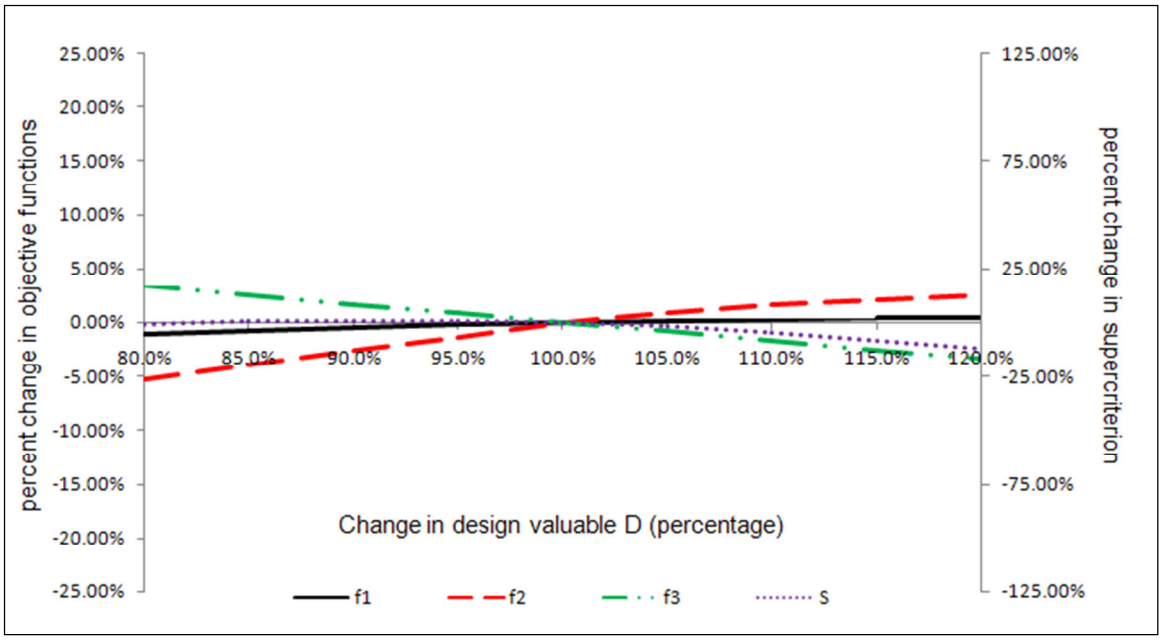

Figure 2-6 Sensitivity analysis with respect to the design valuable D

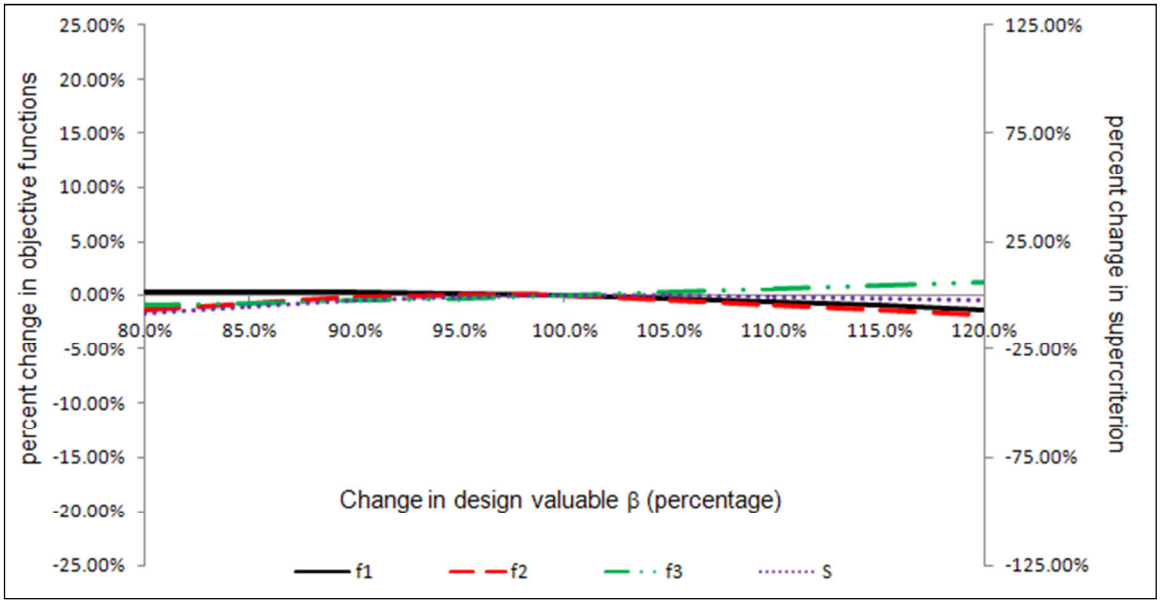

Figure 2-7 Sensitivity analysis with respect to the design valuable β

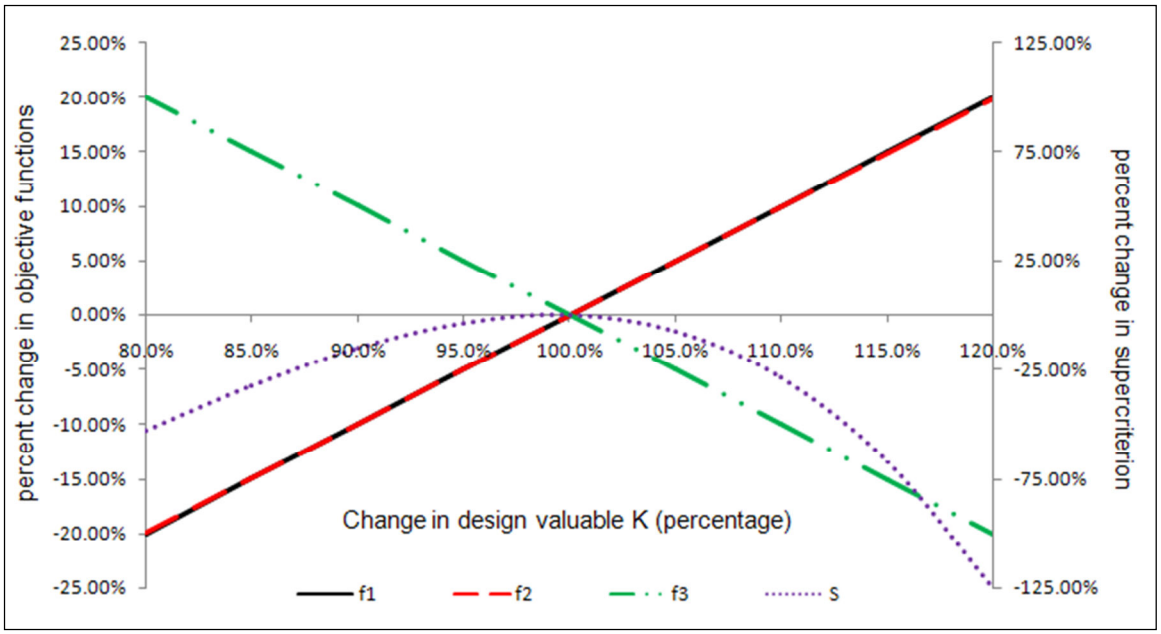

Figure 2-8 Sensitivity analysis with respect to the design valuable K

2.5.2 Probabilistic optimization

1. Single objective optimization: Minimization of $(\overline{f_1} + \sigma_{f_1})$:

Figure 2-9 (a) – (e) present the variation of the mean values of design variables at the optimum solutions found by minimizing $(\overline{f_1} + \sigma_{f_1})$ with different values of probabilities specified for constraint satisfaction. Curves corresponding to different levels of uncertainty of the random variables (coefficient of variation ranging from 1% to 5%) are also shown in the figures. As can be seen from these figures, when the probability of constraint satisfaction is 50%, all the design variables remain the same irrespective of the coefficient of variation of the random parameters. The reason is that the probabilistic approach degenerates to the determinist optimization for this case.

As the probability of constraint satisfaction increases from 50%, the constraints tend to be tighter, and hence the optimization problems become more difficult to solve. Some design variables—the distance between two neighboring rows and tilt angle—increase when the probability of constraint satisfaction increases while the remaining design variables—the height of collector, width of collector—decrease when the probability of constraint satisfaction increases. Because the number of rows is not a random variable and it can only be integral numbers, the optimum values of this design variable result in non-smooth curves as shown in Fig. 2-9(e).

It is observed that the optimum values of some design variables approach the lower (upper) bounds at 50% probability of constraint satisfaction; the optimum values tend to increase (decrease) gradually with an increase in the probability of constraint satisfaction. The reason is that with an increase in the probability of constraint satisfaction, the constraint tends to be tighter, which leads to a large deviation of the optimum values from their respective upper / lower bounds.

In all the figures, optimum values of design variables at 50% constraint satisfaction have been set as reference values (base values). It can be seen from the figures, that with an increase in the value of constraint satisfaction up to 99% (for any specified variability (constant coefficient of variation of the random parameters), the change in the optimum values of the design variables is gradual and less than or equal to about 10%, whereas at 99.99997% constraint satisfaction, the optimum values suddenly shoot to larger / higher levels. This phenomenon is especially prominent for two design variables, namely, the distance between two neighboring rows and tilt angle.

Figures 2-10 (a) – (c) present the values of the mean values of the three objective functions at the optimum solutions found by minimizing $(\overline{f_1} + \sigma_{f_1})$ at different values of constraint satisfaction with different levels of uncertainty (different values of coefficient of variation of all random variables). Similarly, Figures 9 (d) – (f) give the values of $(\overline{f_i} + \sigma_{f_i})$, (i = 1, 2, 3) at optimum solutions found by minimizing $(\overline{f_1} + \sigma_{f_1})$. It can be noticed that the curves in Figs. 2-10 (a), (b) and (c) have almost the same trends exhibited by Figs. 2-10 (d), (e) and (f), respectively. This is because the mean $\overline{f_i}$ of objective i (i = 1, 2, 3) is much greater than its standard deviation, σ_{f_i} (i = 1, 2, 3).

With an increase in the level of constraint satisfaction probability, the absolute values of the objective functions decrease because of tighter constraints. It can be seen from Figs. 2-10 (d) – (f) that with increasing values of the constraint satisfaction level up to 99% (at constant standard deviations of random variables), the change in the objective function values is gradual and is less than 20%, whereas at the 99.99997% constraint satisfaction level, the optimum values suddenly shoot to a newer levels and as a result, the objective function values lie far away from the base values. A larger value of the standard deviation of all random variables makes the absolute value of each objective function decrease rapidly.

The mean values of the objective functions, $\overline{f_1}$ and $\overline{f_2}$, vary between -10% and 50% of the baseline values and exhibit similar characteristics whereas the objective function value, $\overline{f_3}$, has a conflicting characteristic and varies between -40 and 10% of the baseline value.

2. Single objective optimization: Minimization of $(\overline{f_2} + \sigma_{f_2})$:

In this case, the minimization of $(\overline{f_2} + \sigma_{f_2})$ is carried for different values of probabilities specified for constraint satisfaction using several values of the coefficient of variation for all the random variables. It is observed that the minimizations of $(\overline{f_1} + \sigma_{f_1})$ and $(\overline{f_2} + \sigma_{f_2})$ exhibited similar behaviors. The primary reason for this behavior can be attributed to the low altitude of the specific location (Miami) used in the numerical computations. For example, the variation in the monthly average temperature between summer months and winter months is not as significant (see Table 2-5) as for locations such as Chicago.

Table 2-5 Monthly average temperature of Miami (Weather Channel, 2010)

Month	Jan	Feb	Mar	Apr	May	Jun	Jul	Aug	Sep	Oct	Nov	Dec	Ave
Average High (°F)	76	78	81	84	87	90	91	91	89	85	81	78	84
Average Low (°F)	60	61	64	68	72	75	77	76	76	72	68	62	69

As indicated in Table 2-5, the lowest temperate generally recorded in the month of January is between 60 and 76 °F. This is almost 90% of the yearly average temperature. Gong et al. (2005) presented the output in winter and the yearly average output of a photovoltaic system in Carbondale, Illinois based on different designs. The energy output in winter is only 50-70% of the yearly average energy output depending on different design. Wei et al. (2007) compared the solar radiation in two cities of China, Kunming (latitude 25.04° N) and Beijing (latitude 39.55°N). They concluded that the solar collectors in Kunming have much less seasonal fluctuation in yearly energy output compared to those in Beijing. Since the winter period for the cities like Chicago or Beijing, is relatively long, designers should consider to add maximization of the incident

solar energy for the whole winter time as one objective function instead of only the lowest month. The present approach and methodology can be applied to any location using the corresponding solar data.

3. Single objective optimization: Minimization of $(\overline{f_3} + \sigma_{f_3})$:

Figures 2-11 (a) – (e) present the mean values of design variables at the optimum solutions found by minimizing f_3 with different values of probabilities specified for constraint satisfaction. The minimization of $\overline{f_3} + \sigma_{f_3}$ has been carried by varying the probability level of constraint satisfaction for different values of the coefficient of variation of the random parameters. The results of this study exhibited some features similar to those found in the case of minimizations of $(\overline{f_1} + \sigma_{f_1})$ and $(\overline{f_2} + \sigma_{f_2})$. For example, when the probability of constraint satisfaction is 50%, all the design variables remain the same as the determinist optimum solution irrespective of standard deviation values of the design variables.

The number of cases in which the optimum solutions are found is lesser in this case compared to the previous two cases because of the two extra constraints, Eq. (53) – (54), added in this case. When the standard deviation assumed for the random variables is only 1% and 2%, the optimum solutions are found for all levels of probabilities of constraint satisfaction. But when the standard deviation assumed for all the random variables goes up to 3% and then 4%, no feasible solution can be found when the probability of constraint satisfaction is 99.99997%. When the standard deviation assumed for all the random variables further increases to 5%, optimum solution could only be found when the probability of constraint satisfaction is less than or equal to 95%.

It is found that the design variables—the width of the collector, tilt angle and number of rows—increased by up to nearly 30%, 30% and 10%, respectively, with an increase of the probability of constraint satisfaction while the design variable, height of collector, decreased up to nearly 10% with an increase of the probability of constraint satisfaction. The design variable, distance between two neighboring rows, has experienced nearly ±4% fluctuation about the base value.

Figures 2-12 (a) – (c) present the values of $\overline{f_i}$ (i = 1, 2, 3) at the optimum solution found by minimization of $(\overline{f_3} + \sigma_{f_3})$ for different values of probability of constraint satisfaction at different values for the coefficient of variation of the random variables. Figures 2-12 (d) – (f) present the corresponding values of $(\overline{f_i} + \sigma_{f_i})$ (i = 1, 2, 3). It has been observed that the curves in Figs.2-12 (a), (b) and (c) and those in Figs.2-12 (d), (e) and (f) exhibit similar trends. This is because the mean value is very high compared to the standard deviation for any objective function i.

When the probability of constraint satisfaction is 50%, all the values of $\overline{f_i}$, (i = 1, 2, 3), remain the same irrespective of the standard deviation of the design variables as shown in Figs. 2-12 (a) to (c). However, in Figs. 2-12 (d) to (f), at any particular value of constraint satisfaction including 50%, curves corresponding to different values of the standard deviations of the random variables lead to different values of σ_{f_i}, (i = 1, 2, 3) with larger standard deviations resulting in larger values.

With increasing values of probability of constraint satisfaction, the absolute values of the objective functions increase because of tighter constraints. Larger values of standard

deviation of the random variables result in a rapid increase in the absolute values of each of the objectives.

The mean values of the objective functions, $\overline{f_1}$ and $\overline{f_2}$, vary between -40% and 0% of the respective baseline values and exhibit similar nature whereas the value of $\overline{f_3}$, is conflicting and varies between 0 and 40% of the baseline value.

4. Multi-objective optimization using game theory:

The results of multi-objective optimization (using game theory) obtained with the coefficient of variation of the random variables varying from 1% to 5% are given in Table 2-6 and with the probability of constraint satisfaction varying from 50% to 99.99997% are given in Table 2-7. It is observed that with a coefficient of variation of random variables equal to 1%, the optimum values of design variables D (distance between two neighboring rows of collectors) attained its lower bound value and the design variables H (height of collector) and L (length of solar collector) attained their upper bound values when the probability of constraint satisfaction is 50%. As the probability of constraint satisfaction increased from 50% to 99.99997%, the optimum values of these design variables deviated gradually from their respective bounds. The optimum value of the tilt angle of the collector (the design variable β) increased gradually from 30º to 34º and the optimum number of rows of collectors (the design variable K) essentially remained constant at 79 as the probability of constraint satisfaction increased from 50% to 95% and slightly fluctuated from 77 to 80 as the probability of constraint satisfaction increased to 99% and finally to 99.99997%.

The annual average incident solar energy decreased from 1.3665×10^6 W to 1.1931×10^6 W and the average incident solar energy for the lowest month also decreased from 1.0966×10^6 W to 1.0013×10^6 W and the cost of the solar collector decreased from \$ 1.0758×10^6 to \$ 0.9694×10^6 as the probability of constraint satisfaction increased from 50% to 99.99997%. The maximum value of game theory objective, - (FC - S), also decreased from 0.1402 to 0.0903 as the probability of constraint satisfaction varied from 50% to 99.99997%.

Figures 2-13 (a) - (e) present the mean values of design variables at the optimum solution of the multi-objective optimization problem found for different values of probabilities specified for constraint satisfaction with different values of the coefficient of variation specified for all the random variables. As shown in these figures, when the probability of constraint satisfaction is 50%, as expected, all the design variables remain the same irrespective of standard deviation values of these design variables. Not only that, the probabilistic optimum solution is same as that of the deterministic optimum solution.

Since game theory approach uses the results of single objective optimizations, it cannot be used for cases in which any of the single objective optimization problems result in infeasible designs. In the present case, the minimization of f_3 considers additional constraints and hence yields the least optimum value. Thus the number of multi-objective optimization problems solved (for different cases) is same as the number of different cases that have feasible solutions during the minimization of f_3. It is found that the distance between two neighboring rows and the tilt angle increased up to 18% and 30%, respectively, while the remaining design variables—the height of collector, width of collector—decreased up to 10% when the probability of constraint satisfaction increased

from 50% to 99.99997%. The number of rows, as the only one design variable that is not random variable, has a small fluctuation (±2.6%) when the probability of constraint satisfaction increased from 50% to 99.99997%.

An observation on the variation of the weights (c_1, c_2, c_3) used in the Pareto optimal solutions indicated that f_1 is dominant in the multi-objective optimization problems that the probability of constraint satisfaction is less than or equal to 95%. In these cases, the weight of the objective function of f_1 is found to gradually drop from 80% to 65% with an increase in either the standard deviation of the random variables or the probability of constraint satisfaction. The weights of the second and third objective function are found to be slightly increased from 10% to 15%. When the probability of constraint satisfaction increases to 99%, the weight of the second objective function suddenly increase to a higher level, around 20-40%, and when the probability of constraint satisfaction finally increases to 99.99997%, it shoot to almost 80%. The weight of the third objective function never dominates in any case of the Pareto optimal solution.

Figures 2-14 (a) – (c) present the values of $\overline{f_i}$, (i = 1, 2, 3) achieved as a result of multi-objective optimization under probabilistic uncertainty. Figures 2-14 (d) – (f) give the values of $(\overline{f_i} + \sigma_{f_i})$, (i = 1, 2, 3) at the optimum solutions obtained by multi-objective optimization. It can be noticed that the two sets of curves [Figs. 2-14 (d), (e) and (f), and Figs. 2-14 (a), (b) and (c)] exhibit similar trends. The reason is that the mean value is much larger than the standard deviation for each objective function.

As expected, in Figs. 2-14 (a) – (c), when the probability of constraint satisfaction is 50%, the values of $\overline{f_i}$ remain the same irrespective of the standard deviation values of the

design variables for any i (i = 1, 2, 3). However, in Figs. 2-14 (d) to (f), when the probability of satisfaction is 50%, different objective functions have different standard deviations and hence the curves start at different points on the vertical axis. Although a 50% constraint satisfaction with relatively larger standard deviation can result in superior energy output, it may not be suitable for practical applications. With an increase in the probability of constraint satisfaction, the absolute values of the objective functions decrease because of tighter constraints. The values of $\overline{f_1}$ and $\overline{f_2}$ vary between -10% and 20% of the baseline values and exhibit similar variations whereas the value of $\overline{f_3}$ varies between -20 and 10% of the baseline.

Table 2-6 Effect of Variability (C.V.) on Multi-objective Optimization (Probability of constraint satisfaction: 95%)

c.v. of uncertain parameters	Optimal design parameters (mean values)					Optimal objective function (FC-S), at $\overrightarrow{X^*}$	value† of $\vec{f} = \begin{Bmatrix} \overline{f_1} \\ \overline{f_2} \\ \overline{f_3} \end{Bmatrix}$ at $\overrightarrow{X^*}$
	H (m)	L (m)	D (m)	β (deg)	K		
0.01	1.9676	29.5145	0.8134	31.3127	79	-0.1264	$\begin{Bmatrix} -1.3184 \\ -1.0649 \\ 1.0444 \end{Bmatrix}$
0.02	1.9363	29.0444	0.8272	32.6980	80	-0.1107	$\begin{Bmatrix} -1.2720 \\ -1.0346 \\ 1.0145 \end{Bmatrix}$
0.03	1.9059	28.5891	0.8415	34.1617	80	-0.0998	$\begin{Bmatrix} -1.2272 \\ -1.0055 \\ 0.9861 \end{Bmatrix}$
0.04	1.8765	28.1479	0.8563	35.7100	80	-0.0489	$\begin{Bmatrix} -1.1836 \\ -0.9774 \\ 0.9589 \end{Bmatrix}$
0.05	1.8480	27.7200	0.8717	37.3499	81	-0.0034	$\begin{Bmatrix} -1.1412 \\ -0.9503 \\ 0.9331 \end{Bmatrix}$

†: Units: 10^6 W for f_1, 10^6 W for f_2, 10^6 \$ for f_3.

Table 2-7 Variation of Constraint Satisfaction Probability on Multi-objective Optimization (Coefficient of variation of uncertain parameters: 0.01)

Probability of constraint satisfaction	Optimal design parameters (mean values)					Optimal objective function (FC-S), at $\overrightarrow{X^*}$	value† of $\vec{f} = \begin{Bmatrix} \overline{f_1} \\ \overline{f_2} \\ \overline{f_3} \end{Bmatrix}$ at $\overrightarrow{X^*}$
	H (m)	L (m)	D (m)	β (deg)	K		
0.50	2.0000	30.0000	0.8000	30.0000	79	-0.1402	$\begin{Bmatrix} -1.3665 \\ -1.0966 \\ 1.0758 \end{Bmatrix}$
0.80	1.9833	29.7492	0.8068	30.6640	79	-0.1330	$\begin{Bmatrix} -1.3416 \\ -1.0802 \\ 1.0595 \end{Bmatrix}$
0.90	1.9747	29.6203	0.8104	31.0170	79	-0.1294	$\begin{Bmatrix} -1.3289 \\ -1.0718 \\ 1.0512 \end{Bmatrix}$
0.95	1.9676	29.5145	0.8134	31.3127	79	-0.1264	$\begin{Bmatrix} -1.3184 \\ -1.0649 \\ 1.0444 \end{Bmatrix}$
0.99	1.9545	29.3172	0.8191	31.8796	80	-0.1213	$\begin{Bmatrix} -1.2989 \\ -1.0522 \\ 1.0318 \end{Bmatrix}$
0.9999997	1.9048	28.5714	0.9362	34.2212	77	-0.0903	$\begin{Bmatrix} -1.1931 \\ -1.0013 \\ 0.9694 \end{Bmatrix}$

†: Units: 10^6 W for f_1, 10^6 W for f_2, 10^6 \$ for f_3.

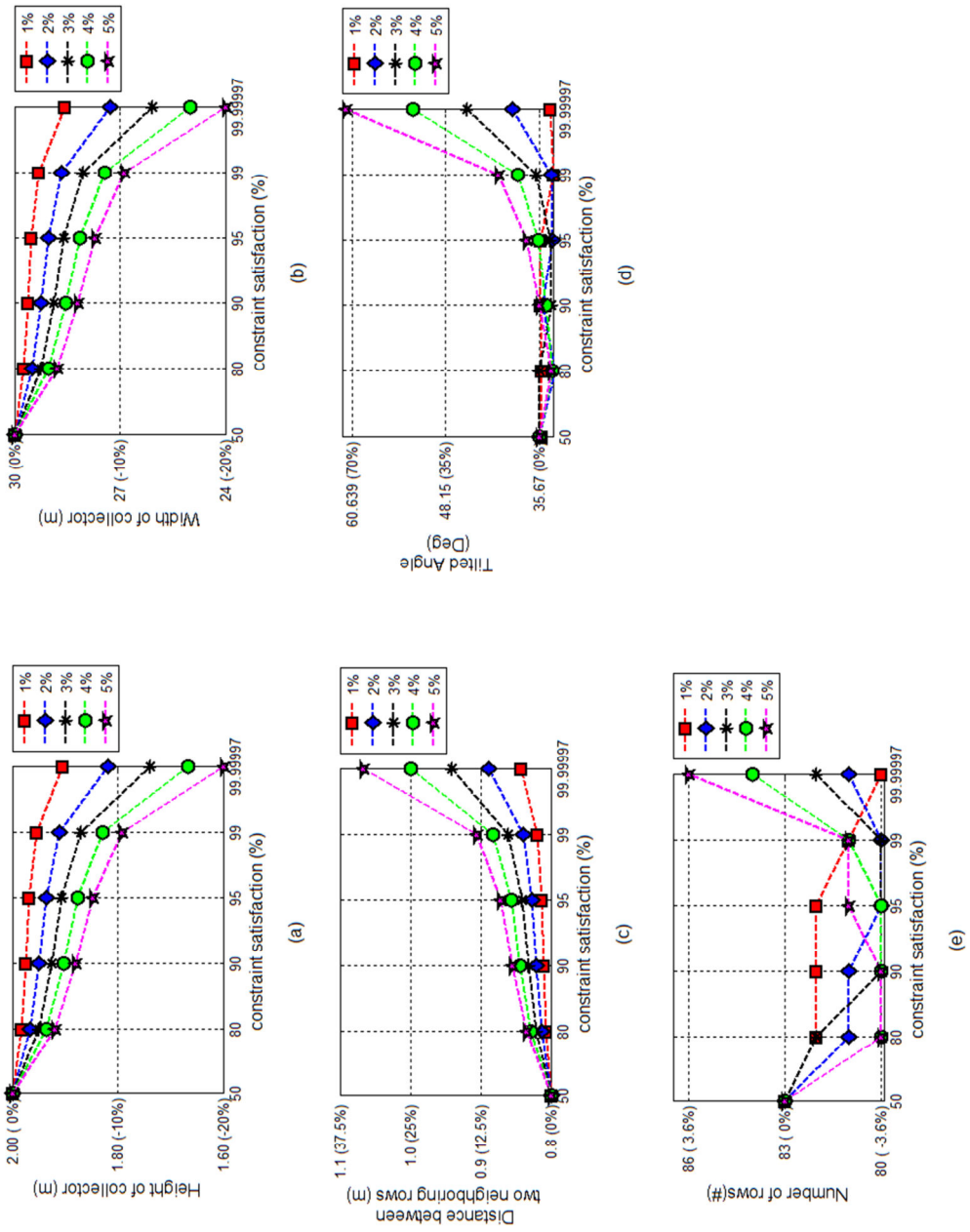

Figure 2-9 Probabilistic single objective optimization; Minimization of $\overline{f_1} + \sigma_{f_1}$; Variation of design variables

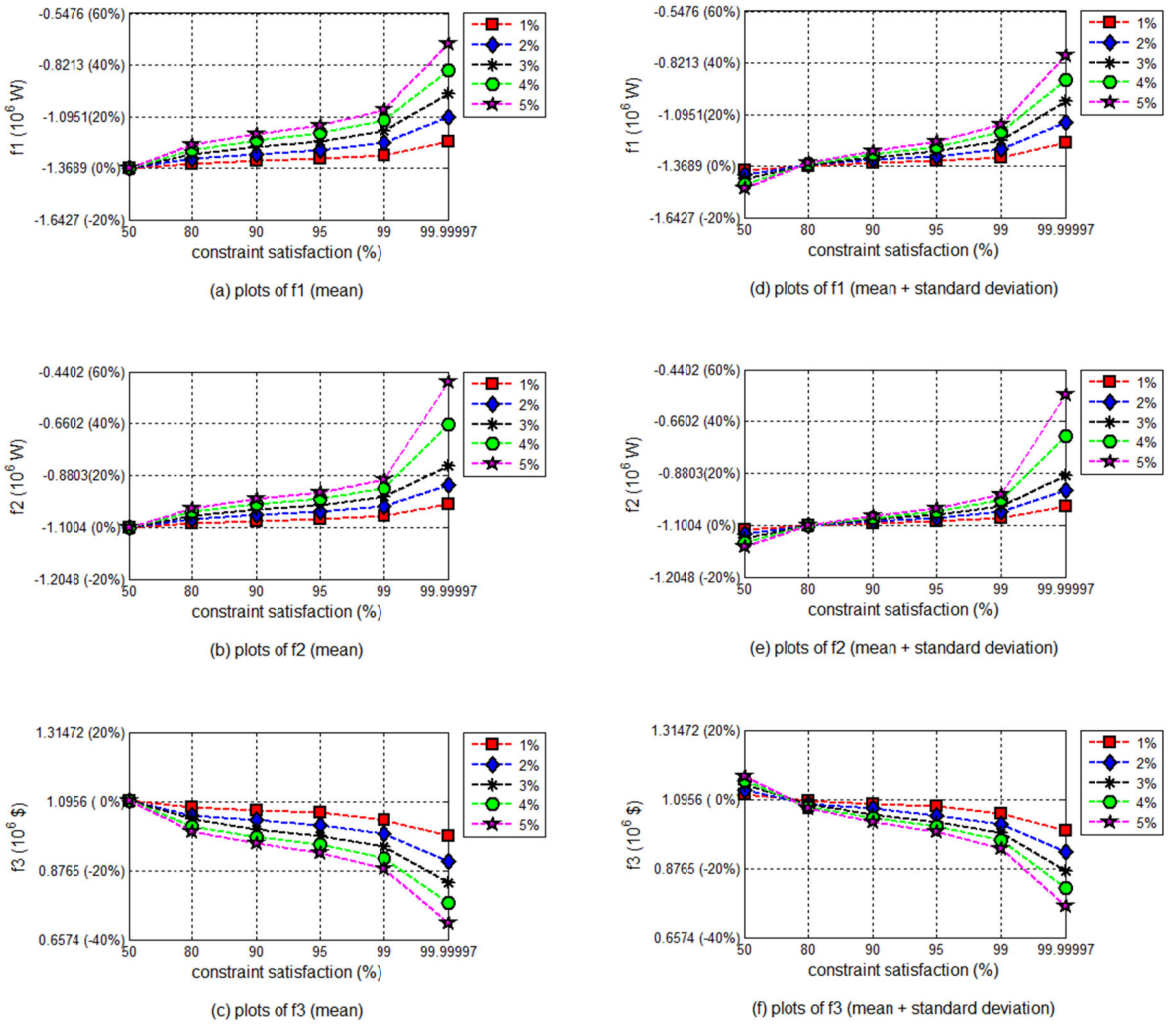

Figure 2-10 Probabilistic single objective optimization; Minimization of $\overline{f_1} + \sigma_{f_1}$; Variation of objective functions

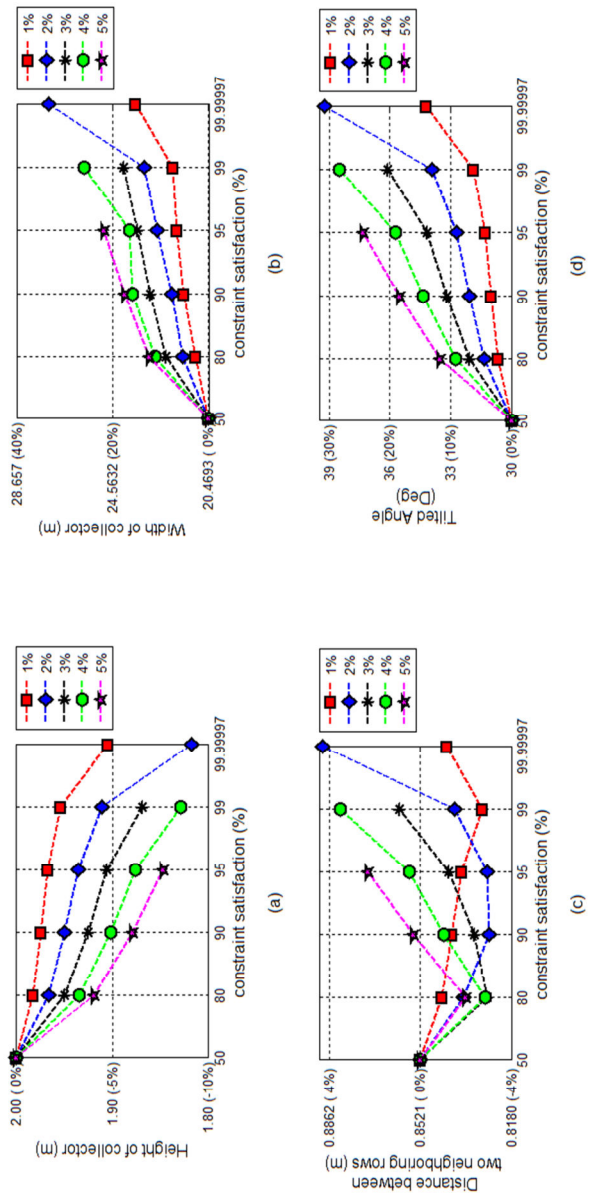

Figure 2-11 Probabilistic single objective optimization; Minimization of $\overline{f_3} + \sigma_{f_3}$; Variation of design variables

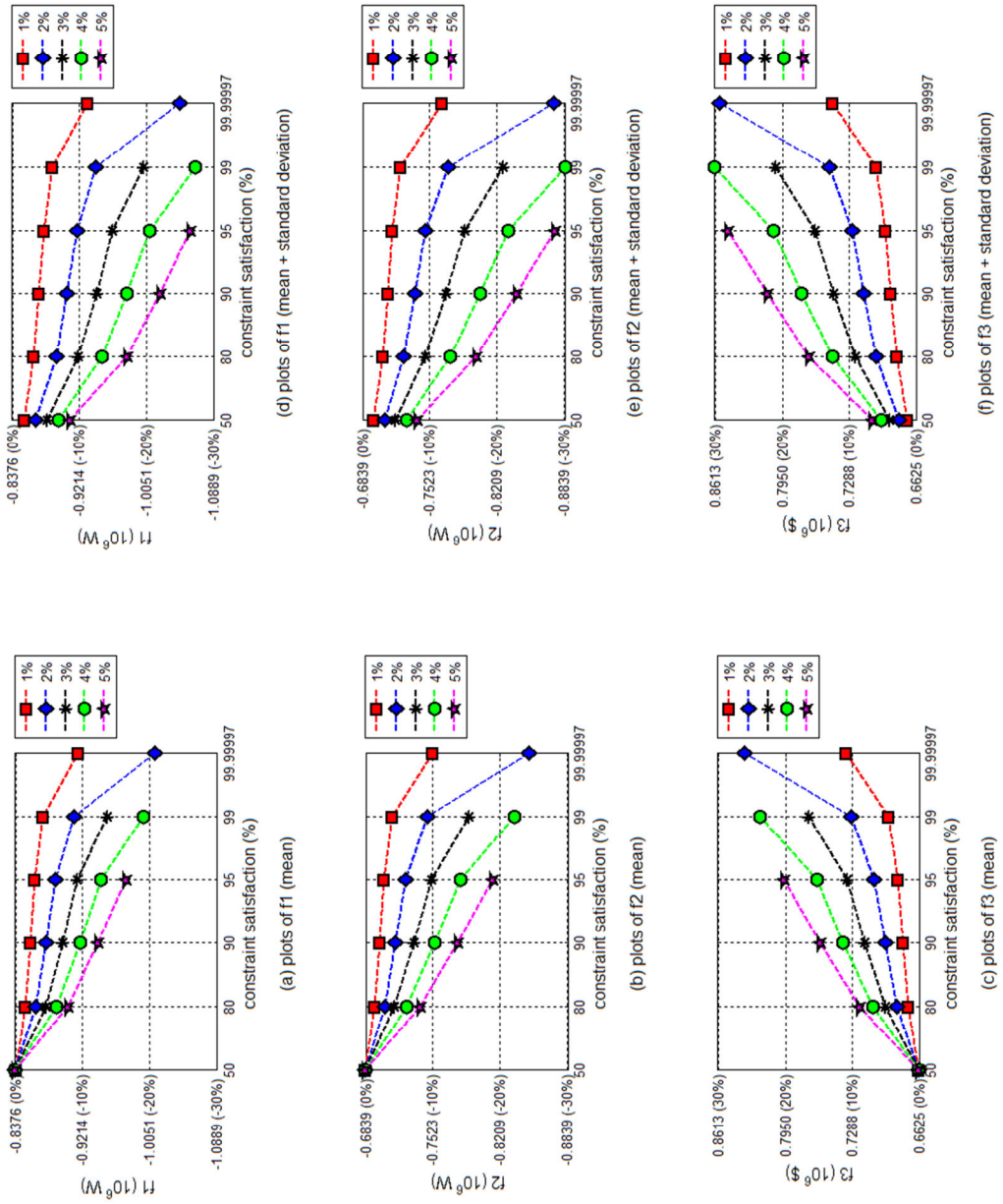

Figure 2-12 Probabilistic single objective optimization; Minimization of $\overline{f_3} + \sigma_{f_3}$; Variation of objective functions

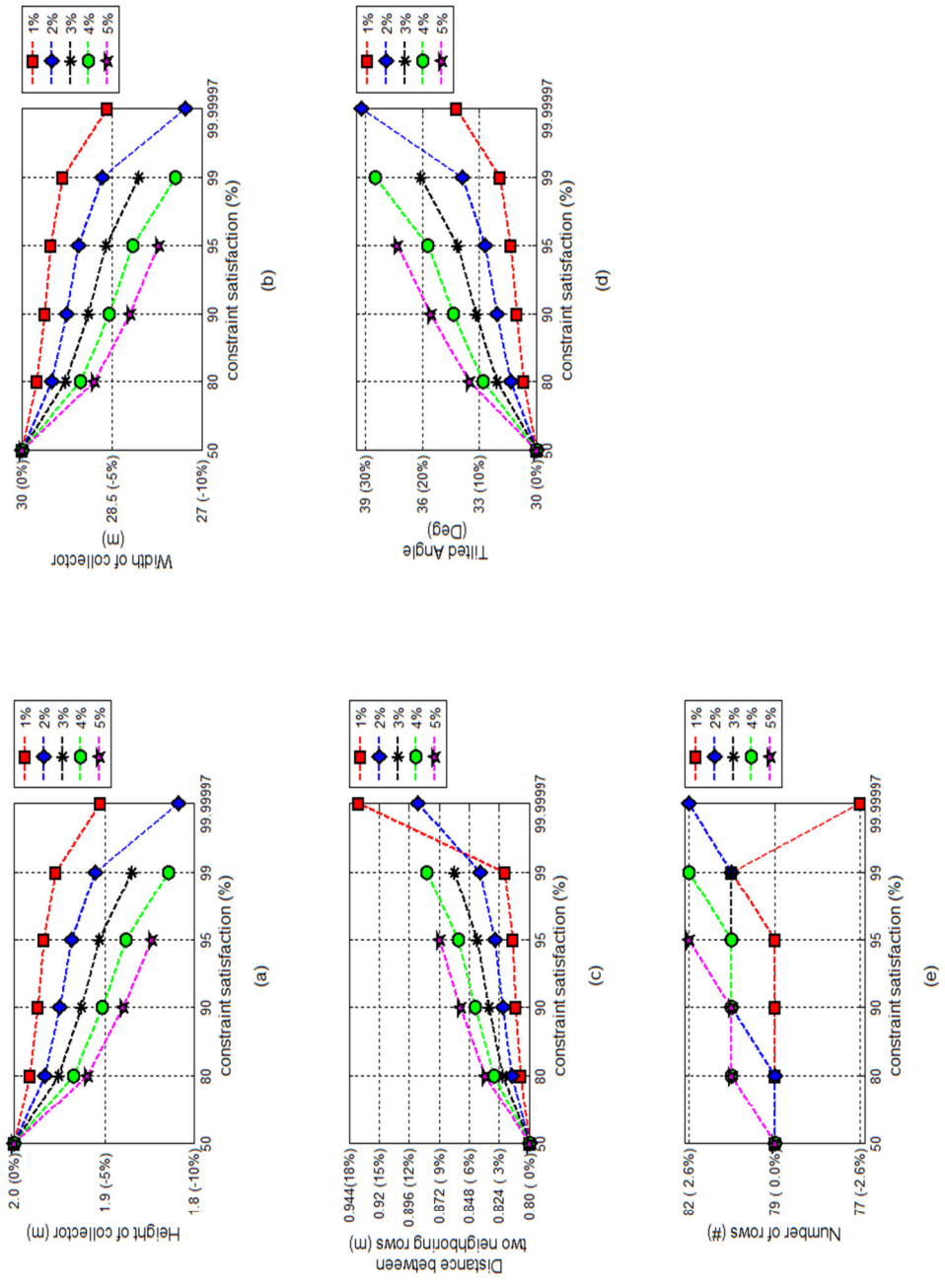

Figure 2-13 Probabilistic multi-objective optimization (Game theory); Variation of design variables

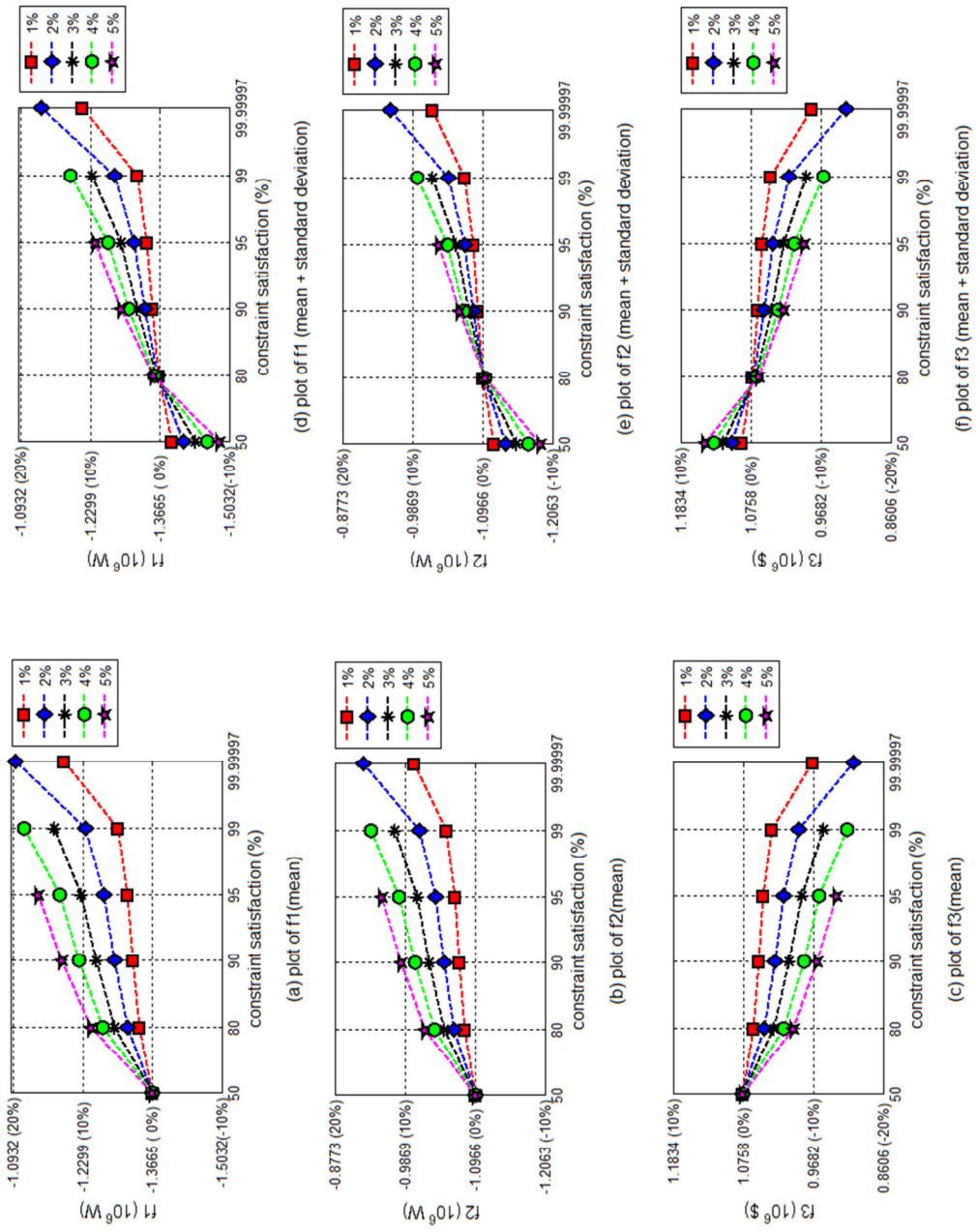

Figure 2-14 Probabilistic multi-objective optimization (Game theory); Variation of objective functions

2.6 Conclusions

The multi-objective optimum design of flat-plate solar collectors is presented with a consideration of solar radiation with shading effect. Three objectives, namely, the maximization of the annual average incident solar energy, the maximization of the lowest month incident solar energy and minimization of the cost, are considered. Most of the design variables and the altitude, solar constant and typical day of each month are treated as random variables following normal distribution. Game theory methodology with probabilistic uncertainty is used for the solution of the three objective constrained optimization problems to find a balanced solution. The solution represents the best compromise based on the terms of the super-criterion selected. Numerical results are obtained at a specific location (Miami, USA). The sensitivity analysis based on the results of deterministic approach is conducted at the optimum solution. Since the design parameters of the solar collector are subject to manufacturing and installation errors, a sensitivity study was conducted to find the influence of the design variables, as they change by ±20% about their respective optimal values, on the three objective functions as well as the supercriterion. It was observed that the construction parameters—height, length and number of rows—have more influence than the installation factors—tilt angle and distance between two adjacent panels—on the objective functions. The standard deviation of each of the random parameters is varied from 1% to 5% of the respective mean values to find the influence of uncertainty on different objective functions. The numerical results are given to show the influence of the level of probability of constraint satisfaction and the coefficient of variation of the random variables. It is observed that the absolute value of each objective function is decreased with an increase in either the

probability of constraint satisfaction or the coefficient of variation of the random variables. Better objective function values can be obtained with a lower value of probability of constraint satisfaction, but it might not be suitable (safe) for practical applications. A relatively higher constraint satisfaction (like 99.9997%) would result in worse objective function values. The results of the present study help designers in producing optimum solar collectors based on customer requirements. As seen from the present results, there is a trade-off between the absolute values of the various objectives and the probability of constraint satisfaction. From practical point of view, an increase in the overall objective implies improvement in a combination of annual energy output, winter energy output and cost of manufacture. With a higher probability of constraint satisfaction, the manufacture has to sacrifice the energy values as well as the profit if the costs of raw and processed materials are relatively large.

CHAPTER 3

Optimal Design of Compound Parabolic Concentrator (CPC) Solar Collector System

3.1 Introduction and Literature Review

The compound parabolic concentrator (CPC), first proposed by Winston and Hinterberger (1975), has the capability of reflecting all the insolation to the absorber over a relatively wide range of angles. Figure 3-1 presents a typical CPC, in which AB and CD are parabolic reflectors, which have the foci at C and B, respectively, and BC is a flat plate receiver. Any radiation within the collector acceptance angle enters through the aperture and finds its way to absorber surface by multiple internal reflections. Improving the efficiency and reducing the cost of these solar collectors is a hot research topic in the field of solar collectors. Abdul-Jabbar (1998) concluded through a series of experiments in the middle-east that the CPC solar collectors with double axis tracking system can get up to 75% more insolation. Kim *et al.* (2008) used both numerical and experimental methods to achieve the thermal efficiency of a CPC solar collector with single-axis tracking system is about 14.9% higher than a stationary CPC solar collector. Weinstock and Appelbaum (2009) compared the energy outputs of stationary flat plate solar collectors and flat plate solar collectors with various tracking systems. They found that the East-West horizontal axis multi-row PV panels with a North-South tracking

performed 16% better than the stationary PV panels while the North-South horizontal axis PV panels with an East-West tracking system could provide 17% extra power compared to the stationary PV panels. But from the cost point of view, stationary solar collector system is the most economic choice compared to the solar collectors with any tracking system. Small concentration ratio truncated CPC solar collectors without a tracking system are widely used in practice. Since the higher part of the parabola will prevent the radiation during some specific times, it will make the overall performance of the CPC solar collectors poor. Truncated CPC solar collectors are usually applied because a large portion of the reflector area can be eliminated in order to save the cost without seriously reducing the concentration. Many papers (Rabl, 1976, Derrick *et al.*1986, Carvalho *et al.* 1987 and Suzuki and Kobayashi 1995) discussed and recommended that the acceptance angle of CPC solar collectors should lie between 25° to 55° depending on the environment. Some researchers (Mills and Giutronich, 1977, Trupanagnostopolos *et.al*, 2000, Mallick, et al. 2004, 2007) designed different asymmetric parabolic reflectors in order to attract more insolation. Mills and Giutronich (1977) concluded based on a comparative study of symmetrical and asymmetrical parabolic concentrators that asymmetrical design could collect higher and more stable energy. Trupanagnostopolos *et.al* (2000) compared the performance of three small CPC units and one large CPC unit, with the aperture area of the larger unit equal to three times more than that of the smaller units through experiments and confirmed that the three smaller units performed better than the large unit. Mallick et al. (2004, 2007) designed, constructed and experimentally tested a prototype asymmetric CPC solar collector. For the same receiving area, the power output of the CPC collector was found to be 1.62

times more than that of a flat plate photovoltaic panel. Other researchers focused on the design of different types of receivers. In general, receivers can be designed as flat plates (as shown in Fig 3-1), V-type (Fraidenraich *et al.*, 2008) or cylindrical (Trupanagnostopolos and Souliotis, 2004). Other practical designs with multichannels (Tripanagnostopoulos and Yianoulis, 1996) and bifacial absorbers (Tripanagnostopoulos *et al*, 2000) have also been used.

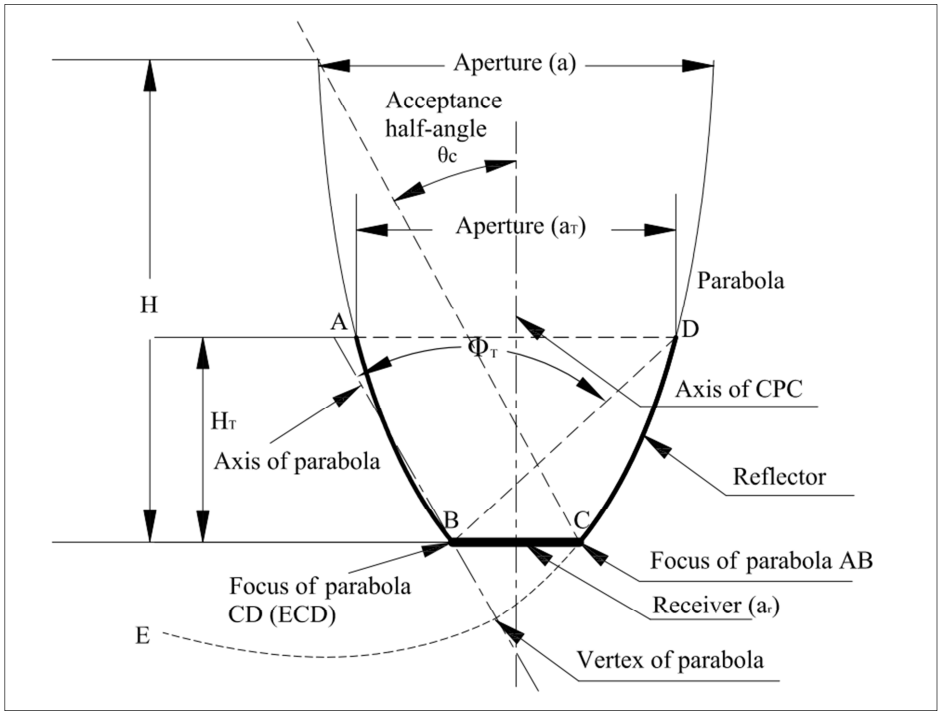

Figure 3-1 Geometric cross section of a truncated compound parabolic solar collector

Since a CPC solar collector has the merits of flat plate solar collector and concentrating collector, it is an excellent substitute for a flat plate solar collector. The CPC solar collectors can offer superior yearly energy delivery at comparable cost and reach considerably higher temperatures than most flat-plate collectors in thermal applications. Similar to flat plate solar collectors, the CPC solar collectors are also used for increasing

the intensity of irradiation in order to improve the performance of photovoltaic solar panels. For large area solar panel applications, a multi-row CPC solar (photovoltaic) collector system needs to be designed and optimized. As shown in Fig. 3-2, increasing the number of solar collector rows and height of the collector will definitely increase the total collector area; however, it also increases the shading area which will reduce the radiation energy received from the sun. Weinstock and Appelbaum (2004, 2007, 2009), Hu and Rao (2009) and Rao and Hu (2010) considered different types of optimum designs for large area multi-row flat plate solar collector systems with shading effects. However, the shading effect has not been considered in a large area multi-row CPC panel design problems until now. The present work is to incorporate the shading effect in a large area multi-row optimum design problem. Three objectives, including the maximization of the annual average incident solar energy, maximization of the incident solar energy for the lowest month and minimization of cost, are considered separately and simultaneously under both deterministic and probabilistic uncertainty.

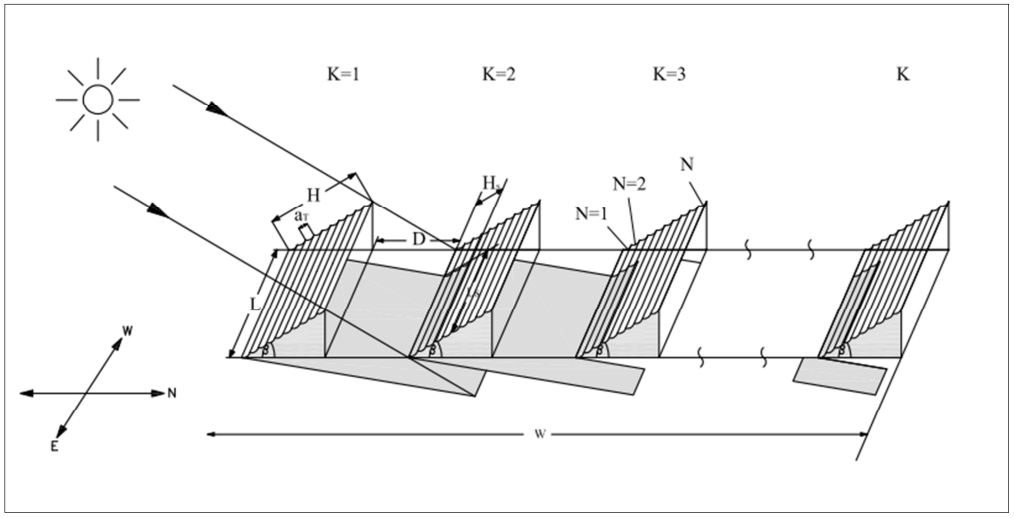

Figure 3-2 Multi-row compound parabolic collector in a given area

3.2 Deterministic Single-objective Optimization of CPC solar collector system

The optimal design of a CPC solar collector system involves of several design variables, several random variables, a set of linear and nonlinear equality and inequality constraints and an objective function. Mathematically, it can be stated in the following general form:

Minimize or maximize f(X) with respect to X,

subject to: $$g_j(X) = 0, \qquad j = 1,2,....m \tag{3.1}$$

$$h_j(X) \le 0, \qquad j = 1,2,....n \tag{3.2}$$

$$a_k \le x_k \le b_k, \qquad k = 1,2,....l \tag{3.3}$$

where x_k is the k^{th} component of the design vector X, and a_k and b_k are the lower and upper bounds on the design variable x_k, respectively.

3.2.1 Maximization of annual average incident solar energy

The general aim of a CPC solar collector design is to obtain maximum incident energy on a given horizontal land with fixed dimensions L × W (length × width). A CPC solar collector system includes K rows of solar collectors with distance D between two neighboring rows and each row of collectors consists of N small CPC units. The small CPC unit has a receiver of length a_r, an acceptance angle of θ_c and is truncated at a height ratio r_T (the height of truncated CPC / the height of full CPC). All the solar collectors are inclined at an angle β with respect to the horizontal. The design vector of the problem is:

$$\vec{X} = \{a_r \;\; \theta_c \;\; L \;\; \beta \;\; D \;\; K \;\; N \;\; r_T\}^T \tag{3.4}$$

The objective function is taken as the negative of the average incident solar energy of the field (for maximization):

$$Q_1 = a_r \times L \times r_{cpc}^T \times N \times \left[q_b \tau_{cpc,b} + q_d \tau_{cpc,d} + (K-1)(q_b^{sh} \tau_{cpc,b} + q_d^{sh} \tau_{cpc,d})\right] \quad (3.5)$$

$$f_1(\vec{Y}) = -Q_1 \quad (3.6)$$

where r_{cpc}^T can be calculated using Eqs. 3.7~3.14:

$$f = a_r(1 + sin\theta_c) \quad (3.7)$$

$$a = a_r/sin\theta_c \quad (3.8)$$

$$h = fcos\theta_c/sin^2\theta_c \quad (3.9)$$

$$a_T = \frac{fsin(\emptyset_T - \theta_c)}{sin^2(\emptyset_T/2)} - a_r \quad (3.10)$$

$$h_T = \frac{fcos(\emptyset_T - \theta_c)}{sin^2(\emptyset_T/2)} \quad (3.11)$$

$$r_T = \frac{\cos(\emptyset_T - \theta_c) sin^2(\emptyset_T/2)}{sin^2(\emptyset_T/2) cos\theta_c} \quad (3.12)$$

$$r_{cpc}^{full} = \frac{1}{sin\theta_c} = \frac{a}{a_r} \quad (3.13)$$

$$r_{cpc}^T = \frac{a_T}{a_r} \quad (3.14)$$

The expressions for computing $q_b, q_d, q_b^{sh}, q_d^{sh}$ are given in the section 2.2.

For the constraints, the total length of each collector plate (H) should be less than or equal to a maximum value and the total width (length) of the collectors must be less than or equal to the maximum width (length) of the available land:

$$KNa^T cos\beta + (K-1)D - W \leq 0 \tag{3.15}$$

The side constraints are taken as:

$$H = N \cdot a_T \leq H^{max} \tag{3.16}$$

$$a_r^{min} \leq a_r \leq a_r^{max} \tag{3.17}$$

$$\theta_c^{min} \leq \theta_c \leq \theta_c^{max} \tag{3.18}$$

$$0 \leq \beta \leq 90 \tag{3.19}$$

$$L_{min} \leq L \leq L_{max} \tag{3.20}$$

$$D_{min} \leq D \tag{3.21}$$

$$0 \leq r_T \leq 1 \tag{3.22}$$

$$1 \leq K \leq K_{max} \tag{3.23}$$

$$1 \leq N \leq N_{max} \tag{3.24}$$

$$1 \leq r_{cpc}^T \leq 2 \tag{3.25}$$

along with a positive integer requirement (constraint) for the number of rows N and the number of units K:

$$N \in \{\text{Positive Integers}\} \tag{3.26}$$

$$K \in \{\text{Positive Integers}\} \tag{3.27}$$

The integer requirement constraints, Eqs. (3.26~3.27), are handled using the following procedure:

Step1: Solve the optimization problem by treating all the design variables to be continuous. Let the optimum solution give the non-integer number for the rows K and for the units N.

Step2: Fix the number of rows K and number of units N at integer values in the close neighborhood of the respective values found by the continuous variable optimization approach. If the optimal values of the number of rows and units found in step1 are K = 72.2 and N = 15.2, for example, we fix an integer value for K and N out of the values, K= 71, 72 or 73 and N = 14, 15 or 16, one at a time, successively and solve the corresponding continuous variable optimization problems.

Step3: Compare the optimum values of the objective functions given by the solution of the various optimization problems formulated with different settings of the values of K and N. Choose the result corresponding to the best objective function and the corresponding integer numbers of rows and units used as the final (approximate) optimum solution of the problem with the constraint of Eqs. (3.26) ~ (3.27).

3.2.2 Maximization of average incident solar energy for the lowest month

In general, the incident solar energy is more in summer than in winter; however, consumers need more heat energy in winter. It is therefore necessary to consider the maximization of incident solar energy for the lowest month as the objective function:

$$f_2 = -\text{ lowest incident monthly solar energy} \tag{3.28}$$

The design variables and constraints will be same as in the case of the optimization problem stated in section 3.2.1.

3.2.3 Minimization of cost

Another important objective in the design of a solar collector is the minimization of cost. The design variables are same as those indicated earlier. The objective function (cost) to be minimized can be expressed as:

$$Cost = Cost_{PV} + Cost_{reflector} + Cost_{land} \tag{3.29}$$

$$Cost_{PV} = S_1 a_T L \tag{3.30}$$

$$Cost_{reflector} = S_2 A_{reflector} \tag{3.31}$$

$$A_{reflector} = A_s(1 + sin\theta_c)\left\{\frac{cos\theta_c}{sin^2\theta_c} + log\left[\frac{(1+sin\theta_c)(1+cos\theta_c)}{sin\theta_c[cos\theta_c+\sqrt{2(1+sin\theta_c)}]}\right] - \frac{\sqrt{2}cos\theta_c}{(1+sin\theta_c)^{1.5}}\right\} \tag{3.32}$$

$$Cost_{land} = S_3 LW \tag{3.33}$$

where s_1 is the unit cost of receiver (photovoltaic solar panel), s_2 is the unit cost of reflector and s_3 is the unit cost of land. Note that additional cost components such as those associated with piping, backup energy equipment, maintenance cost could also be added to the objective function if necessary.

The following additional constraints are considered while minimizing f_3. The daily average incident solar energy in any month should be at least some percentage (P between 70%-100%) of the daily optimum value found in the case of the problem described in section 3.2.1 (Q^*):

$$Q_1 - (P) \times Q_1^* \leq 0 \tag{3.34}$$

3.2.4 Numerical Example

The single and multi-objective optimization of CPC solar collectors is illustrated by considering a numerical example. The game theory approach is considered for the multi-objective optimum design problem. The following data are assumed:

$a_r^{min} = 0.10\ (m)$, $a_r^{max} = 0.30\ (m)$, $\theta_c^{min} = 25\ (deg)$, $\theta_c^{max} = 90\ (deg)$, L_{min} = 15m, L_{max} = 30m, H_{min} = 0.5m, H_{max} = 2m, D_{min} = 0.8m, K_{max} = 150, N_{max} = 150, P = 80%, s_1 = 100 \$/m^2, s_2 = 20 \$/m^2, s_3 = 1/20/50 \$/m^2, $\tau_{cpc,b} = 1.0$, $\tau_{cpc,d}$ = 1.0

The solar collector is assumed to be installed in a specific location, Miami (USA), where the latitude is 25.4°N and the altitude is 5m, and the solar collector is assumed to face the equator (south). The starting design vector is chosen as:

$$\vec{X} = \{a_r\ \ \theta_c\ \ L\ \ \beta\ \ D\ \ K\ \ N\ \ r_T\}^T = \{0.10\ 40\ 25\ 40\ 1.0\ 70\ 10\ 0.5\}^T \qquad (3.35)$$

The result of the single-objective optimization problems, along with the initial design, are listed in Tables 3-1 (a) and (b). It can be noticed that the optimum value of the truncation ratio r_T is almost zero for the optimization problems involving the minimizations of f_1 and f_2; this indicates that the optimum CPC solar collectors are totally truncated and tend to reach flat plate solar collectors in these cases. As a result, the optimum values of the design variables L, β, D, and K are very similar to those obtained in the case of flat plate solar collectors. One more integer constraint (N must be integer) makes the values of the objective functions f_1 and f_2 slightly less than the corresponding optimum results obtained in the case of flat plate solar collectors. In Table 3-2(b), the cost per unit watt (\$/W), corresponding to the minimizations of f_1 and f_2 are 0.4516 and 0.5286, respectively, while the value reduces to 0.3642 in the case of minimization of f_3. The results indicate

that the primary (significant) objective in designing CPC solar collector systems is to reduce the cost per unit energy instead of getting more solar radiation. Since a reflector cannot direct 100% of radiation to the receiver, the theoretical insolation achieved by a CPC solar panel will be less than the incident energy received by a flat plate solar panel in any given area. However, the compound parabolic concentrator is usually much cheaper than the price of solar cells. O'Gallagher (2008) reported that the price of the concentrator is approximately 20% of the solar cell. Therefore it is practical to design a more economic multi-row solar collector system by using CPC units.

Table 3-1(a) Initial design and single-objective optimization results (design variables)

	Design variables							
Objectives	A_r (m)	θ_c (deg)	W (m)	β (deg)	D (m)	K	N	r_T
Initial	0.20	40.00	25.00	40.00	1.00	70	10	0.5000
Min f_1	0.10	89.90	30.00	35.94	0.80	83	20	0.0010
Min f_2	0.10	89.90	30.00	51.36	0.80	98	20	0.0010
Min f_3	0.10	25.00	29.22	21.20	0.80	70	10	0.2680

Table 3-1(b) Initial design and single-objective optimization results (objective functions and other outputs)

	objectives and other outputs							
Objectives	cpc ratio	f_1 ($10^6\times$W)	f_2 ($10^6\times$W)	f_3 ($10^6\times$\$)	solar cell ($10^6\times$\$)	land ($10^6\times$\$)	reflector ($10^6\times$\$)	f_3/f_1 (\$/W)
Initial	1.4450	-1.2675	-1.0230	0.5517	0.3500	0.1120	0.0897	0.4353
Min f_1	1.0000	-1.3685	-1.0967	0.6180	0.4980	0.1192	0.0000	0.4516
Min f_2	1.0000	-1.3395	-1.1225	0.7080	0.5846	0.1200	0.0000	0.5286
Min f_3	1.8095	-1.0954	-0.8828	0.3989	0.2163	0.1056	0.0770	0.3642

3.2.5 Sensitivity Analyses

In the first single-objective optimization problem, the result provides a flat plate solar collectors design which has a maximum average incident solar energy of $Q_1^* = 1.3685 \times 10^6$ W. The primary objective for the optimum design of CPC solar panel system is aiming at reducing overall cost and cost per unit energy of solar energy system. Therefore, this section investigates the sensitivity analyses with respect to the energy output expectation ratio (P), mathematically formulated as Q/Q_1^*, in the range of 70% to 100%. Sensitivity analyses with respect to lower values of P (less than 70%) have limited significance and therefore they are excluded in the current analysis. Since these solar panels can be installed in a rural place or in an urban area, the price of land (s_3) can be variable. Three different levels of land prices—low s_3 = 1 \$/m^2, medium s_3 = 20 \$/m^2 and high s_3 = 50 \$/m^2—are incorporated and compared in the sensitivity analyses. This section investigates primarily on the effects of the design variables as well as the CPC ratio and the cost.

The variations of the design variables with respect to the change of P under different land prices are presented in Fig. 3-3 (a) – (h) respectively. Each figure demonstrates that the optimum result of each design variable is singular when P = 100% regardless of the unit price of land. Hence, the optimum values corresponding to P = 100% were set as the reference values (base lines) in Fig. 3-3 (a) – (h). The horizontal axis presents the value of P in the range from 70% to 100% and the vertical axis presents the different values of corresponding design variables. The variation of the design variable x_1, namely the width of receiver, is presented in Fig. 3-3 (a). In this figure, most of the optimum results stay at the bottom of the graph, in a range from 0 to 10% above the lower bound except for the

optimum results under relatively lower P value (70% and 75%) and medium or high land cost (s_3 = 20 and 50). The numerical observation matches with the experimental results concluded by Trupanagnostopolos *et.al* (2000) that multiple small CPC units can perform better than one large CPC unit. When the value of P decreases, however, less energy output is expected and therefore larger CPCs are recommended due to economic reasons. Figure 3-3 (b) shows the variation of the design variable x_2, namely half of the acceptance angle. The angle remains essentially the same in the lower bound (25 degree) when the value of P is less than or equal to 85%. When the values continue increasing to 90% and 95%, the optimum value increases dramatically and eventually all of the curves converged to one point which is the upper bound (90 degree) when the value of P is equal to 100%. Fig.3-3 (c) presents the variation of the third design variable, namely the width of the CPC solar panel. The results of this design variable remain at the upper limit regardless of the energy expectation ratio when the unit price of land is relatively low (s_3 = 1). However, when the unit price of land is medium or high, the optimum results no longer reach the upper limit at relatively lower energy expectation ratio. Thus, higher unit prices of land lead to lower optimum values in any given energy expectation ratio lower than 100%. Figure 3-3 (d) demonstrates the variation of the optimum results for the design variable x_4. When the energy expectation ratio is between 70% and 95%, the optimum values fluctuate in the range of 20 to 27 degrees. In order to bring energy output expectation ratio to 100%, the optimum results shifts to flat plate solar collectors design. As a result, the optimum values suddenly shoot to 35.9394 degree which is much higher than any of the other optimum values. Fig. 3-3 (e) presents the variation of the optimum values of the design variable x_5, namely the distance between two neighboring rows. It is

clear that the optimum results remain essentially in the lower bound when the unit price of land is medium or high. In contrast, when the unit price of land is low, the distance between two neighboring rows no longer adheres to the lower limit and shading effects can be decreased with increase of the value for this design variable. Figures 3-4 (f) and (g) show the variation of the optimum values of the design variables, namely, number of rows and number of the CPC units in one panel, respectively. The tendency of all the curves in the two figures appears to be similar. Under the relatively lower energy output expectation ratio, fewer rows and CPC units per row are needed in the optimum design. Figure 3-3 (h) provides the variation of the design variable x_8, namely truncated ratio of CPC. It is clear that the height of the truncated CPC is less than 30% of the height of the full CPC. This indicates that all of the optimum CPC units should be truncated by more than 70%.

Figure 3-3 (i) gives the variation of the CPC ratio with respect to the optimum energy output expectation ratio under different unit prices of land. The CPC ratio fluctuates in a small range between 1.70 and 1.85 when the energy output expectation ratio varies between 70% and 85%. With the energy output expectation ratio continuing to increase, the CPC ratio decrease dramatically and finally reaches one when the energy output expectation ratio hits 100% and the optimum result shifts to flat plate solar collectors. Figure 3(j) presents the relationship between the cost per unit energy and the energy expectation ratio under different unit prices of land. It is clear that the three curves are parallel with each other. For any given unit price of land, the cost per unit energy is almost constant when the value of the energy output expectation ratio is lower than 85%. When the value of energy output expectation ratio increases to more than 85%, the cost

per unit energy starts to increase. The value continuously increases until it reaches a peak value, when the energy output expectation ratio arrives 100%.

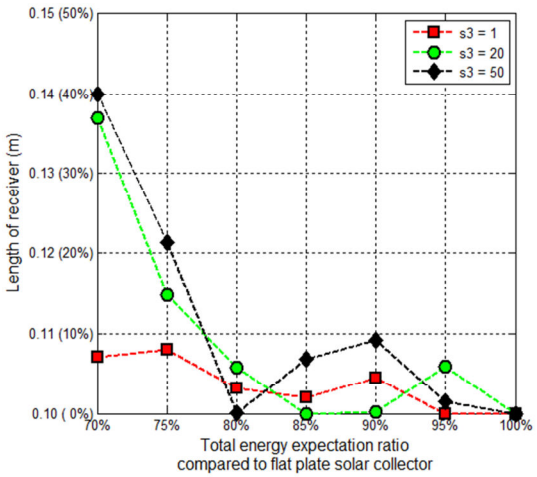

(a)

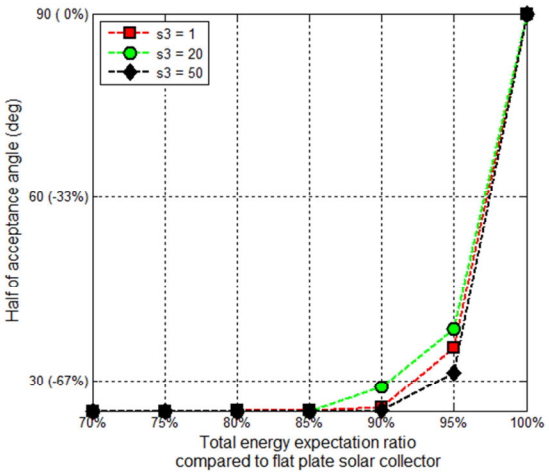

(b)

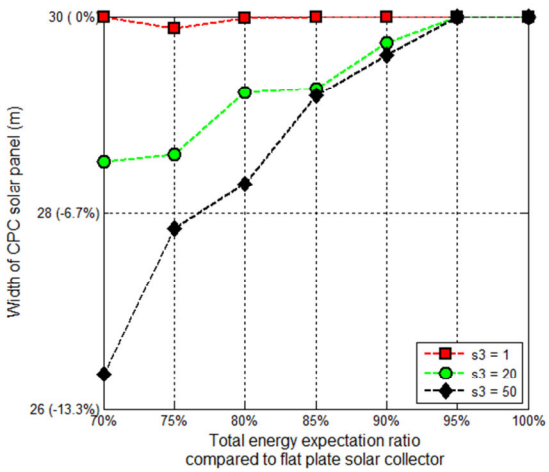

(c)

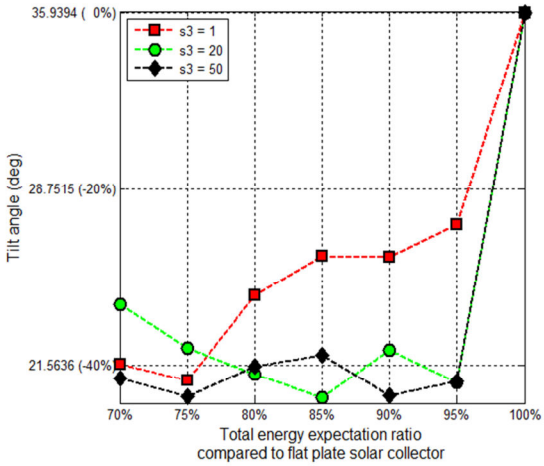

(d)

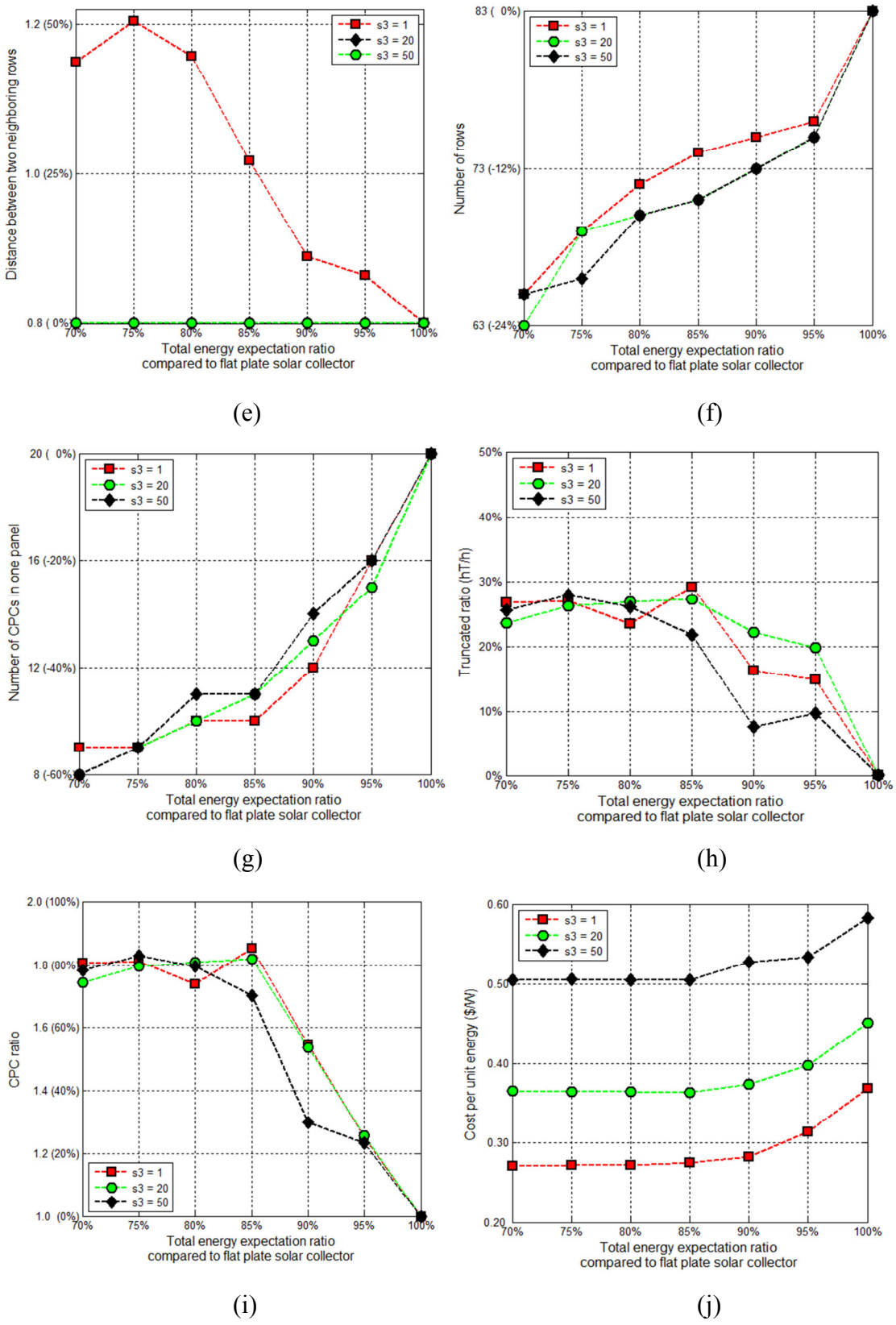

Figure 3-3 Sensitivity Analysis with respect to P and S_2

3.3 Optimization of CPC solar collector system Under probabilistic uncertainty

The procedure of solving optimization problems under probabilistic uncertainty is provided in the section of 2.3.2 and the procedure of formulating multi-objective optimization problem is given in section 2.4. Similar to the example illustrated in the flat-plate solar collector design, a numerical example of multi-objective optimum design of stationary CPC solar panel is considered under probabilistic uncertainty in this section. In addition to the parameters assumed in the deterministic numerical example in section 3.2.4, the following extra conditions are assumed: all of the design variables except number of rows (K) and number of the CPC units in each solar panel (N) are assumed to have a standard deviation with 1% to the corresponding mean value. Other uncertain parameters including altitude, solar constant and typical day of each month are assumed to have a standard deviation with 5% of the corresponding mean value.

3.3.1 Numerical example of single-objective optimization problems under probabilistic uncertainty

Three different single objective functions, namely, maximization of the annual average incident solar energy, maximization of the incident solar energy for the lowest month and minimization of the cost, were considered. A sensitivity analysis with respect to the constraint satisfaction which varies in six different levels—50%, 80%, 90%, 95%, 99%, and 99.99997%—is given as part of the numerical example. Figure 3-4 (a) – (p) demonstrate the variation of the design variables, objective functions, as well as CPC ratio and cost with respect to the probability of constraint satisfaction.

Several common features can be found through all the figures. For example, the number of cases in which the optimum solutions found in minimization of the cost (f_3) is lesser compared to maximization of the average incident solar energy (f_1) and maximization of the incident solar energy of the lowest month (f_2) because of the extra constraint, Eq. (3.34). No feasible solution can be found when probability of constraint satisfaction is 99.99997%. When the probability of constraint satisfaction is 50%, all the design variables remain exactly the same as the determinist optimum solution.

Figure 3-4 (a) – (h) presents the variation of the design variables with respect to the probability of constraint satisfaction. Most of the design variables, namely, length of receiver (Fig. 3-4(a)), half of acceptance angle (Fig. 3-4(b)), width of CPC solar panel (Fig. 3-4(c)), number of rows (Fig. 3-4(f)), number of CPCs in one panel (Fig. 3-4(g)), behave consistently for the first two objectives and conflict with the third objective function. The optimum values of the design variable, namely tilt angle (Fig. 3-4(d)), do not affect too much with respect to the increase of the probability of constraint satisfaction under a given objective function. The design variable, namely, distance between two neighboring rows (Fig. 3-4(e)) increases with the increase of the probability of constraint satisfaction irrespective of the objective functions. The optimum value of the design variable, namely, truncated ratio (Fig. 3-4(h)), is very close to zero for the first two objective functions. It means the CPC collector is almost fully truncated and shift to flat plate solar collector. The feature can also be detected in Fig. 3-4 (i), namely, CPC ratio. The CPC ratio corresponding to the first two objective functions are almost zero irrespective to the variation of the probability of constraint satisfaction. The CPC ratio corresponding to the objective function f_3 is fluctuated in a small range between 1.72 and

1.77. As shown in Fig. 3-4 (j), it is clearly that the cost per unit energy does not affect too much with the change of the probability of constraint satisfaction, and the values are approximately equal to 0.45, 0.51 and 0.36 $/W corresponding to objective functions f_1, f_2 and f_3, respectively.

Figure 3-4 (k), (m) and (o) presents the variation of deterministic objective functions (f_i, i = 1, 2, 3), respectively and Fig. 3-4 (l), (n) and (p) presents the variation of probabilistic objective functions ($\overline{f_i} + \sigma_{f_i}$, j = 1, 2, 3), respectively, with respect to the change of probability of constraint satisfaction. The curves of the deterministic objective functions (f_i, i = 1, 2, 3) exhibit very similar trend to the corresponding curves of probabilistic objective functions ($\overline{f_i} + \sigma_{f_i}$, j = 1, 2, 3) for any single-objective optimization problem. With increasing values of probability of constraint satisfaction, the value of annual average incident solar energy and the incident solar energy for the lowest month is always decreasing and the value of cost is always increasing because of tighter constraints.

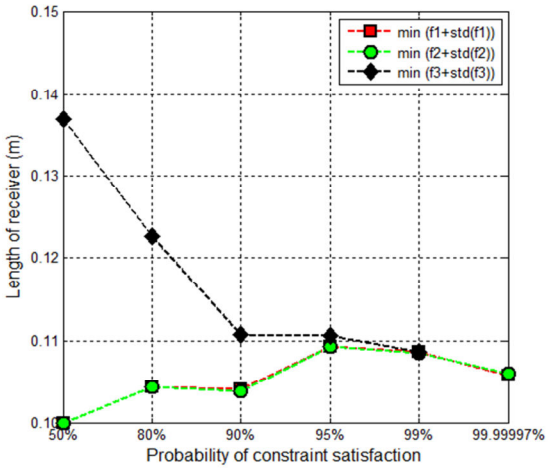

(a)

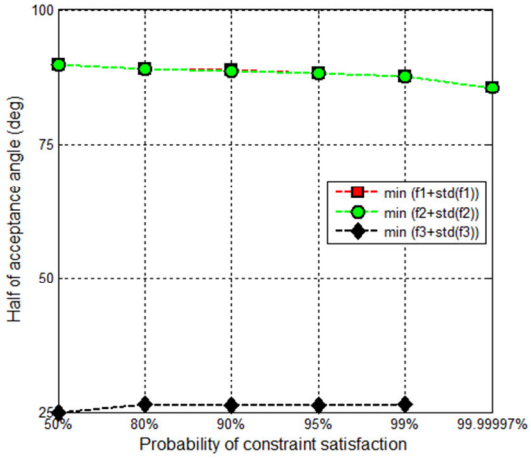

(b)

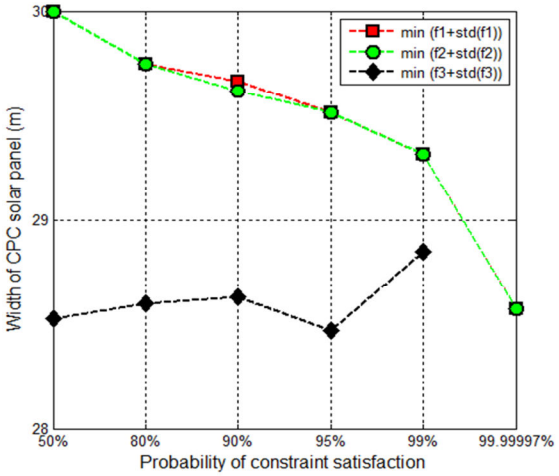
min (f1+std(f1))
min (f2+std(f2))
min (f3+std(f3))
Width of CPC solar panel (m)
30
29
28
50%
80%
90%
95%
99%
99.99997%
Probability of constraint satisfaction

(c)

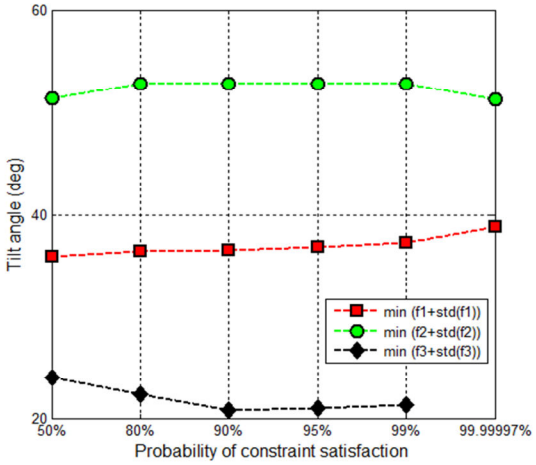
min (f1+std(f1))
min (f2+std(f2))
min (f3+std(f3))
Tilt angle (deg)
60
40
20
50%
80%
90%
95%
99%
99.99997%
Probability of constraint satisfaction

(d)

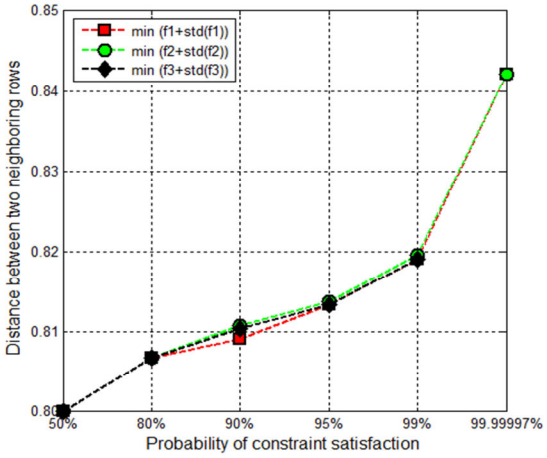
min (f1+std(f1))
min (f2+std(f2))
min (f3+std(f3))
Distance between two neighboring rows
0.85
0.84
0.83
0.82
0.81
0.80
50%
80%
90%
95%
99%
99.99997%
Probability of constraint satisfaction

(e)

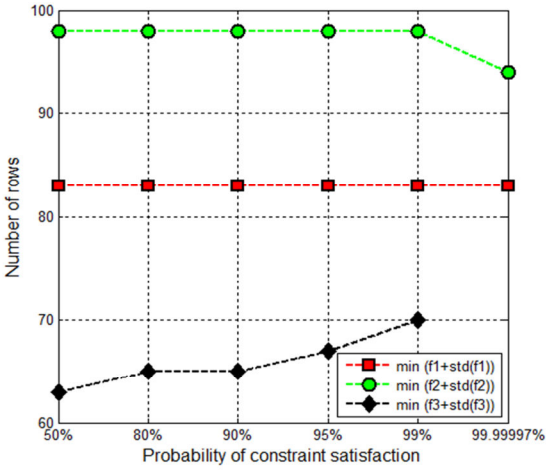
min (f1+std(f1))
min (f2+std(f2))
min (f3+std(f3))
Number of rows
100
90
80
70
60
50%
80%
90%
95%
99%
99.99997%
Probability of constraint satisfaction

(f)

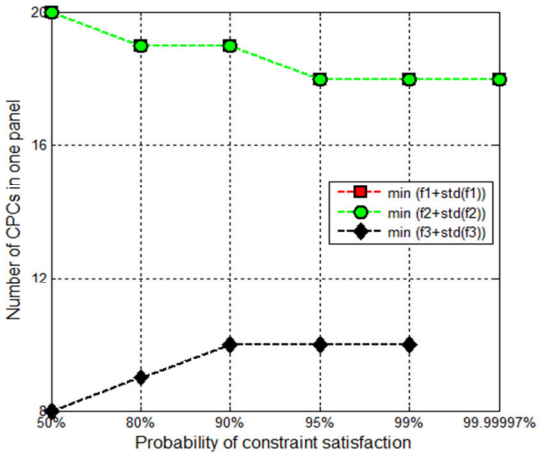
min (f1+std(f1))
min (f2+std(f2))
min (f3+std(f3))
Number of CPCs in one panel
20
16
12
8
50%
80%
90%
95%
99%
99.99997%
Probability of constraint satisfaction

(g)

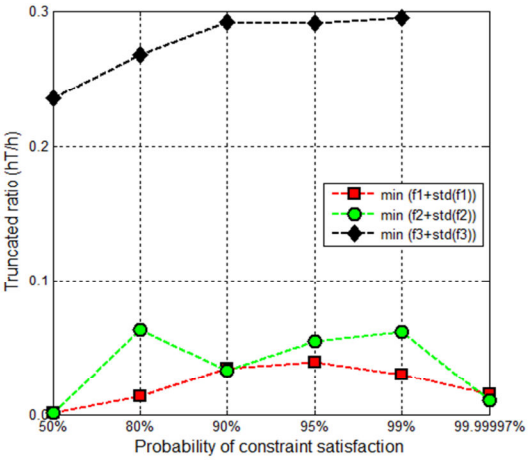
min (f1+std(f1))
min (f2+std(f2))
min (f3+std(f3))
Truncated ratio (hT/h)
0.3
0.2
0.1
0
50%
80%
90%
95%
99%
99.99997%
Probability of constraint satisfaction

(h)

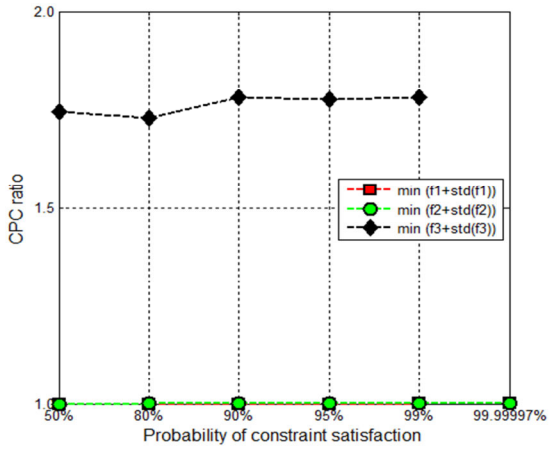
CPC ratio
2.0
1.5
1.0
min (f1+std(f1))
min (f2+std(f2))
min (f3+std(f3))
50%
80%
90%
95%
99%
99.99997%
Probability of constraint satisfaction

(i)

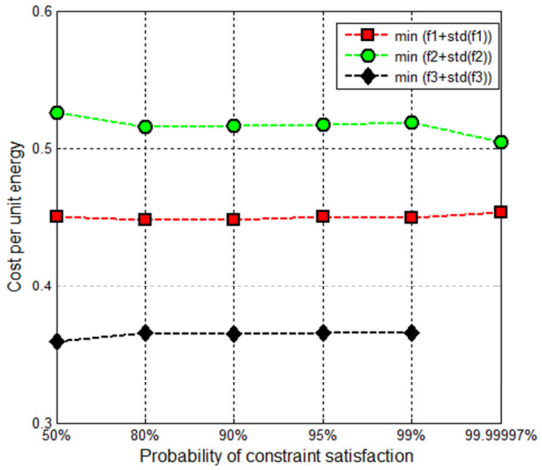
Cost per unit energy
0.6
0.5
0.4
0.3
min (f1+std(f1))
min (f2+std(f2))
min (f3+std(f3))
50%
80%
90%
95%
99%
99.99997%
Probability of constraint satisfaction

(j)

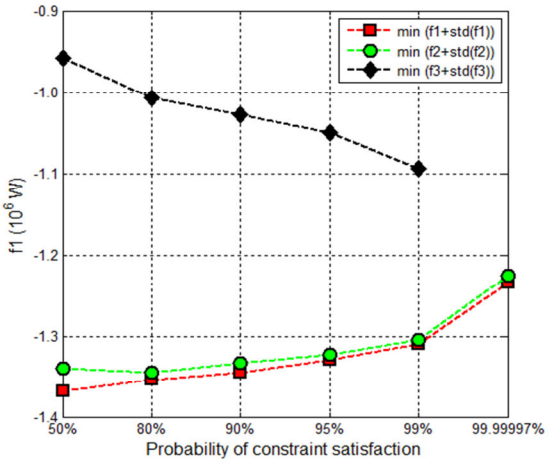
f1 (10^6 W)
-0.9
-1.0
-1.1
-1.2
-1.3
-1.4
min (f1+std(f1))
min (f2+std(f2))
min (f3+std(f3))
50%
80%
90%
95%
99%
99.99997%
Probability of constraint satisfaction

(k)

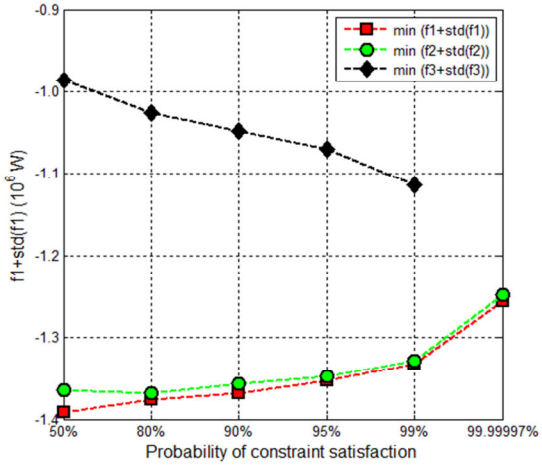
f1+std(f1) (10^6 W)
-0.9
-1.0
-1.1
-1.2
-1.3
-1.4
min (f1+std(f1))
min (f2+std(f2))
min (f3+std(f3))
50%
80%
90%
95%
99%
99.99997%
Probability of constraint satisfaction

(l)

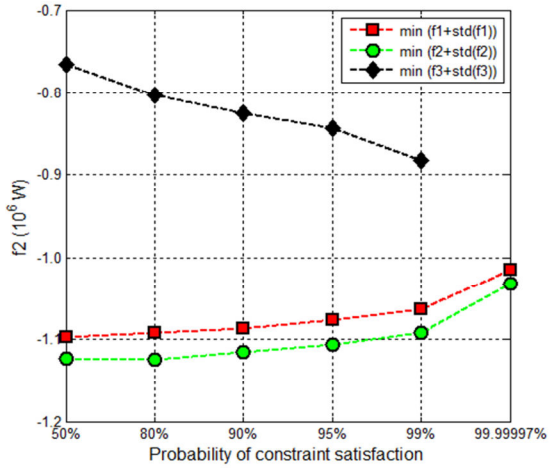
f2 (10^6 W)
-0.7
-0.8
-0.9
-1.0
-1.1
-1.2
min (f1+std(f1))
min (f2+std(f2))
min (f3+std(f3))
50%
80%
90%
95%
99%
99.99997%
Probability of constraint satisfaction

(m)

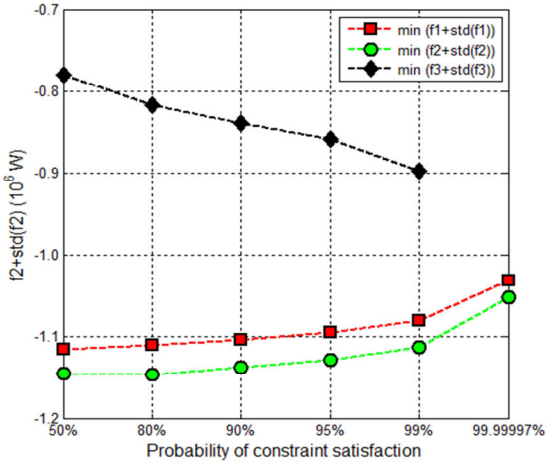
f2+std(f2) (10^6 W)
-0.7
-0.8
-0.9
-1.0
-1.1
-1.2
min (f1+std(f1))
min (f2+std(f2))
min (f3+std(f3))
50%
80%
90%
95%
99%
99.99997%
Probability of constraint satisfaction

(n)

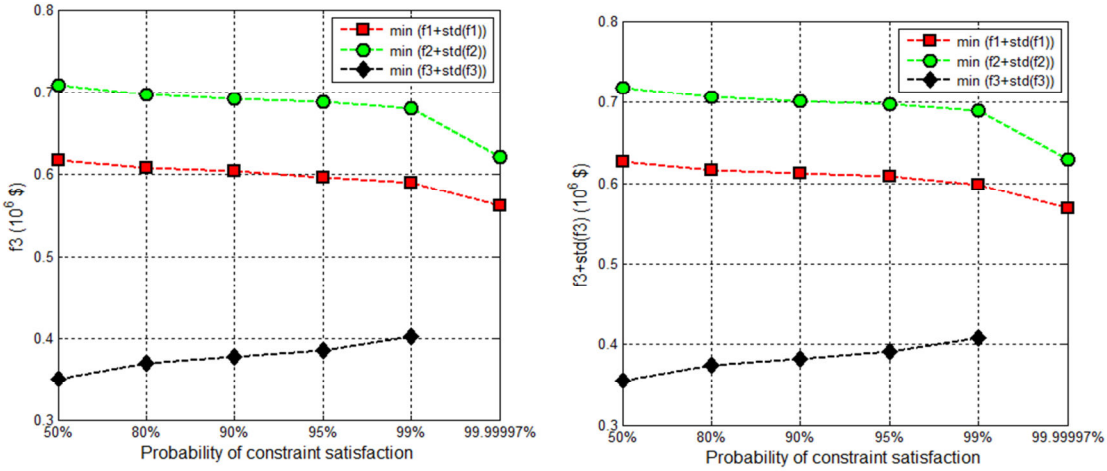

(o) (p)

Figure 3-4 Sensitivity Analysis with respect to probability of constraint satisfactions

3.3.2 Numerical example of multi-objective optimization problems under probabilistic uncertainty

Based on the results from the single-objective optimization, multi-objective optimization problems are generated and solved by using the game theory approach (Eq. 2-68) under probabilistic uncertainty; and the results are listed in Table 3-2 (a)-(b).

Since game theory approach uses the results of single objective optimizations, it cannot be used for cases in which any of the single objective optimization problems result in infeasible designs. In the present case, the minimization of f_3 considers additional constraints and hence yields the least optimum values. Thus the number of multi-objective optimization problems solved (for different cases) is same as the number of different cases that have feasible solutions during the minimization of f_3.

An observation on the variation of the weights (c_1, c_2, c_3) used in the Pareto optimal solutions indicated that f_3 is dominant in the any of the multi-objective optimization

problems. The weights of the first and second objective function are found to lie between 10% and 11% in all the cases. Hence, the results of multi-objective optimization problem are far away from the optimum solutions of the first two single-objective optimization problem, which are flat plate solar collector designs.

The design variables including the length of receiver, width of the solar collector, tilt angle, and truncated ratio are fluctuated in a small range (less than ±10%) with increase of the probability of constraint satisfaction. The design variables including half of the acceptance angle and distance between two neighboring rows are increasing up to 2.38% and 3.84% respectively, with the increase of the probability of constraint satisfaction. The design variable, namely, number of rows, increases from 67 to 70 and the design variable, namely, number of the CPC units in one panel, increases from 9 to 11 with the increase of the probability of constraint satisfaction. The CPC ratios corresponding to the results of multi-objective optimization are fluctuated in the range between 1.75 and 1.85.

Table 3-2(a) Multi-objective optimization results (design variables)

	Design variables							
Probability (P)	A_r (m)	θ_c (deg)	W (m)	β (deg)	D (m)	K	N	r_T
50%	0.1102	25.0000	28.1187	20.1543	0.8000	67	9	0.2799
80%	0.1016	25.2505	28.1392	21.7599	0.8068	68	10	0.2998
90%	0.1028	25.3247	28.9000	22.6211	0.8168	68	10	0.2874
95%	0.1076	25.6793	29.1394	25.5123	0.8166	69	10	0.2592
99%	0.1024	25.5961	27.7827	22.0266	0.8307	70	11	0.2707

Table 3-2(b) Multi-objective optimization results (objective functions and other outputs)

Objectives and other outputs								
Probability (P)	cpc ratio	f_1 (10^6×W)	f_2 (10^6×W)	f_3 (10^6×$)	$f_1+\sigma f_1$ (10^6×$)	$f_2+\sigma f_2$ (10^6×$)	$f_3+\sigma f_3$ (10^6×$)	Obj
50%	1.8325	-0.9596	-0.7744	0.3503	-1.0109	-0.8160	0.3555	0.1987
80%	1.8537	-1.0022	-0.8143	0.3676	-1.0614	-0.8577	0.3731	0.1977
90%	1.8269	-1.0261	-0.8359	0.3770	-1.0807	-0.8804	0.3825	0.1998
95%	1.7536	-1.0513	-0.8480	0.3879	-1.1077	-0.8931	0.3936	0.2075
99%	1.7801	-1.0921	-0.8745	0.3984	-1.1504	-0.9210	0.4043	0.1971

3.3.3 Numerical example with a constraint on the CPC ratio

As observed in the previous sections, the maximization of the annual average incident solar energy and maximization of average incident solar energy for the lowest month resulted in the flat plate solar collector as the best system. In order to achieve a CPC solar collector that is still optimum, the optimization problems are solved by imposing an additional constraint that the minimum CPC ratio should be at least 1.2 along with the rest of the constraint.

The results of the single-objective optimization problems, along with the initial design used, are summarized in Tables 3-3 (a) and (b). It can be noticed that the optimum values of the CPC ratio hit the lower bound value of 1.2 in the minimizations of f_1 an f_2. As a result, the cost corresponding to the minimization of f_1 or f_2 has been slightly reduced compared to the corresponding optimum value without the extra constraint. The result of the minimization of f_3 remains essentially the same as the result given in Table 3-1 (without the extra constraint). The cost per unit watt ($/W) of power corresponding to the minimum of f_3 is still much lower than those of the first two optimizations.

Table 3-3(a) Initial design and single-objective optimization results (design variables)

Design variables								
Objectives	A_r (m)	θ_c (deg)	W (m)	β (deg)	D (m)	K	N	r_T
Initial	0.20	40.00	25.00	40	1.00	70	10	0.5000
Min f_1	0.1191	54.9440	30.0000	37.3840	0.80	84	14	0.6663
Min f_2	0.1387	55.4760	30.0000	47.9550	0.80	94	12	0.7281
Min f_3	0.1000	25.0000	29.2210	21.2010	0.80	70	10	0.2680

Table 3-3(b) Initial design and single-objective optimization results (objective functions and other outputs)

objectives and other outputs								
Objectives	cpc ratio	f_1 (10^6×W)	f_2 (10^6×W)	f_3 (10^6×\$)	solar cell (10^6×\$)	land (10^6×\$)	reflector (10^6×\$)	f_3/f_1 (\$/W)
Initial	1.4450	-1.2675	-1.0230	0.5517	0.3500	0.1120	0.0897	0.4353
Min f_1	1.2000	-1.3430	-1.0877	0.6083	0.4202	0.1200	0.0682	0.4530
Min f_2	1.2000	-1.3324	-1.1091	0.6705	0.4694	0.1201	0.0812	0.4995
Min f_3	1.8095	-1.0954	-0.8828	0.3989	0.2163	0.1056	0.0770	0.3642

The results of multi-objective optimization with the additional constraint under probabilistic uncertainty are listed in Tables 3-4 (a) - (b). The results exhibit similar features as those given in Tables 3-2 (a) – (b) without the extra constraint on the CPC ratio. The absolute values of the objective functions increase with an increase in the level of constraint satisfaction. Since f_3 is dominant in the multi-objective optimization problem, the values of the CPC ratio at the optimum points flunctated in a small range around 1.8 (from 1.7721 to 1.8458). Note that the result corresponding to the probability level of 50% for the constraint satisfaction are equivalent to those of the deterministic problem.

Table 3-4(a) Multi-objective optimization results with an additional constraint that CPC ratio should be at least 1.2 (design variables)

Design variables								
Probability (P)	A_r (m)	θ_c (deg)	W (m)	β (deg)	D (m)	K	N	r_T
50%	0.1107	25.0000	28.5462	21.0610	0.8000	67	9	0.2602
80%	0.1125	25.2505	28.3256	23.6503	0.8068	67	10	0.2753
90%	0.1089	25.3247	28.4509	21.3337	0.8185	68	10	0.2979
95%	0.1079	25.6793	28.5236	22.0256	0.8185	68	11	0.2689
99%	0.1121	25.5961	27.5689	23.8862	0.8307	69	11	0.2986

Table 3-4(a) Multi-objective optimization results with an additional constraint that CPC ratio should be at least 1.2 (objective functions and other outputs)

Objectives and other outputs								
Probability (P)	cpc ratio	f_1 ($10^6\times$W)	f_2 ($10^6\times$W)	f_3 ($10^6\times$\$)	$f_1+\sigma f_1$ ($10^6\times$\$)	$f_2+\sigma f_2$ ($10^6\times$\$)	$f_3+\sigma f_3$ ($10^6\times$\$)	Obj
50%	1.7941	-0.9648	-0.7815	0.3520	-1.0163	-0.8233	0.3571	0.2356
80%	1.8088	-1.0683	-0.8483	0.3910	-1.1308	-0.8935	0.3968	0.2256
90%	1.8458	-1.0804	-0.8688	0.3956	-1.1382	-0.9150	0.4015	0.2168
95%	1.7721	-1.1395	-0.8993	0.4152	-1.2004	-0.9472	0.4213	0.2365
99%	1.8307	-1.1756	-0.9235	0.4330	-1.2383	-0.9727	0.4395	0.2109

3.4 Conclusions

The optimum design of CPC solar collectors under deterministic and probabilistic uncertainty is presented with a consideration of solar radiation with shading effect. Three objectives, namely, the maximization of the annual average incident solar energy, the maximization of the lowest month incident solar energy and minimization of the cost, are considered. Most of the design variables and the altitude, solar constant and typical day of each month are treated as random variables following normal distribution. Game theory methodology with probabilistic uncertainty is used for the solution of the three

objective constrained optimization problems to find a balanced solution. The solution represents the best compromise based on the terms of the super-criterion selected. Numerical results are obtained at a specific location (Miami, USA). The maximization of the annual average incident solar energy and maximization of average incident solar energy for the lowest month resulted in the flat plat solar collector as the best system. Since the price of reflector is much cheaper compared to the solar cell, the primary objective of the CPC solar panel system design is to reduce the area of solar cell by increasing the area of reflectors. Therefore, the minimization of the cost resulted in CPC solar collector designs, which had CPC ratios around 1.8. Sensitivity analyses are presented with respect to the total energy expectation ratio (compared to flat plate solar collectors) and different land price. It is found that the cost per unit energy can be significantly reduced by 10% to 23% depending on different land prices if the total energy output can be sacrificed by 15% or more compared to the flat-plate solar collector system. In the probabilistic approach, most of the design variables vary with 1% of the respective mean value and other random variables including altitude, solar constant, and typical day of each month vary with 5% of the respective mean value to find the influence of uncertainty on different objective functions. The numerical results are given to show the influence of the level of probability of constraint satisfaction. It is observed that the value of the annual average incident solar energy and the average solar energy for the lowest month are decreased with an increase in the probability of constraint satisfaction while the cost is increased with an increase in the probability of constraint satisfaction. The minimization of the cost is dominant in the multi-objective optimization problem. Hence, the compromise solutions resulted in CPC solar collectors which had

CPC ratios around 1.8 irrespective of the additional CPC ratio constraint. Better values of objective function can be obtained with a lower value of probability of constraint satisfaction, but it might not be suitable (safe) for practical applications. The results of the present study are expected to help designers in producing a more economic solar panel system based on customer requirements. As seen from the present results, there is a trade-off between the absolute values of the various objectives and the probability of constraint satisfaction. From practical point of view, an increase in the overall objective implies improvement in a combination of annual energy output, winter energy output and cost of manufacture. With a higher probability of constraint satisfaction, the manufacture has to sacrifice the energy values as well as the profit if the costs of raw and processed materials are relatively large.

CHAPTER 4

Optimum Design of Horizontal Axis Wind Turbine System

4.1 Introduction and Literature Review

In recent years, the growing demand for electricity, environmental issues like global warming, and the rising cost of fossil fuels have created an urgent need to seek renewable energy sources such as wind energy. At the end of 2009, the worldwide capacity of wind power reached 159 gigawatts which accounted for 1.5% of the worldwide electricity usage (Ren21, 2010). The horizontal-axis wind turbines (HAWTs) are dominating the global wind turbine market due to their high power production capability and better efficiency. Since the HAWT industry is still in the emerging stages, the optimization of this type of wind turbines becomes important. The focus of this research is to optimize the parameters of the turbine such as blade and rotor size, tip speed ratio as well as twist and pitch angles to maximize the wind turbine performance and / or minimize the cost. Negm and Maalawi (2000) developed different optimization strategies to minimize weight and vibration, and to maximize stiffness and stiffness/mass ratio of wind turbine towers. Jureczko et al. (2005) implemented a modified genetic algorithm for maximizing energy output and minimizing blade vibration and blade material cost. Martin (2006) optimized the rotor-to-generator size in order to get maximum annual energy production (AEP) under specified wind conditions and budget constraints. Thumthae and

Chitsomboon (2009) used both numerical simulation and experimental methods to find different optimum pitch angles of untwisted blades of HAWTs under different wind velocities. Lanzafame and Messina (2009) maximized AEP by optimizing the twist angle of a wind turbine blade. It can be seen from the available literature that the Taguchi optimization method or its extension to address multiple objective functions and / or multiple constraints has not been used in the area of optimal design of wind turbines.

The Taguchi method of fractional design of experiments was first developed by Genichi Taguchi to improve the quality of manufactured goods in 1956. He suggested that the quality and robustness of a product should be controlled during the design stage instead of checking the products after they were manufactured. Unlike traditional quality control methods which include a range for the acceptable quality, the Taguchi method introduces a loss function for any product that fails to function at its designed performance level. Thus the quality of a product can be made to achieve a desired level instead of making it fall within a range of acceptance values (Kackar, 1985, Ross, 1988). The Taguchi method utilizes orthogonal arrays to conduct the design of experiments, and this results in a minimization of the variation of a quality characteristic in the presence of reasonable variations in the design of experiments. Since the method could efficiently seek the combination of optimized design parameters, more and more designers and researchers have been applying it in many different engineering fields. Ku et al. (1998) extended the Taguchi method to handle both positive and negative objective function values in engineering optimization problems in the presence of both single and multiple objective functions. Lu et al. (2003) successfully improved the quality of solar water heater products by exploiting the Taguchi method to find a set of optimum manufacturing

factors. Chiang (2006) applied the Taguchi method and the analysis of variance (ANOVA) for designing the heat sink module and wind capacity of a fan for computer CPUs. Kim et al. (2006) reduced the stress value of the lower control arm in the systematic process of vehicle suspension systems by using the Taguchi method. Wu et al. (2009) applied the Taguchi method to determine the optimal combination of six primary operating parameters of a PEM fuel cell, and simulated the phenomenon and electrochemical reactions under the optimal conditions. In all these works, no constraints are considered during the process of implementing the Taguchi method. Jung et al. (2009) proposed a penalized multi-response Taguchi method in the experimental design of finishing hard materials with magnetorheological fluid. They considered a lower bound for the maximization problem and an upper bound for the minimization problem as a constraint; however, no other behavior constraints are considered in the experimental design. In the present work, all geometric parameters, including the blade and rotor sizes, tip speed ratio, and twist and pitch angles, the behavior constraints, including the maximum stress induced and the minimum power coefficient, as well as the manufacturing quality and cost of the unit are all important in achieving a robust HAWT design. The work extends the conventional Taguchi method for solving multi-objective and constrained optimization problems and obtaining an optimum combination of design parameters as well as their tolerances using only limited numbers of experiments.

4.2 Aerodynamic theory

Since the wind turbine blade is an aerodynamic structural component, with an airfoil cross section, HAWT design relies heavily on the aerodynamic theories. The blade parameters, such as length of blade, chord length, pitch angle, twist distribution, taper and blade pre-cone angle should be compatible with the selected airfoil section. Extensive aerodynamic calculations are required during the design approach. Wilson and Lissaman (1974) analyzed the aerodynamic performance of wind turbines using axial momentum theory. This theory assumes the wind to correspond to a one dimensional, incompressible non-viscous flow. It is realized that this theory alone is not enough to provide the information for an accurate design of wind turbines. The blade element momentum theory, originally developed for propellers by Glauert (1935), is combined with the axial momentum theory for analyzing wind turbine performance. Numerous of papers (Maalawi and Badawy, 2001, Maalawi and Badr, 2003, Duquette and Visser, 2003, Buhl, 2005, Lanzafame and Messina, 2007) simulated of wind turbine performance by combining the two theories.

4.2.1 Axial momentum theory

Based on the momentum model, wind turbine blades are replaced by an actuator disk which has no thickness. Momentum is imported to the flow that crosses the disk. The disk is divided into concentric annuli. The stream lines that pass through the boundary of each annulus define a set of concentric annular control volumes. As the theory is based on the one-dimensional assumption (Fig. 4-1), the following equations are applicable:

Continuity equation

$$\rho AV = \rho A_T V_T = \rho A' V' \tag{4.1}$$

Momentum equation

$$T = \rho AV^2 - \rho A' V'^2 \tag{4.2}$$

Bernoulli equation

$$P_0 + 0.5\rho V^2 = P_U + 0.5\rho V_T^2 \tag{4.3}$$

$$P_0 + 0.5\rho V'^2 = P_D + 0.5\rho V_T^2 \tag{4.4}$$

Equations (4.3) and (4.4) yield

$$\Delta P = P_U - P_D = 0.5\rho(V^2 - V'^2) \tag{4.5}$$

$$V_T = 0.5(V + V') \tag{4.6}$$

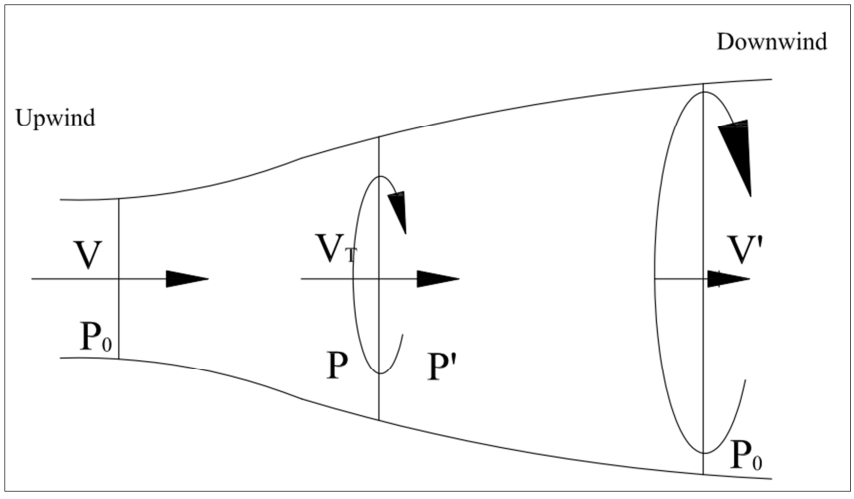

Figure 4-1 Axial flow model

Thus the velocity of the wind stream at the rotor section is the average of the velocities at its upsteam and downsteam sides. By introducing the axial induction factor a as

$$a = \frac{V - V_T}{V} \tag{4.7}$$

V_T and V' can be expressed in terms of V as

$$V_T = V(1 - a) \tag{4.8}$$

$$V' = V(1 - 2a) \tag{4.9}$$

The power developed by the turbine due to the transfer of kinetic energy is given by

$$P_T = 0.5\rho A_T V_T\left(V^2 - V'^2\right) \tag{4.10}$$

Substitution of Eq. (4.8) into Eq. (4.10) yields

$$P_T = 2\rho A_T V^3 a(1 - a) \tag{4.11}$$

By defining the power coefficient as

$$C_p = \frac{P_T}{0.5\rho V^3 A_T} \tag{4.12}$$

Eq. (4.11) can be substituted into Eq. (4.12) to obtain

$$C_p = 4a(1 - a)^2 \tag{4.13}$$

When a = 1/3, Eq. (4.10) has a maximum point equal to 16/27, which is known as the Betz limit.

In order to make the results more realistic, the effect of wake rotation must be considered. Two assumptions must be made in order to describe this effect. The upstream flow is assumed to be entirely axial while the downstream flow is assumed to have rotation at an

angular speed ω. By considering the tangential flow behind the rotor, another factor termed the tangential induction factor a' is introduced:

$$a' = \frac{\omega}{2\Omega} \tag{4.14}$$

where ω is the induced tangential angular velocity of flow and Ω is the angular speed of the rotor.

Equations for the toque and power can be obtained by considering the flow through an annulus at radius r with area

$$A = 2\pi \mathrm{rdr} \tag{4.15}$$

Thus, the thrust force and torque experienced by the annular element may be expressed as

$$dT = 4a(1-a)\frac{1}{2}\rho V^2 2\pi r dr \tag{4.16}$$

$$dM = 4a'(1-a)\frac{1}{2}\rho V^2 2\pi r dr \Omega r^2 \tag{4.17}$$

The power developed by the rotor is equal to the product of this annular elemental torque and the angular velocity, integrated over the total blade span. Thus the power is given by

$$P = \int_0^R \Omega\, 4a'(1-a)\frac{1}{2}\rho V 2\pi r dr \Omega r^2 \tag{4.18}$$

and the power coefficient by

$$C_p = \frac{2}{\rho A_T V^3}\int_0^R \Omega\, 4a'(1-a)\frac{1}{2}\rho V 2\pi r dr \Omega r^2 \tag{4.19}$$

4.2.2 Blade element momentum theory

The blade element momentum (BEM) theory divides the whole rotor blade into a series of airfoil sections, calculates the power, thrust, torque, and other features of each airfoil section, and sums the results. Two assumptions are made in applying the BEM theory:

(1) There is no aerodynamic interaction between the elements.

(2) The force on the blades is determined solely by the lift and drag characteristics of the airfoil shape of the blades.

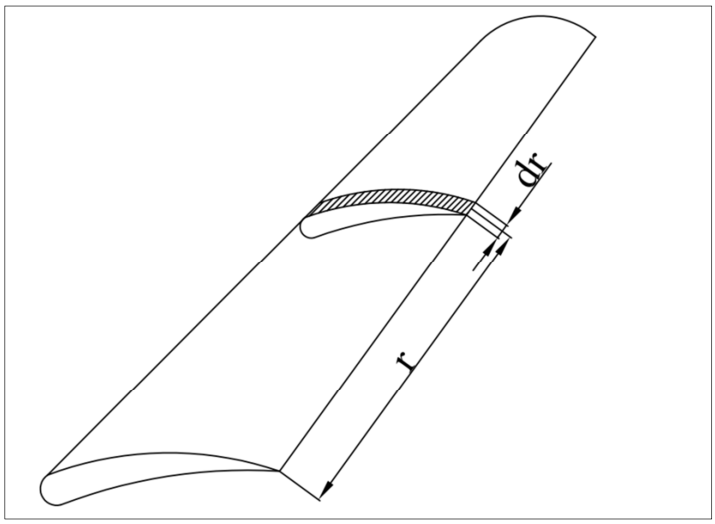

Figure 4-2 A blade element

Consider a blade element of length dr at distance r from the rotor axis as shown in Fig.4-2. The magnitudes of the lift and drag forces developed in this blade element are given by (Bhadra et al., 2005).

$$dF_L = \frac{1}{2}\rho dA_b W^2 C_L \tag{4.20}$$

$$dF_D = \frac{1}{2}\rho dA_b W^2 C_D \tag{4.21}$$

Their resultant gives the total aerodynamic force dF, which can be resolved into the axial thrust dF_T and the moment producing force dF_M . The forces are related to dF_L and dF_D as Fig.4-3:

$$dF_T = dF_L cos\phi + dF_D sin\phi \tag{4.22}$$

$$dF_M = dF_L sin\phi - dF_D cos\phi \tag{4.23}$$

$$dM = r(dF_L sin\phi - dF_D cos\phi) \tag{4.24}$$

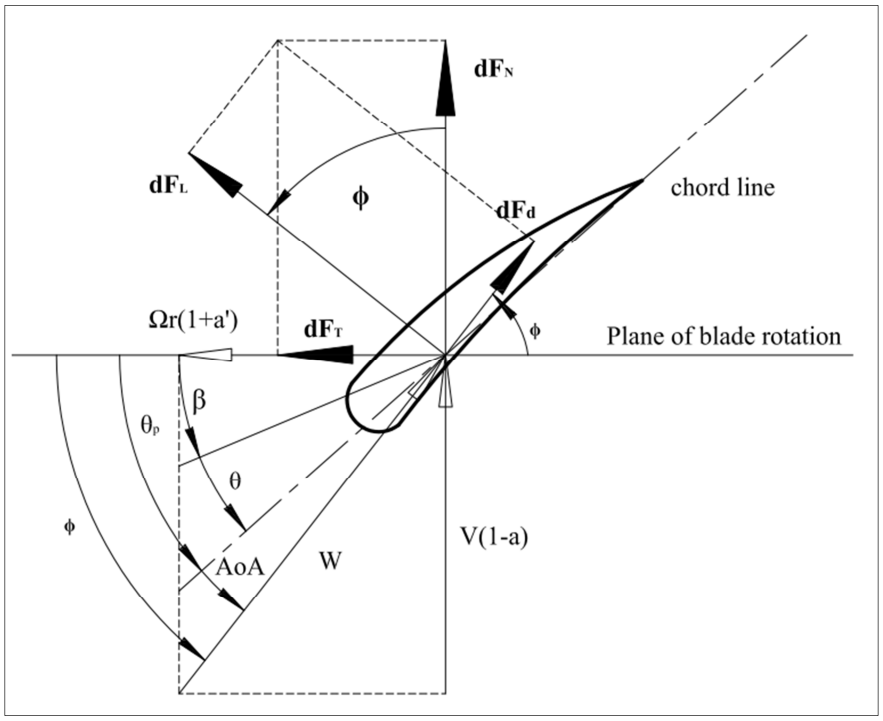

Figure 4-3 Blade geometry for analysis of a horizontal axis wind turbine

The relative wind speed W can be expressed as a function of the wind speed and rotational speed as:

$$W = \frac{V(1-a)}{sin\phi} \tag{4.25}$$

$$W = \frac{\Omega r(1+a')}{cos\phi} \tag{4.26}$$

Substituting Eqs. (4.20),(4.21),(4.25) and (4.26) into Eqs.(4.22) and (4.24) yields

$$dF_T = \frac{1}{2}B\rho dA_b \frac{V^2(1-a)^2}{sin^2\phi}(C_L cos\phi + C_D sin\phi) \tag{4.27}$$

$$dM = \frac{1}{2}B\rho dA_b r \frac{V^2(1-a)^2}{sin^2\phi}(C_L sin\phi - C_D cos\phi) \tag{4.28}$$

$$dP = \omega dM = \frac{1}{2}B\rho dA_b \frac{V^2(1-a)^2}{sin^2\phi}\Omega r(C_L sin\phi - C_D cos\phi) \tag{4.29}$$

It is evident that the torque and the power depend on the angle φ, which is determined by the wind speed and rotational speed. The lift and drag coefficients depend on the angle of attack, which is equal to φ minus the sum of the pitch angle (β) and the twisted angle (θ). The lift and drag coefficient are tested and reported in the literature (Selig et al., 1995, 1996, Selig and Mcgranahan, 2004, Lyon et al., 1998). A simulation program XFOIL, first developed by Drela in 1986 and modified subsequently (Drela, 2001), is also widely used by many designers to find the lift and drag coefficients. In this work, XFOIL version 6.94 is used for calculating the lift and drag coefficients of wind turbine blades.

The force, torque, and power of the entire blade are calculated by adding the corresponding values of all blade elements.

4.2.3 Solution procedure and computer codes

Equations (4.16), (4.18), (4.27) and (4.29) denote the four governing equations for each annular control volume. First, divide the blade into several elements and stat to assume an initial axial induction factor and an initial tangential induction factor in one element.

Then the angle of attack, lift and drag coefficients, thrust and torque distribution along the blade can be calculated by the BEM theory. Next the governing equations can be solved and axial induction and tangential induction factors can be updated until convergence. This process is repeated for other elements to complete the calculation. Some researchers [Benini and Toffolo, 2002, Lanzafame and Messina, 2007, Gur and Rosen, 2008] developed computer codes based on this logic but for different purposes and / or outputs. In this work, the program, WT_Perf from the National Renewable Energy Laboratory, is utilized. WT_Perf uses both the axial momentum and BEM theories to predict the performance of wind turbines. It is a descendent of the PROP code that was originally developed at Oregon State University in 1985 and modified and improved by Jim Tangler of Solar Energy Research Institute (SERI) / National Renewable Energy Laboratory (NREL) and Buhl, Marshall of NREL in the following years (Buhl, 2004).

4.3 Wind Speed Distribution

4.3.1 Wind speed variation with height

The wind data available in the literature is reported by meteorological stations by collecting the data at a special sensor height. In most cases, the data are logged at 10 m as recommended by the World Meteorological Organization. However, designers are more concerned about the wind speed at the height of hub center of HAWTs. The most common expression used for the wind speed is the power law, expressed as:

$$V = V_0(\frac{z}{z_0})^{\alpha} \tag{4.30}$$

where V is the wind speed estimated at the desired height z; V_0 is the wind speed reported at a reference height z_0; and α is the ground surface friction coefficient, given in Table 4-1.

Table 4-1 Friction Coefficient α of Various Terrains (Patel, 2006)

Terrain Type	α
Lake, ocean and smooth, hard ground	0.10
Foot-high grass on level ground	0.15
Tall crops, hedges, and shrubs	0.20
Wooded country with many trees	0.25
Small town with some trees and shrubs	0.30
City area with tall buildings	0.40

4.3.2 Probability density function

HAWTs can be designed to maximize the energy output according to a given wind speed distribution function. Weibull distribution is commonly used to describe the frequency distribution of wind speed.

$$f(v) = \frac{k}{c}(\frac{V}{c})^{k-1} exp\left[-\left(\frac{V}{c}\right)^{k}\right] \tag{4.31}$$

where k denotes the shape factor and c indicates the scale factor. Both these factors are functions of the mean wind speed $\bar{V}$ and the standard deviation of wind speed σ_V, as given by (Justus, 1978, Lysen, 1983):

$$k = \left(\frac{\sigma_V}{\bar{V}}\right)^{-1.086} \tag{4.32}$$

$$\frac{c}{\bar{V}} = (0.568 + \frac{0.433}{k})^{-\frac{1}{k}} \quad (4.33)$$

4.3.3 Average power in the wind

For a unit area of the rotor, the power available at a given wind speed v is

$$P_V = 0.5\rho V^3 \quad (4.34)$$

The total energy of a unit rotor area contributed by all possible wind speeds can be formulated as

$$P_w = \int_0^\infty P_V f(V) dV \quad (4.35)$$

If f(V) follows Weibull distribution, the average power becomes (Lu *et al.* 2002)

$$P_w = \frac{\rho A V^3 \Gamma(1+3/k)}{2(\Gamma(1+1/k))^3} \quad (4.36)$$

4.3.4 Optimum wind speed

The optimum wind speed, u_{op}, is the speed that produces the most energy in a given period, like one day, one month or one year. The wind turbine should be chosen with a rated wind speed that matches this maximum energy wind speed for the purpose of maximizing the energy output. The optimum wind speed can be obtained for any specific probability distribution of the wind speed. If the wind speed follows Weibull distribution, the optimum wind speed can be expressed as (Johnson, 1985)

$$U_{op} = c(\frac{k+2}{k})^{1/k} \quad (4.37)$$

Once the optimum wind speed is known at a given site, the optimal rated wind speed of a wind turbine can also be found. This will help the designer in maximizing the wind energy output based on a relatively simple method.

4.4 Taguchi Method of Design

Taguchi method uses orthogonal arrays to estimate the effects of factors on the mean and variation of the response. Orthogonal arrays allow the investigation of each effect independently and reduce the time and cost associated with the experiment. Standard orthogonal arrays (Lorenzen and Anderson, 1993) are used in most engineering design problems. The purpose of Taguchi-based designs is to reduce the variability in order to achieve the mean value closer to the target. The Taguchi method combines the effects of individual noise factors and computes a signal-to-noise (S/N) ratio for each experiment. There are three commonly used S/N ratios—smaller-the-better, larger-the-better, and nominal-the-better—depending on the desired mean square deviation. Mathematically they are formulated as follows:

Smaller-the-better:

$$\frac{S}{N} = -10log_{10}\left\{\frac{1}{n}\left[\sum_{i=1}^{n}(y_i)^2\right]\right\} \tag{4.38}$$

Larger-the-better:

$$\frac{S}{N} = -10log_{10}\left\{\frac{1}{n}\left[\sum_{i=1}^{n}\left(\frac{1}{y_i}\right)^2\right]\right\} \tag{4.39}$$

Nominal-the-better:

$$\frac{S}{N} = -10log_{10}[S^2] \tag{4.40}$$

where y_i is the i^{th} experimental value, n is the number of experiments and S^2 is the variance of the experimental results.

Taguchi method has been applied mostly for single-objective unconstrained optimization problems. However, in many engineering problems, the design variables are to be selected to optimize multiple objectives and to satisfy a specified set of functional and other requirements (constraints). In this work, a novel extended penalized Taguchi method is proposed for the solution of constrained optimization problems. In this method, the constrained problem is first transformed into an unconstrained optimization problem using the concept of penalty function in nonlinear programming and the resulting unconstrained problem is then solved by the traditional Taguchi method.

Minimize $f(\vec{X})$

subject to: $$g_i(\vec{X}) \leq 0, i = 1,2 \dots, m \tag{4.41}$$

$$h_j(\vec{X}) = 0, j = 1,2 \dots, n \tag{4.42}$$

The equivalent unconstrained optimization problem is formulated as:

$$\text{Minimize } f(\vec{X}) + \sum_{i=1}^{m} R_i \Phi\left(g_i(\vec{X})\right) + \sum_{j=1}^{n} Q_i \Psi\left(h_j(\vec{X})\right) \quad i = 1,2, \dots m; j = 1,2, \dots n \tag{4.43}$$

where Φ and Ψ are the penalty terms defined as

$$\Phi(Y) =< Y >^2 \tag{4.44}$$

where

$$< Y > \; = \begin{Bmatrix} Y & if\ Y > 0 \\ 0 & if\ Y \leq 0 \end{Bmatrix} \tag{4.45}$$

$$\Psi(Z) =< Z >^2 \tag{4.46}$$

where

$$< Z > \; = \begin{Bmatrix} Z & if\ Z > 0 \\ 0 & if\ Z \leq 0 \end{Bmatrix} \tag{4.47}$$

and R_i and Q_j are termed the penalty factors.

4.5 Numerical Example of Robust Design of Wind Turbine Using Taguchi Method

The robust design of wind turbines using Taguchi method is considered to illustrate the proposed methodology. In this work, the robust design includes both parameter design and tolerance design. Parameter design is the process of identifying the optimum settings of the design parameters in order to achieve the maximum wind energy. Tolerance design is the process of seeking optimum setting of the tolerances of design variables in order to control the manufacturing cost and quality.

4.5.1 Parameter design

As indicated in section 4.3, Eq. (4.30) – (4.33) can be used to determine the scale factor c and the shape factor k of Weibull distribution of wind velocity based on original

meteorological data at any specific location. The scale factor c is the mean value of wind speed calculated at the hub height and the shape factor k usually ranges between 1.8 and 2.3 (Bhadra et al. 2005). In this work, k = 1.8 and c = 8 are used. The optimum wind speed computed from Eq. (4.37) is given by:

$$U_{op} = c(\frac{k+2}{k})^{1/k} \approx 12\ m/s \tag{4.48}$$

By using the optimum wind speed as the rated speed, the problem of maximizing the annual wind energy production can be converted to the simpler problem of maximizing the power output in the optimum wind speed.

1. Design parameters and levels

Based on the aerodynamic theories, ten design variables—the chord length at the blade root, twist angles at four locations along the blade, number of blades, rotational speed, pitch angle, rotor radius and hub radius—are chosen for the parameter design with three different levels for each design variable as indicated in Table 4-2.

The chord length at the blade root (design variable A), is chosen to determine the shape of the blade. In order to make the total blade area at the three different design levels competitive, the chord length is assumed to be uniform along the rotor radius at level 1 and change linearly along the blade in levels 2 and 3 as shown in Fig.4-4. In practice, the twist angles (design variables B - E), usually decrease from the tip to the root of a blade, and reach a particular value close to zero at the blade root. Based on this fact, three different sets of twist angles are considered for each blade element as shown in Table 4-2. Numerical values for the various design levels of the rest of design variables are also

listed in Table 4-2. A three-blade tapered profile with practical twist and pitch angles coupled with a rotor having a relatively lower speed is used for the initial design.

The lift and drag coefficients are functions of the angle of attack which can be calculated using the software Xfoil. The selection of a suitable blade profile depends on the performance criterion chosen. More than one airfoil section can be chosen to fit the chosen thickness distribution. Usually a thicker section is need closer to the root for structural reasons, while a thinner section is used along the outboard region with a smooth transition from the root to the tip. Thus, the lift and drag coefficients of different types of airfoils should be fed to different airfoil sections to predict the aerodynamic performance of any arbitrary blade profile. NACA23018 is chosen to specify the airfoil profile along the blade in this study to demonstrate the methodology for simplicity.

Table 4-2 Design variables and their levels

	Design Variable	Unit	Level 1	Level 2	Level 3
A	Blade Chord length (Root)	m	0.50	0.70	0.90*
B	Twist Angle for Element1	deg	8	12*	16
C	Twist Angle for Element2	deg	4	6*	8
D	Twist Angle for Element3	deg	2	3*	4
E	Twist Angle for Element4	deg	0*	1	2
F	Number of Blade	#	2	3*	4
G	Rotational Speed	rpm	75*	125	175
H	Pitch Angle	deg	0	3*	6
I	Rotor Radius	m	4.00	4.25	4.50*
J	Hub Radius	m	0.50	0.75	1.00*

*: Initial design are randomly chosen for comparsion purpose

Other parameters such as the coning angle, tilt angle and yaw angle can also be treated as design variables. However, they are not used in the present work for simplicity. The

coning angle is used for structural reasons rather than for aerodynamic purposes; it is assumed as 0 degrees in this work. The tilt angle, the angle between the wind direction and the rotor axis of rotation, is used for tower accommodation purpose and is assumed as 0 degrees. Finally the yaw angle, which is the misalignment angle between wind and turbine pointing directions, is also assumed as 0 degrees in this work.

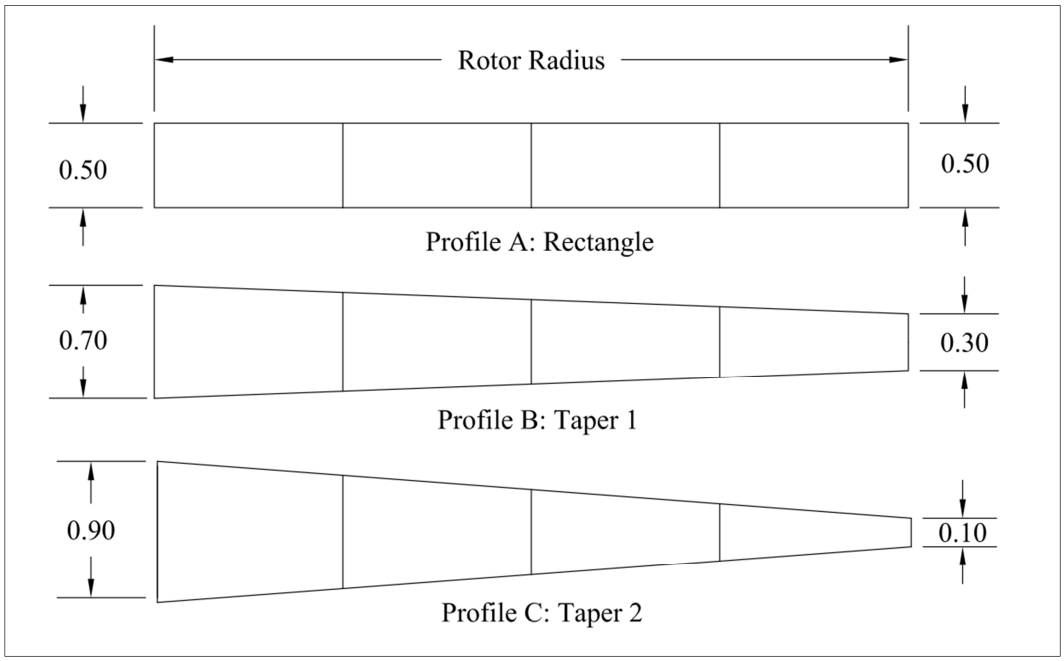

Figure 4-4 Three different levels of shape profiles

Table 4-3 Noise factors and levels

	Design Variable	Unit	Level 1	Level 2
A	Blade Chord length (Root)	m	-0.005	+0.005
B	Twist Angle for Element1	deg	-1	+1
C	Twist Angle for Element2	deg	-0.5	+0.5
D	Twist Angle for Element3	deg	-0.25	+0.25
E	Twist Angle for Element4	deg	-0.125	+0.125
G	Rotational Speed	rpm	-5	+5
H	Pitch Angle	deg	-1	+1
I	Rotor Radius	m	-0.005	+0.005
J	Hub Radius	m	-0.005	+0.005

2. Noise factors and levels

In order to understand the sensitivity of the performance characteristic with respect to variations in the design parameters, noise experiments must be introduced as outer loops. The procedure involves perturbing the design parameters in order to evaluate the effect that the noise factors have on the performance characteristic and to make the factor combination responsible for the noise factors. As shown in Table 4-3, some realistic tolerances have been assumed to all the design variables, except for the number of blade, as noise factors in the parameter design.

3. Parameter design using Taguchi method

The parameter design using Taguchi method uses two matrices—the design parameter matrix and the noise matrix—as shown in Table 4-4. The factional factorial design uses a standard L_{27} (3^{10}) orthogonal array for the inner loop and a standard L_{12} (2^9) orthogonal array for each outer loop. Table 4 shows both the inner array and a typical outer array corresponding to the first run of the inner array. Each inner array has a corresponding outer array. There are 27 inner arrays in all with 12 runs in each outer array, which means that $27 \times 12 = 324$ runs are to be carried out in the experiment. The results of the numerical simulation (experiments) are used to compute the S/N ratio corresponding to larger-the-better performance characteristic as defined in Eq. (39).

Item	Chord length on the Root of the Blade	Twist Angle 1	Twist Angle 2	Twist Angle 3	Twist Angle 4	No. of Blades	Rotational Speed	Pitch	Rotor Radius	Hub Radius
	A	B	C	D	E	F	G	H	I	J
Unit	m	deg	deg	deg	deg	#	rpm	deg	m	m
1	0.5	16	8	4	2	2	75	0	4.00	0.50
2	0.5	16	8	4	1	3	125	3	4.25	0.75
3	0.5	16	8	4	0	4	175	6	4.50	1.00
4	0.5	12	6	3	2	2	75	3	4.25	0.75
5	0.5	12	6	3	1	3	125	6	4.50	1.00
6	0.5	12	6	3	0	4	175	0	4.00	0.50
7	0.5	8	4	2	2	2	75	6	4.50	1.00
8	0.5	8	4	2	1	3	125	0	4.00	0.50
9	0.5	8	4	2	0	4	175	3	4.25	0.75
10	0.7	16	6	2	2	3	175	0	4.25	1.00
11	0.7	16	6	2	1	4	75	3	4.50	0.50
12	0.7	16	6	2	0	2	125	6	4.00	0.75
13	0.7	12	4	4	2	3	175	3	4.50	0.50
14	0.7	12	4	4	1	4	75	6	4.00	0.75
15	0.7	12	4	4	0	2	125	0	4.25	1.00
16	0.7	8	8	3	2	3	175	6	4.00	0.75
17	0.7	8	8	3	1	4	75	0	4.25	1.00
18	0.7	8	8	3	0	2	125	3	4.50	0.50
19	0.9	16	4	3	2	4	125	0	4.50	0.75
20	0.9	16	4	3	1	2	175	3	4.00	1.00
21	0.9	16	4	3	0	3	75	6	4.25	0.50
22	0.9	12	8	2	2	4	125	3	4.00	1.00
23	0.9	12	8	2	1	2	175	6	4.25	0.50
24	0.9	12	8	2	0	3	75	0	4.50	0.75
25	0.9	8	6	4	2	4	125	6	4.25	0.50
26	0.9	8	6	4	1	2	175	0	4.50	0.75
27	0.9	8	6	4	0	3	75	3	4.00	1.00

Inner array L_{27} (3^{10})

Item	Shape Profile	Twist Angle 1	Twist Angle 2	Twist Angle 3	Twist Angle 4	Rotational Speed	Pitch	Rotor Radius	Hub Radius
	A	B	C	D	E	G	H	I	J
Unit	m	deg	deg	deg	deg	rpm	deg	m	m
1	0.495	15	7.5	3.75	1.875	70	-1	3.95	0.495
2	0.495	15	7.5	3.75	1.875	80	1	4.05	0.505
3	0.495	15	8.5	4.25	2.125	70	-1	3.95	0.505
4	0.495	17	7.5	4.25	2.125	70	1	4.05	0.495
5	0.495	17	8.5	3.75	2.125	80	-1	4.05	0.495
6	0.495	17	8.5	4.25	1.875	80	1	3.95	0.505
7	0.505	15	8.5	4.25	1.875	70	1	4.05	0.495
8	0.505	15	8.5	3.75	2.125	80	1	3.95	0.495
9	0.505	15	7.5	4.25	2.125	80	-1	4.05	0.505
10	0.505	17	8.5	3.75	1.875	70	-1	4.05	0.505
11	0.505	17	7.5	4.25	1.875	80	-1	3.95	0.495
12	0.505	17	7.5	3.75	2.125	70	1	3.95	0.505

Outer array L_{12} (2^9)

Table 4-4 Specific values chosen for the design parameters (Inner Array) and values of noise factor (Outer Array)

Table 4-5 Results of the 27 experiments of parameter design

Chord length on the Root of the Blade (m)	Twist Angles (1-4) (deg)				No. of Blades	Rotational Speed (rpm)	Pitch (deg)	Rotor Radius (m)	Hub Radius (m)	Mean (kW)	S/N (kW)
0.5	16	8	4	2	2	75	0	4	0.5	12.99	22.27
0.5	16	8	4	1	3	125	3	4.25	0.75	26.46	28.45
0.5	16	8	4	0	4	175	6	4.5	1	14.39	23.16
0.5	12	6	3	2	2	75	3	4.25	0.75	15.36	23.73
0.5	12	6	3	1	3	125	6	4.5	1	25.24	28.04
0.5	12	6	3	0	4	175	0	4	0.5	21.48	26.64
0.5	8	4	2	2	2	75	6	4.5	1	16.69	24.45
0.5	8	4	2	1	3	125	0	4	0.5	24.4	27.75
0.5	8	4	2	0	4	175	3	4.25	0.75	26.9	28.59
0.7	16	6	2	2	3	175	0	4.25	1	26.44	28.45
0.7	16	6	2	1	4	75	3	4.5	0.5	28.32	29.04
0.7	16	6	2	0	2	125	6	4	0.75	17.27	24.75
0.7	12	4	4	2	3	175	3	4.5	0.5	29.86	29.5
0.7	12	4	4	1	4	75	6	4	0.75	20.41	26.2
0.7	12	4	4	0	2	125	0	4.25	1	24.02	27.61
0.7	8	8	3	2	3	175	6	4	0.75	17.26	24.74
0.7	8	8	3	1	4	75	0	4.25	1	23.8	27.53
0.7	8	8	3	0	2	125	3	4.5	0.5	25.66	28.19
0.9	16	4	3	2	4	125	0	4.5	0.75	31.36	29.93
0.9	16	4	3	1	2	175	3	4	1	18.03	25.12
0.9	16	4	3	0	3	75	6	4.25	0.5	17.63	24.92
0.9	12	8	2	2	4	125	3	4	1	22.94	27.21
0.9	12	8	2	1	2	175	6	4.25	0.5	16.14	24.16
0.9	12	8	2	0	3	75	0	4.5	0.75	20.47	26.22
0.9	8	6	4	2	4	125	6	4.25	0.5	22.89	27.19
0.9	8	6	4	1	2	175	0	4.5	0.75	28.52	29.1
0.9	8	6	4	0	3	75	3	4	1	15.4	23.75

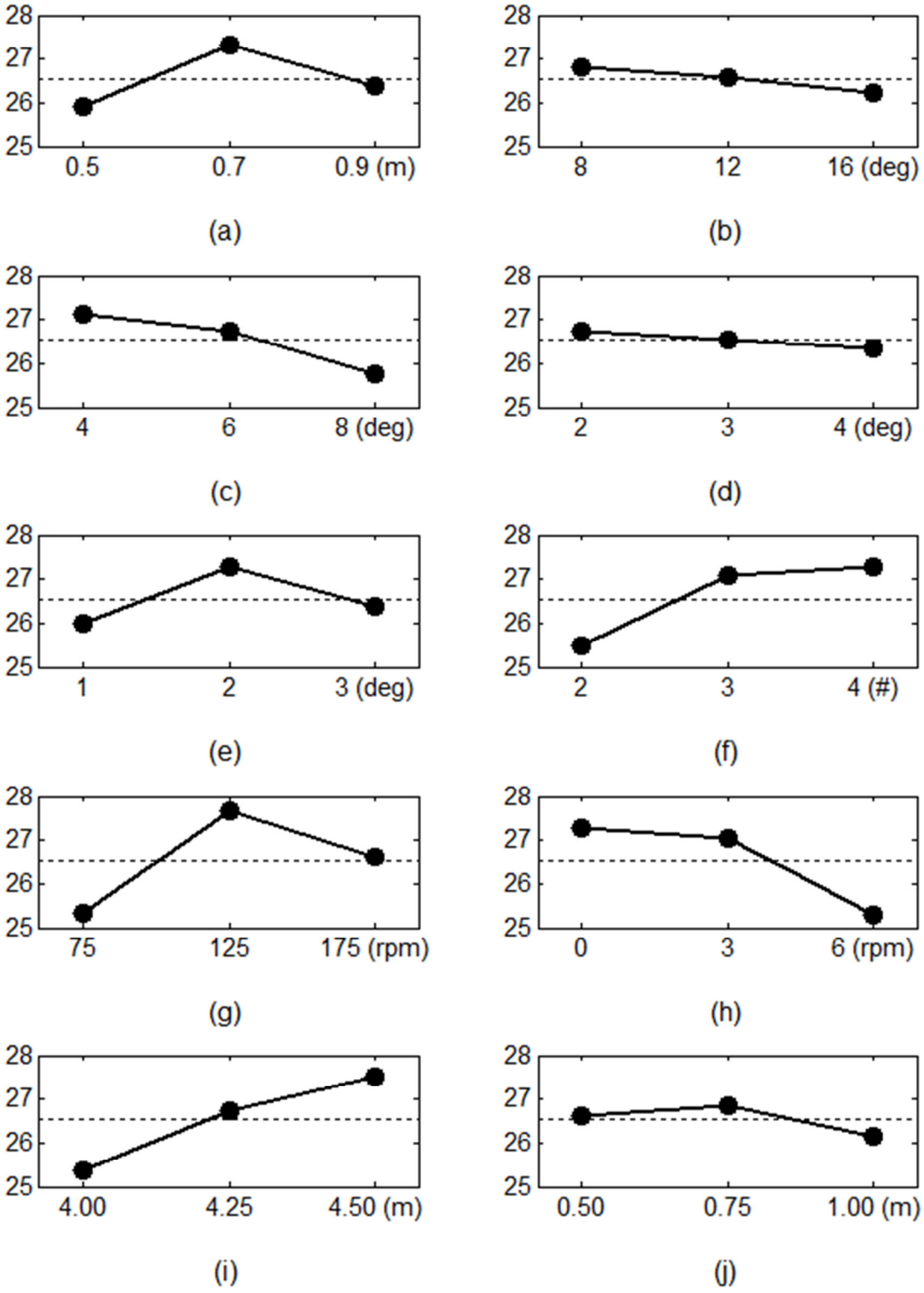

Figure 4-5 Response graphs for the S/N ratio (Parameter design)

Table 4-6 Results of analysis of variance (ANOVA) for S/N ratios

	Item	Degree of Freedom (DF)	Sum of Square (SS)	Mean of Square (MS)	F	P	Rank
A	Chord length on the Root of the Blade	2	9.553	4.7767	3.95	0.081	5
B	Twist Angle 1	2	1.534	0.7672	0.63	0.563	9
C	Twist Angle 2	2	8.726	4.3628	3.6	0.094	6
D	Twist Angle 3	2	0.631	0.3154	0.26	0.779	10
E	Twist Angle 4	2	7.76	3.8802	3.21	0.113	7
F	Number of Blades	2	15.871	7.9353	6.56	0.031	4
G	Rotational Speed	2	24.578	12.289	10.15	0.012	1
H	Pitch	2	21.444	10.722	8.86	0.016	2
I	Rotor Radius	2	21.014	10.507	8.68	0.017	3
J	Hub Radius	2	2.363	1.1816	0.98	0.429	8
	Error	6	7.262	1.2104			
	Total	26	120.73				

All the 27 simulation results are summarized in Table 4-5. The factor response graphs, based on their S/N ratios, of the design variables are shown in Fig.4-5. The results indicate the design of HAWT for maximum power (correspond to the larger-the-better characteristic of the S/N ratio) and the optimum design correspond to the settings A_2, B_1, C_1, D_1, E_2, F_3, G_2, H_1, I_3, and J_2. The results of the analysis of variance (ANOVA) of the S/N ratios are shown in Table 4-6. The P value is usually used to identify the significance of different design variables with a smaller P value indicating that the corresponding design value is statistically more important.

It is evident that the rotational speed (G) has the lowest P-value and hence is statistically the most important parameter with respect to S/N ratio among all the design variables and G_2, a rotational speed of 125 rpm, turns out to be the best choice. The pitch angle (H) stands at rank 2 with respect to the S/N ratio and H_1 is the best choice. It can be observed

that the S/N ratio reduces only a little when the pitch angle changes from 0 to 3 degrees. However, when the pitch angle changes from 3 to 6 degrees, the S/N ratio reduces dramatically. The rotor radius (I), which has a slightly larger P-value than that of the pitch angle, is the third important design parameter with respect to the S/N ratio. It is obvious that the larger the radius, the better the performance. Hence, I_3 emerges as the optimum design. The number of blades (F) is the fourth important design variable in terms of the S/N ratio. As indicated in Fig.4-5, a four-blade design (F_3) seems to be the best choice since it displays the highest S/N ratio. However, it can be detected from the plots that the power output of the three-blade wind turbine (F_2) is considerably larger than that of the two-blade design (F_1) but the improvement of the four-blade wind turbine (F_3) is negligible compared to the three-blade design (F_2). Since increasing the number of blades by one will significantly increase the cost of the wind turbine system, the three-blade wind turbine design (F_2) is clearly the best choice in this optimization problem. The chord length at the blade root ranks fifth, and a tapered shape design (A_2) proves to have the largest S/N ratio and obviously becomes the best choice. Similarly B_1, C_1, D_1, E_2 and J_2 are the optimum settings for the twist angles at locations 1 to 4 and hub radius respectively. It can be noticed that these design parameters rank from 6 to 10 and have relatively larger P-values compared to the previous design variables in ANOVA. This indicates that these design variables are not statistically as significant as the previously discussed design variables with respect to the S/N ratio. As a result, the design combination A_2, B_1, C_1, D_1, E_2, F_2, G_2, H_1, I_3, and J_2 is chosen as the optimum solution. The design variable settings for both the initial design and optimum design are summarized in Table 4-7. The power output of the optimum design is 32.76 kW

compared to a value of 21.11 kW at the initial design; thus an improvement of 55% has been achieved through optimization.

Table 4-7 Comparison of Initial design and optimum design

Design Variable		Initial	Optimum
Chord length on the Root of the Blade	(m)	0.9	0.7
Twist Angle 1	(deg)	12	8
Twist Angle 2	(deg)	6	4
Twist Angle 3	(deg)	3	2
Twist Angle 4	(deg)	0	1
No. of Blades		3	3
Rotational Speed	(rpm)	75	125
Pitch	(deg)	3	0
Rotor Radius	(m)	4.50	4.50
Hub Radius	(m)	1.00	0.75
Power	(kW)	21.11	32.76

4. Parameter design with constraints using penalized Taguchi method

The parameter design using the traditional Taguchi method can be considered as an unconstrained optimization method. However, most practical problems involve some behavior constraints. In the HAWT design problem, the power coefficient, defined as the ratio of the actual power developed by the rotor to the theoretical power available in the wind, is an important index that can be used as a measure of the efficiency of a wind turbine. Hence a minimum acceptable value of the power coefficient can be specified as a constraint (Eq. (4.49)).

$$C_p - C_{p,min} \geq 0 \qquad (4.49)$$

The cyclic load acting on the structure of a wind turbine could cause fatigue failure. Hence a constraint can be placed either on the maximum stress induced or the maximum

permissible fractional fatigue damage in the design problem. Since wind turbines are usually fixed in position and rotate for many years, a large safety factor must be considered in the design stage. The stress at the root of the blade is larger than that at other positions along the blade; hence the stress induced at the root of the wing is to be constrained to be less than a particular value (depending on the blade material), by considering a reasonable factor of safety as:

$$\sigma - \frac{\sigma_{max}}{C_{Safety}} \leq 0 \tag{4.50}$$

Additional constraints such as limitations on mass, acoustic and vibration performance as well as cost can also be included in the design optimization problem. In this work, only the constraints (4.49) and (4.50) are considered.

The new objective function can be formulated in the format of Eq. (4.43) by applying the penalty terms. By using the values of $C_{pmin} = 0.35$ and $\sigma_{max}/C_{SAFTY} = 3.5$ MPa with the corresponding penalty factors $R_1 = 20$ and $R_2 = 60$, the original constrained optimization problem is converted into an equivalent unconstrained optimization problem, and the results of the penalized Taguchi approach are shown in Table 4-8. It can be seen from Table 4-8, that no constrained is violated in cases 5, 11, 14, 17, 22 and 25; therefore, the mean values of the new objective functions remain the same as the values of the original objective functions. In other cases, either the constraint of Eq.(4.49) or Eq.(4.50) has been violated; therefore the penalty terms have been added in the new objective functions, which make the mean values of new objective functions less than the original ones. The S/N ratios using the larger-the-better rule (Eq.(4.39)) are calculated using the inner loop

with standard $L_{27}(3^{10})$ orthogonal array and the outer loops with standard $L_{12}(2^9)$ orthogonal array and the results are presented in Table 4-8.

Table 4-8 Results of parameter design using penalized Taguchi method

Outputs	Power (Orginial objective function)	Power coefficient		stress		Y_1	Y_2	New objective function	
Unit	kW	-	Violate constraint (Yes/No)	MPa	Violate constraint (Yes/No)	-	-	Mean	S/N
1	12.99	0.24	Yes	3.26	No	0.31	0	11.14	20.94
2	26.46	0.44	No	3.76	Yes	0	0.07	26.14	28.35
3	18.283	0.27	Yes	2.29	No	0.23	0	17.26	24.74
4	15.36	0.26	Yes	3.22	No	0.27	0	13.89	22.86
5	25.24	0.37	No	3.08	No	0	0	25.24	28.04
6	21.05	0.39	No	4.38	Yes	0	0.25	17.25	24.73
7	16.69	0.25	Yes	3.03	No	0.29	0	14.96	23.5
8	24.4	0.46	No	4.41	Yes	0	0.26	20.31	26.15
9	26.9	0.45	No	3.9	Yes	0	0.11	26.12	28.34
10	26.44	0.44	No	4.2	Yes	0	0.2	24.07	27.63
11	28.32	0.42	No	3.42	No	0	0	28.32	29.04
12	17.27	0.32	Yes	2.31	No	0.07	0	17.16	24.69
13	29.86	0.44	No	4.64	Yes	0	0.33	23.48	27.41
14	20.41	0.38	No	1.81	No	0	0	20.41	26.2
15	24.02	0.4	No	4.36	Yes	0	0.25	20.41	26.2
16	17.26	0.32	Yes	1.82	No	0.07	0	17.15	24.68
17	23.8	0.4	No	2.45	No	0	0	23.8	27.53
18	25.66	0.38	No	5.45	Yes	0	0.56	7.02	16.92
19	31.36	0.46	No	3.71	Yes	0	0.06	31.15	29.87
20	18.03	0.34	Yes	2.62	No	0.03	0	18.01	25.11
21	17.63	0.29	Yes	2.2	No	0.16	0	17.09	24.66
22	22.94	0.43	No	1.82	No	0	0	22.94	27.21
23	16.14	0.27	Yes	2.66	No	0.23	0	15.05	23.55
24	20.47	0.3	Yes	2.96	No	0.13	0	20.11	26.07
25	22.89	0.38	No	2.11	No	0	0	22.89	27.19
26	28.52	0.42	No	5.7	Yes	0	0.63	4.92	13.83
27	15.4	0.29	Yes	1.56	No	0.18	0	14.77	23.39

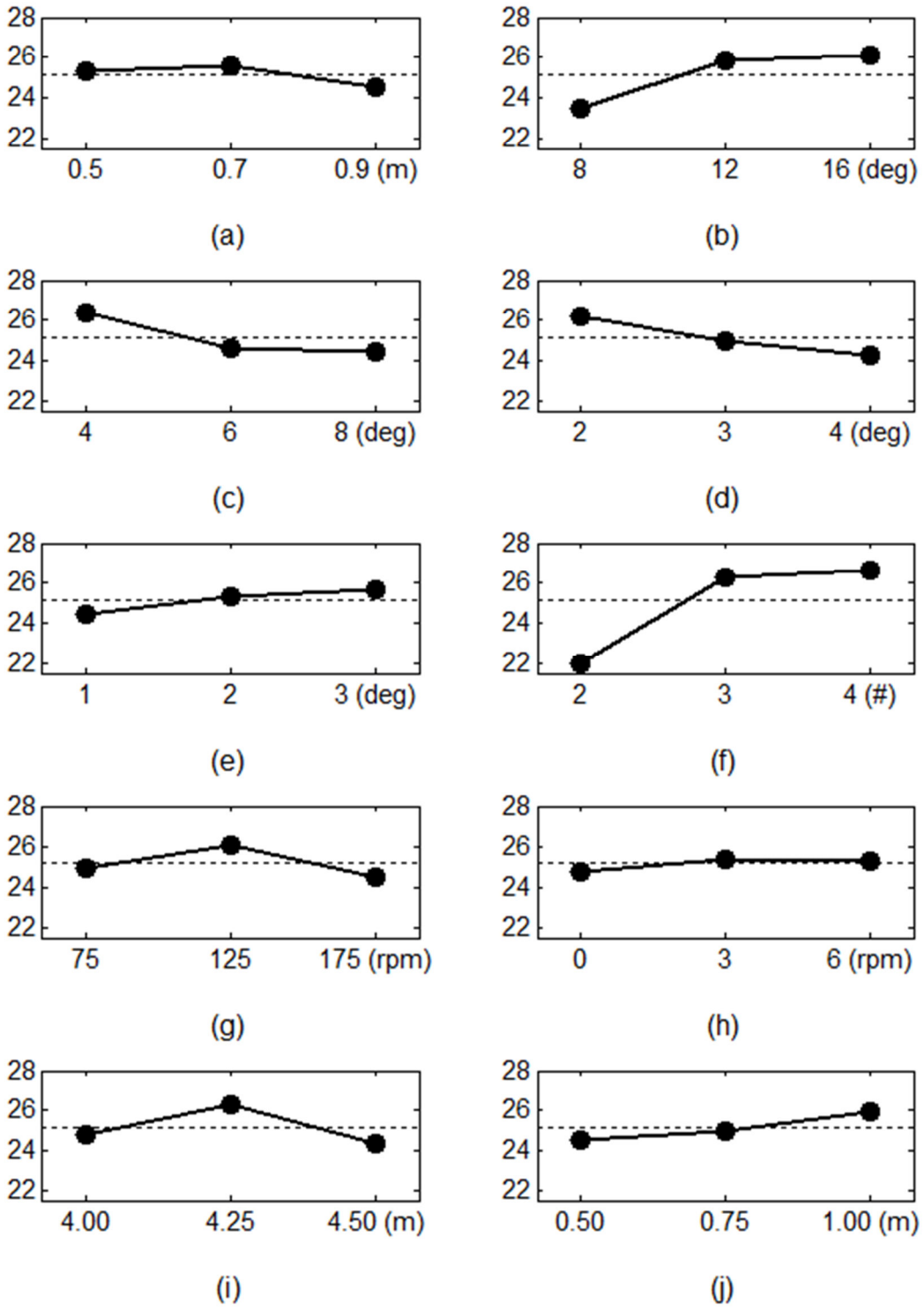

Figure 4-6 Response graph for S/N ratio (Parameter design using Penalized Taguchi Method)

Table 4-9 Comparison of Initial design and Optimum results by Traditional and Penalized Taguchi Methods

Design variable	Power (Original objective function) (kW)	Constraint 1: Power coefficient (Minimum requirement 0.35)		Constraint 2: Stress induced (Maximum limit 3.50)	
		-	Violation of constraint (Yes/No)	(Mpa)	Violation of constraint (Yes/No)
Initial design	21.11	0.31	Yes	2.36	No
Optimum results of traditional Taguchi method	32.24 (+52.7%)	0.48	No	5.31	Yes
Optimum results of penalized Taguchi method	25.76 (+22.0%)	0.43	No	3.04	No
Additional Experiment (Refinement)	27.79 (+31.6%)	0.43	No	3.5	No, but active

The effect of each design variable with respect to the corresponding S/N ratio is shown in Figure 4-6. The optimum design variable combination given by the penalty-based Taguchi method are A_2, B_3, C_1, D_1, E_3, F_3, G_2, H_2, I_2, J_3. Compared to the optimum design variables given by the unconstrained problem, the optimum levels of design variables B, E, H, I and J changed while the the rest of the design variables A, C, D, F and G remained the same with no change. Similar to the adjustment made for the optimum level of the design variable F for the purpose of cost in the previous example, the design level of F_3 is adjusted to F_2 for the same reason in the present case. Therefore, the optimum design variable combination becomes A_2, B_3, C_1, D_1, E_3, F_2, G_2, H_2, I_2, J_3.

The initial design, the optimum design given by the traditional Taguchi method and the optimum design given by the penalized Taguchi method are summarized in Table 4-9. All the constraints are satisfied though the power obtained by the penalized Taguchi method is 6.48 kW less compared to the result given by the traditional (unconstrained) Taguchi method.

In the constrained optimization problem, it can be observed that none of the constraints is close to zero at the optimum point which implies that the optimum point can be further improved. Since the Taguchi optimization method is based on discrete levels of design variables, by refining the design variable levels or by using the response surface methodology, a better optimum solution can be found. In the present case, some of the design variables that have relatively larger influence on the S/N ratio, namely—twist angles 1 and 2, rotational speed rotor radius and pitch angle—are used in conducting an additional fractional factorial design of experiments by using new design levels (settings). The remaining design variables are also incorporated in the additional experimentation by using the old design levels. The new experiment still uses a standard L_{27} (3^{10}) orthogonal array for the inner loop and a standard L_{12} (2^9) orthogonal array for each outer loop. The new design levels (over a smaller range for each variable) are determined based on the results shown in Fig. 6. The results of the new design of experiments are summarized in Table 8 and Fig. 7. The design level combination A_2, B_2, C_1, D_1, E_2, F_2, G_2, H_2, I_3, and J_2 is chosen as the optimum solution. The power output with this choice is further improved by about 9.6%, from 25.76 to 27.79 kW. Although the power is still less than the result obtained with the unconstrained optimization example, the stress constraint is active at the current design (Table 9).

Table 4-10 Refinement of design levels and results by penalized Taguchi method

Outputs	Power (Original objective function)	Power coefficient		stress		Y_1	Y_2	New objective function	
Unit	kW	-	Violate constraint (Yes/No)	Mpa	Violate constraint (Yes/No)	-	-	Mean	S/N
1	19.988	0.3526	No	4.598549	Yes	0.00	0.31	7.08	17.00
2	27.071	0.4498	No	3.8409396	Yes	0.00	0.10	25.89	28.26
3	24.565	0.3852	No	2.5232904	No	0.00	0.00	18.28	25.24
4	20.365	0.3384	Yes	3.8720529	Yes	0.03	0.11	14.66	23.32
5	24.391	0.3825	No	2.8982059	No	0.00	0.00	25.24	28.04
6	24.049	0.4242	No	4.6063273	Yes	0.00	0.32	15.05	23.55
7	19.026	0.2983	Yes	3.1035539	No	0.15	0.00	16.25	24.22
8	26.317	0.4642	No	4.8910142	Yes	0.00	0.40	14.92	23.48
9	27.954	0.4645	No	3.8113819	Yes	0.00	0.09	26.42	28.44
10	27.11	0.4505	No	4.0120629	Yes	0.00	0.15	25.16	28.01
11	30.808	0.4831	No	3.6869287	Yes	0.00	0.05	28.14	28.99
12	18.752	0.3308	Yes	3.0335489	No	0.05	0.00	17.21	24.72
13	29.038	0.4553	No	4.2889714	Yes	0.00	0.23	26.82	28.57
14	24.417	0.4307	No	2.1966005	No	0.00	0.00	20.41	26.20
15	23.993	0.3987	No	4.3792001	Yes	0.00	0.25	20.24	26.12
16	20.93	0.3692	No	2.2728282	No	0.00	0.00	17.26	24.74
17	27.708	0.4604	No	2.9697666	No	0.00	0.00	23.80	27.53
18	24.903	0.3905	No	5.0979178	Yes	0.00	0.46	13.16	22.38
19	29.353	0.4603	No	3.4037974	No	0.00	0.00	31.36	29.93
20	19.176	0.3382	Yes	2.804866	No	0.03	0.00	18.01	25.11
21	21.839	0.3629	No	2.5932954	No	0.00	0.00	17.63	24.92
22	24.543	0.4329	No	2.0659246	No	0.00	0.00	22.94	27.21
23	18.124	0.3012	Yes	2.9339863	No	0.14	0.00	15.75	23.95
24	26.198	0.4108	No	3.4458004	Yes	0.00	0.00	20.47	26.22
25	23.202	0.3855	No	2.1437079	No	0.00	0.00	22.89	27.19
26	26.163	0.4102	No	4.8474556	Yes	0.00	0.38	19.63	25.86
27	21.07	0.3717	No	2.1110389	No	0.00	0.00	15.40	23.75

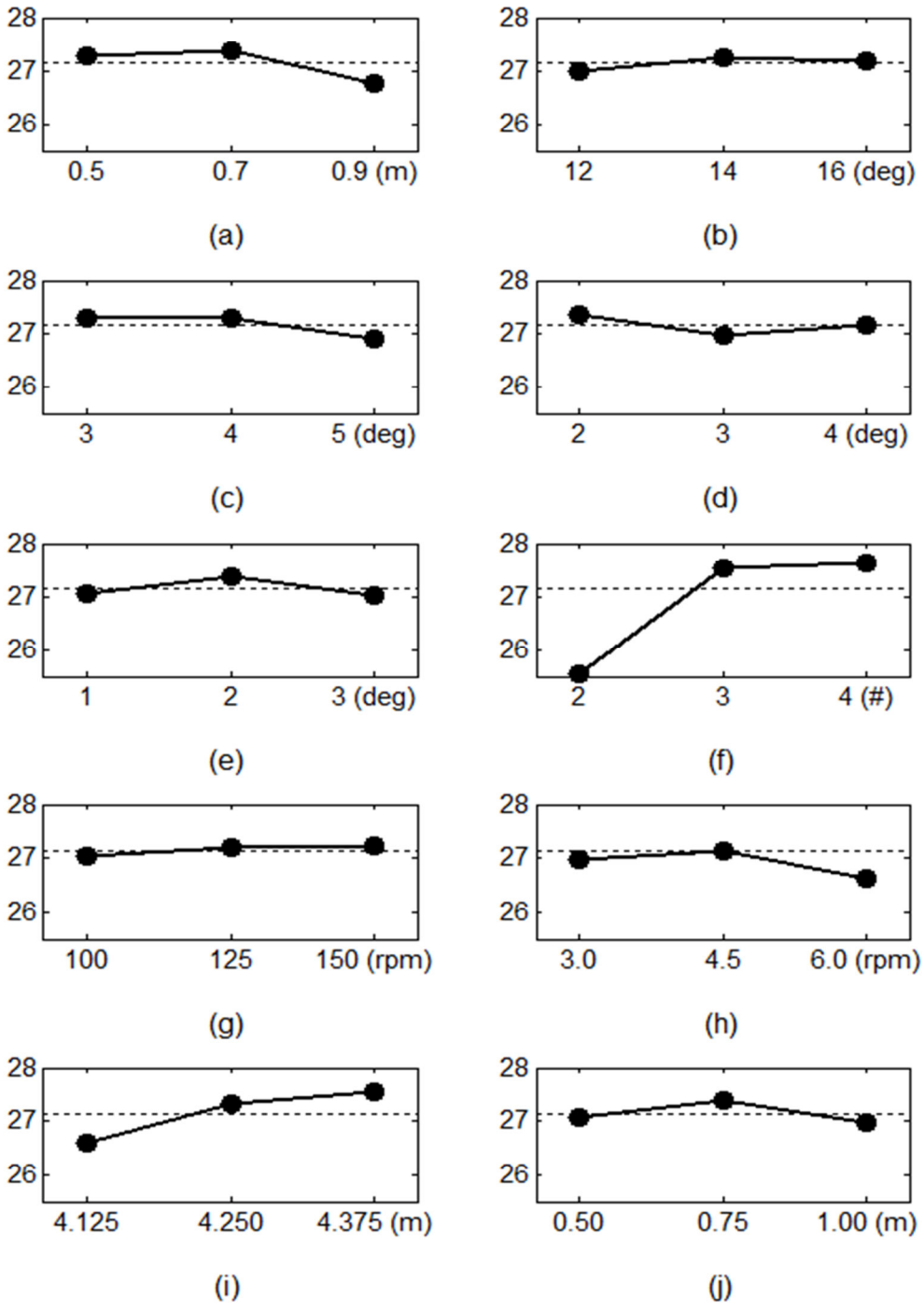

Figure 4-7 Response graph for S/N ratio (Refine Design level in Penalized Taguchi Method)

4.5.2 Tolerance design

In any manufacturing process, it is impractical to achieve the exact values of dimensions. Under certain stable fabrication conditions, the dimensions of each machined / manufactured component vary within a certain small controlled range, called tolerances. The tolerance values are specified for any desired dimensions based on functional requirements as well as cost. The purpose of tolerance design of HAWTs is to achieve quality, reliability and less fluctuation in power at a reasonable cost. However, there is always a conflict between tolerance and the cost of quality control. Smaller tolerances require higher costs and hence a small cost may correspond to large tolerances as well as lower quality. A typical tolerance-cost relation curve is displayed in Fig. 4-8. As tolerance increases, the cost goes down steeply at the beginning, and then the trend becomes gradually less. Since both quality and cost of the product are important in manufacturing, a combination of these two factors is considered as the objective function in the tolerance design process.

1. Tolerance levels and cost

In the tolerance design process, each of the design variables used in the parameter design stage except one, namely the number of blades, are assumed to have three different levels of tolerance as shown in Table 4-11. The relative costs to control each design variable of a HAWT used in this work are summarized in Fig. 4-9. The optimum solution achieved in the parameter design stage is used as the mean value for tolerance design. In this work, the optimum design variables found by the traditional Taguchi method in the parameter stage are assumed as the mean values in the tolerance design.

The chord length, a linear dimension, is assumed to have three different tolerance levels, namely, ±1.0%, ±0.5% and ±0.2%, which correspond to ±7 mm, ±3.5 mm and ±1.4 mm, respectively. The cost to control the tolerance of the chord length is relatively cheap as shown in Fig. 4-9(a), since it is a small dimension. Four different twist angles have been combined into one control (tolerance) factor since one tolerance value is enough to control all the four twist angles during the manufacturing process. As twist angle is more difficult to control compared to linear dimension during manufacturing, three relatively larger tolerance values, namely, ±10%, ±5% and ±2%, are assumed for this factor and the cost of controlling the twist angle is assumed to be five times more than the linear dimension control and is indicated in Fig. 4-9(b). The rotational speed is assumed to have a one side tolerance because a higher rotational speed increases the risk of failure and might result in an extra cost that exceeds the material cost of the whole system. The variations of -6 rpm, -4 rpm and -2 rpm about the optimum value of 125 rpm are set as three different tolerance levels and these levels are not too difficult to achieve in practice. Hence the cost is assumed to be slightly higher than that of controlling a linear dimension as shown in Fig. 4-9(c). The pitch angle is a parameter that needs to be controlled especially for large wind speeds. Any inaccuracy in setting the initial pitch angle may affect the performance at large wind speeds. Therefore, ±1.0º, ±0.5 º and ±0.2º are considered as the tolerance levels for this parameter. Since pitch angle is an angular dimension, the same cost as in the case of controlling the twist angle, is assumed as shown in Fig. 4-9(d). The rotor radius is assumed to have three different levels of tolerance—±0.5%, ±0.2% and ±0.1%—which correspond to physically ±22.5mm, ±9mm and ±4.5mm, respectively. Since this is a large dimension and all three blades must be

controlled simultaneously, it is relatively more expensive than other design variables as indicated in Fig. 4-9(e). Similarly, the hub radius is assumed to have three tolerances, ±1.0%, ±0.5% and ±0.2%, which physically imply ±7.5mm, ±3.75mm and ±1.5mm, respectively. The cost of controling the tolerance of hub radius is assumed to lie between the costs of controlling linear dimensions and angular dimensions and is shown in Fig. 4-9(f).

2. Details of tolerance design

As in the case of parameter design, the tolerance design using Taguchi method involves the use of two matrices—a design parameter matrix and a noise matrix—as shown in Table 12. The fractional factorial design uses a standard L_{27} (3^6) orthogonal array for the inner loop and a standard L_8 (2^5) for each of the outer loops. Table 12 shows both the inner loop and a typical outer loop that corresponds to the first run of the inner loop. There will be 27 outer arrays in all with 8 runs in each outer array, which implies that 27 × 8 = 216 runs will be carried out in the experiment. The results from the numerical experiments are transformed into the S/N ratios. In this case, the smaller-the-better type of performance characteristic is applicable. Mathematically it is formulated as indicated by Eq.(4.38) with y_i is defined as a combination term including fluctuations of both power and cost. It is chosen as the product of the two terms as:

$$y_i = \Delta P_i \times Cost_i \tag{4.51}$$

where ΔP_i is the difference between actual power and optimum power and $Cost_i$ is the total cost of controlling the tolerance of the i^{th} design variable.

Table 4-11 Control factors and levels in tolerance design

	Control factor	Optimum value	Tolerance	
A	Chord length	0.70 m	Level 1	±1.0%
			Level 2	±0.5%
			Level 3	±0.2%
B	Twist angle	$\begin{Bmatrix}8\\4\\2\\1\end{Bmatrix}$ deg	Level 1	±10.0%
			Level 2	±5.0%
			Level 3	±2.0%
C	Rotational Speed	125 rpm	Level 1	-6 rpm
			Level 2	-4 rpm
			Level 3	-2 rpm
D	Pitch Angle	0 deg	Level 1	±1.0 deg
			Level 2	±0.5 deg
			Level 3	±0.2 deg
E	Rotor Radius	4.50 m	Level 1	±0.5%
			Level 2	±0.2%
			Level 3	±0.1%
F	Hub Radius	0.75 m	Level 1	±1.0%
			Level 2	±0.5%
			Level 3	±0.2%

Figure 4-8 Sample tolerance-cost curve

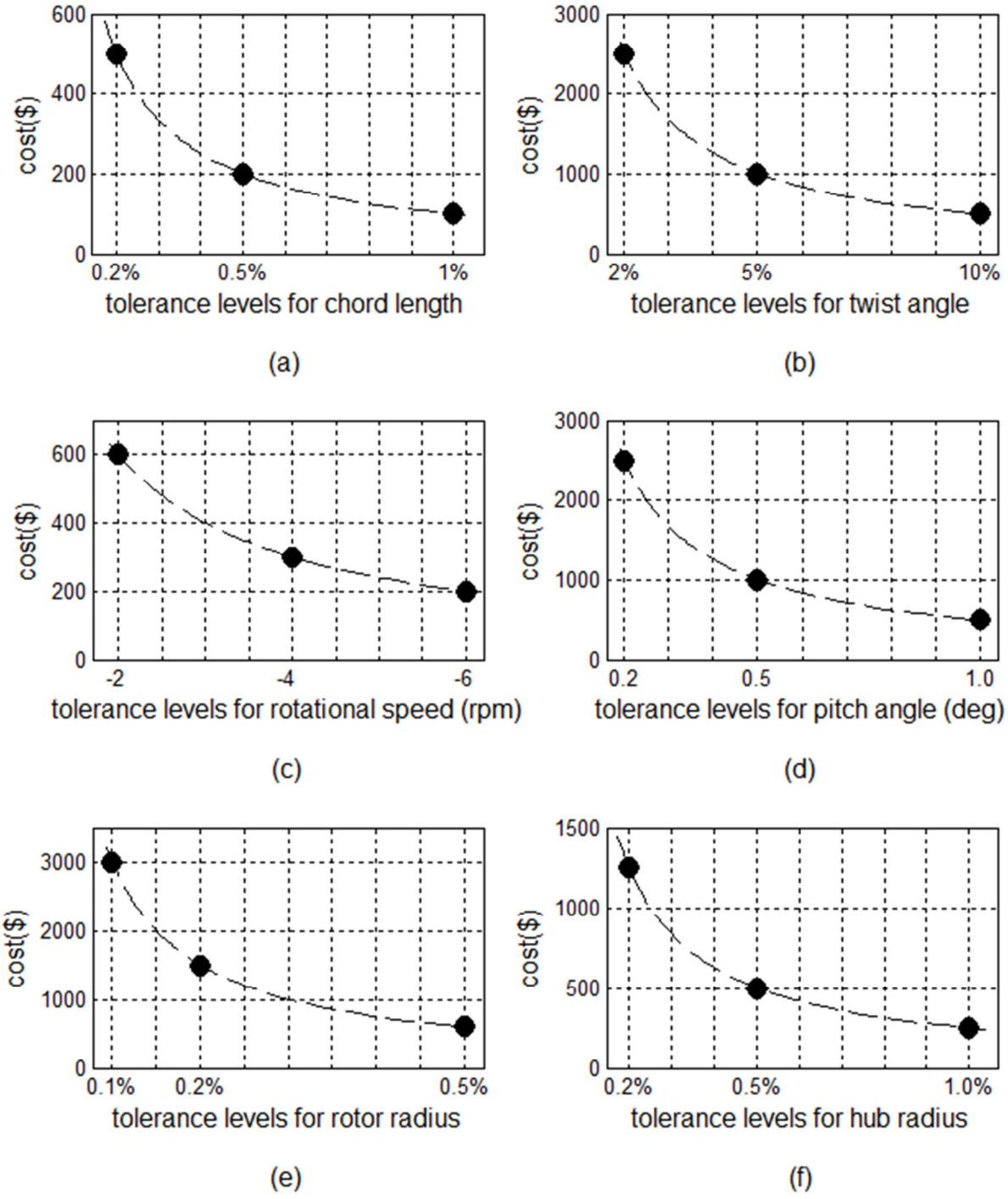

Figure 4-9 Relative cost for different tolerance levels

Table 4-12 Specific values chosen for the tolerance (Inner Array) and values of noise factor (Outer Array)

Item	Chord length on the Root of the Blade	Twist Angle	Rotational Speed	Pitch	Rotor Radius	Hub Radius
	A	K	G	H	I	J
Unit	m	deg	rpm	deg	m	m
Optimum setting	0.7	{8 4 2 1}	125	0	4.5	0.75
1	1.00%	10%	-6	1.00	0.50%	1.00%
2	1.00%	10%	-6	1.00	0.20%	0.50%
3	1.00%	10%	-6	1.00	0.10%	0.20%
4	1.00%	5%	-4	0.50	0.50%	1.00%
5	1.00%	5%	-4	0.50	0.20%	0.50%
6	1.00%	5%	-4	0.50	0.10%	0.20%
7	1.00%	2%	-2	0.20	0.50%	1.00%
8	1.00%	2%	-2	0.20	0.20%	0.50%
9	1.00%	2%	-2	0.20	0.10%	0.20%
10	0.50%	10%	-4	0.20	0.50%	0.50%
11	0.50%	10%	-4	0.20	0.20%	0.20%
12	0.50%	10%	-4	0.20	0.10%	1.00%
13	0.50%	5%	-2	1.00	0.50%	0.50%
14	0.50%	5%	-2	1.00	0.20%	0.20%
15	0.50%	5%	-2	1.00	0.10%	1.00%
16	0.50%	2%	-6	0.50	0.50%	0.50%
17	0.50%	2%	-6	0.50	0.20%	0.20%
18	0.50%	2%	-6	0.50	0.10%	1.00%
19	0.20%	10%	-2	0.50	0.50%	0.20%
20	0.2%	10%	-2	0.50	0.20%	1.00%
21	0.20%	10%	-2	0.50	0.10%	0.50%
22	0.20%	5%	-6	0.20	0.50%	0.20%
23	0.20%	5%	-6	0.20	0.20%	1.00%
24	0.20%	5%	-6	0.20	0.10%	0.50%
25	0.20%	2%	-4	1.00	0.50%	0.20%
26	0.20%	2%	-4	1.00	0.20%	1.00%
27	0.20%	2%	-4	1.00	0.10%	0.50%

Inner array $L_{27}(3^6)$

Item	Shape Profile	Twist Angle	Pitch	Rotor Radius	Hub Radius
	A	K	H	I	J
Unit	m	deg	deg	m	m
1	0.707	+10%	+1	4.5225	0.7575
2	0.707	+10%	+1	4.4775	0.7425
3	0.707	-10%	-1	4.5225	0.7575
4	0.707	-10%	-1	4.4775	0.7425
5	0.693	+10%	-1	4.5225	0.7425
6	0.693	+10%	-1	4.4775	0.7575
7	0.693	-10%	+1	4.5225	0.7425
8	0.693	-10%	+1	4.4775	0.7575

Outer array $L_8(2^5)$

Table 4-13 Results of all 27 runs of tolerance design

Item	Chord length on the Root of the Blade (A)	Twist Angle (K)	Rotational Speed (G)	Pitch (H)	Rotor Radius (I)	Hub Radius (J)	Power difference (ΔP^2)	Cost	S/N
Unit	m	deg	rpm	deg	m	m	kW^2	$	-
1	1.00%	10%	-6	1	0.50%	1.00%	2.07	2150	-78.85
2	1.00%	10%	-6	1	0.20%	0.50%	1.22	3300	-80.25
3	1.00%	10%	-6	1	0.10%	0.20%	1.19	5550	-84.68
4	1.00%	5%	-4	0.5	0.50%	1.00%	1.26	3250	-80.26
5	1.00%	5%	-4	0.5	0.20%	0.50%	0.39	4400	-77.85
6	1.00%	5%	-4	0.5	0.10%	0.20%	0.27	6650	-79.8
7	1.00%	2%	-2	0.2	0.50%	1.00%	1.08	6550	-85.67
8	1.00%	2%	-2	0.2	0.20%	0.50%	0.24	7700	-80.6
9	1.00%	2%	-2	0.2	0.10%	0.20%	0.08	9950	-78.21
10	0.50%	10%	-4	0.2	0.50%	0.50%	1.11	4600	-82.72
11	0.50%	10%	-4	0.2	0.20%	0.20%	0.32	6250	-79.98
12	0.50%	10%	-4	0.2	0.10%	1.00%	0.2	6750	-78.62
13	0.50%	5%	-2	1	0.50%	0.50%	1.61	3400	-81.73
14	0.50%	5%	-2	1	0.20%	0.20%	0.86	5050	-82.46
15	0.50%	5%	-2	1	0.10%	1.00%	0.74	5550	-82.63
16	0.50%	2%	-6	0.5	0.50%	0.50%	1.26	5000	-84.01
17	0.50%	2%	-6	0.5	0.20%	0.20%	0.49	6650	-82.37
18	0.50%	2%	-6	0.5	0.10%	1.00%	0.37	7150	-81.81
19	0.20%	10%	-2	0.5	0.50%	0.20%	1.23	4450	-82.89
20	0.20%	10%	-2	0.5	0.20%	1.00%	0.37	4350	-77.52
21	0.20%	10%	-2	0.5	0.10%	0.50%	0.25	6100	-78.71
22	0.20%	5%	-6	0.2	0.50%	0.20%	1.24	6050	-85.61
23	0.20%	5%	-6	0.2	0.20%	1.00%	0.39	5950	-80.47
24	0.20%	5%	-6	0.2	0.10%	0.50%	0.26	7700	-80.83
25	0.20%	2%	-4	1	0.50%	0.20%	1.72	5650	-86.43
26	0.20%	2%	-4	1	0.20%	1.00%	0.88	5550	-83.37
27	0.20%	2%	-4	1	0.10%	0.50%	0.76	7300	-85.09

3. Results of tolerance design and analysis

The results of the twenty-seven simulations are summarized in Table 4-13. The factor response graphs of design variables, based on the computed S/N ratios are shown in Fig. 10. According to the smaller-the-better criterion, larger values of S/N ratio correspond to smaller values of the product of power fluctuation and cost. Therefore, the optimal design variable combination for tolerance design can be identified as A_1, B_1, C_3, D_2, E_2, and F_1 from Fig. 4-8. Finally, the optimum solution including both the mean values (optimum values found in parameter design) and tolerances (optimum values found in tolerance design) can be identified for all the design variables as shown in Table 4-14.

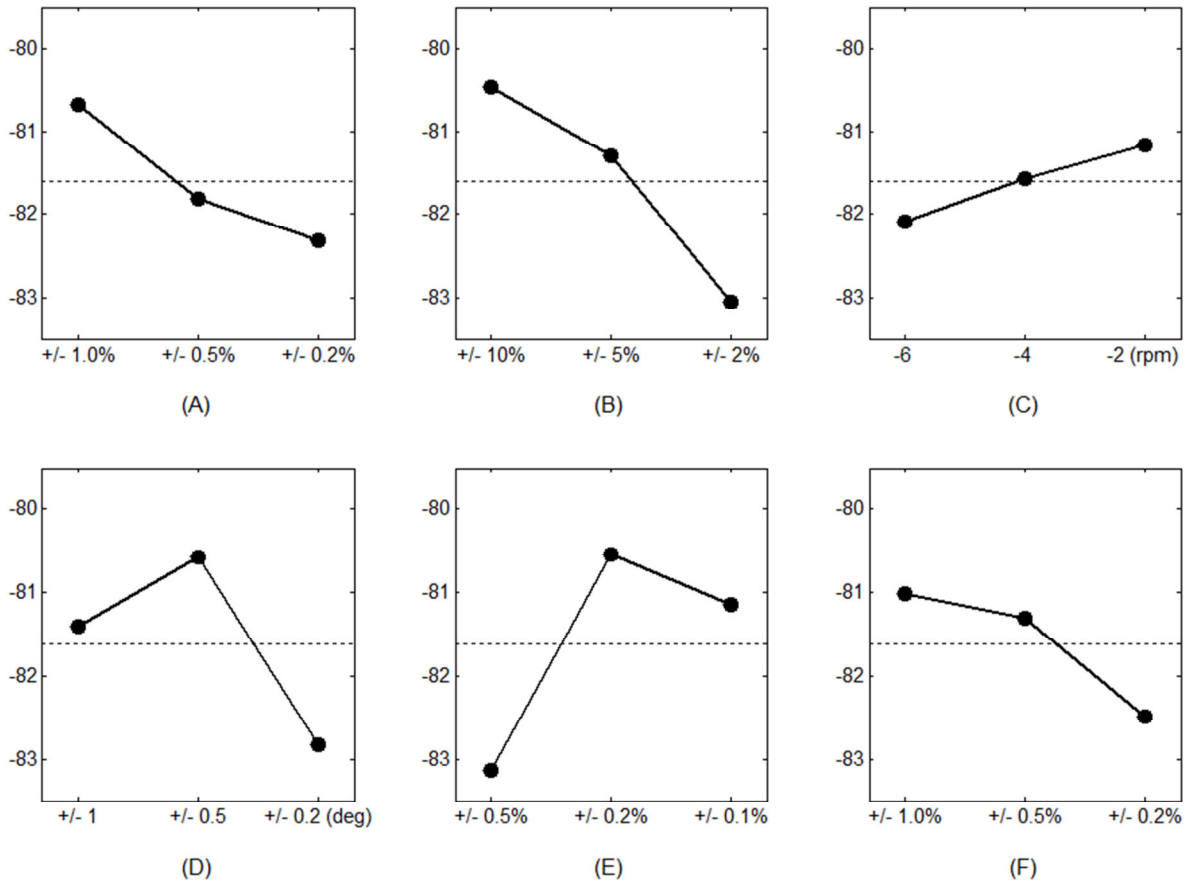

Figure 4-10 Response graphs for the S/N ratio (Tolerance design)

Table 4-14 Optimum mean and tolerance values of design variables

Optimum Values of Design Variable	Unit	Mean	Tolerance
Chord length on the Root of the Blade	m	0.7	± 0.007
Twist Angle 1	deg	8	± 0.8
Twist Angle 2	deg	4	± 0.4
Twist Angle 3	deg	2	± 0.2
Twist Angle 4	deg	1	± 0.1
No. of Blades	#	3	0
Rotational Speed	rpm	125	-2
Pitch	deg	0	± 0.5
Rotor Radius	m	4.5	± 0.009
Hub Radius	m	0.75	± 0.0075

4.6 Conclusions

The work extends the conventional Taguchi method for solving multi-objective constrained optimization problems and obtaining an optimum combination of design parameters as well as their tolerances using only a limited number of experiments. It provides a simple way of designing robust horizontal axis wind turbine systems under realistic conditions. The robust design of HAWT, including both parameter design and tolerance design, is presented.

In the parameter design stage, the energy output of the turbine is maximized by using the Taguchi method and the wind energy output is improved by 52.7%. However, from a practical point of view, the design of HAWT needs to involve some behavior constraints. In this work, two constraints, namely, minimum requirement of power coefficient and maximum limit on the stress induced or permissible fractional fatigue damage, are considered. An application of a novel extended penalty-based Taguchi method is demonstrated through the design of a HAWT example and the energy output is improved

by 31.6%. Although the improvement in the wind energy output is less in the second example, all of the imposed constraints are satisfied.

Based on the results of the parameter design, an appropriate set of tolerance setting of the parameters is established so as to yield an economical design while ensuring a minimal variability of performance of the wind turbine. The resulting objective function is formulated as a multi-objective function and solved by the traditional Taguchi method.

CHAPTER 5

Optimum Design of Direct Methanol Fuel Cell System

5.1 Introduction and Literature Review

A clean source of energy is becoming greatly needed as conventional fuels such as coal and petroleum products have a devastating impact on the environment. When burned, these fuels release large quantities of toxics to the atmosphere causing all sorts of problems from global warming to ozone depletion.

Currently, there are many options for clean sources of energy, including solar, wind and geothermal power sources. The biggest challenge for these types of sources is portability; therefore it becomes necessary to explore power sources for portable applications. Hydrogen energy systems, more specifically, hydrogen based fuel cells are considered as a leading contender to replace internal combustion engines and conventional batteries.

Direct Methanol Fuel Cell (DMFC) is a subcategory of proton exchange membrane fuel cells (PEMFCs) in which methanol is used as the fuel. Since methanol is supplied to the fuel cell in liquid form, it is easy to store, deliver and recharge compared to hydrogen. Despite all these advantages, there are several drawbacks that make DMFCs not yet ready for commercialization. Some of these hindrances are: slow electro-oxidation of methanol at the anode, the undesired methanol crossover from the anode to the cathode and the high cost associated with using high platinum catalyst loadings.

The optimization of the fuel cell operating conditions and flow field geometry is a hot topic in fuel cell research. Unfortunately, the majority of research works have been conducted experimentally in a trial and error fashion. This approach is time consuming and costly and it does not provide a mechanistic explanation for the results. Therefore, the application of numerical optimization techniques becomes necessary in this field.

PEMFC models with different levels of complexity have been used in some optimization studies. Grujicic and Chittajallu (2003) employed a two-dimensional model coupled with a nonlinear constrained optimization algorithm to determine an optimum design of the fuel cell considering the geometrical parameters as well as the operating parameters as design variables. Chen et al. (2006) applied discretization and branch and bound type optimization techniques for obtaining a global optimum point of annualized cost for a specified power production level based on a one-dimensional model. Secanell et al. (2006) used a gradient-based optimization technique to maximize the current density at a given electrode voltage based on a two-dimensional single-phase multi-variable model. Ang et al. (2010) formulated a multi-objective optimization problem by using the weighting method to study the trade-offs between two objectives—the efficiency and the size.

There are few literatures published in the topic of optimization of DMFC. Xu et al. (2005) developed a dynamic DMFC model to decide the optimal methanol feed concentration for maximizing the power density output by using a sensitivity analysis based approach. Yeh and Chen (2007) obtained an optimum combination of the anode and cathode catalyst layers, thickness of membrane, membrane conductivity and methanol concentration by using the factorial design method based on a single-phase, one-dimensional model. Ko et al. (2008) reported in their non-isothermal dynamic

optimization model of DMFC that methanol feed concentration had a significant larger effect on the methanol crossover, temperature, as well as cell voltage and provided an effective optimum operating strategy for the dynamic model. Alotto (2009) applied stochastic particle swarm optimization method to optimize multi-objectives including the maximization of the cell duration between two consecutive fuel recharges and the minimization of the methanol crossover of micro DMFC. Basri et al. (2010) formulated a passive DMFC model and used sequential quadratic programming to minimize the cost. The geometrical parameters of the anode and cathode such as methanol concentration, power density, and catalyst loading were treated as design variables, upper and lower bounds of these parameters were considered as inequality constraints and all of the governing equations of the fuel cell model were included as equality constraints.

It can be noticed that most of these DMFC optimization papers were, in general, based on simple one-dimensional models. Comprehensive analysis of three-dimensional, one or two phase flows were reported (Wang and Wang (2003), Ge and Liu (2005, 2006), Liu et al. (2007)). However, optimization techniques have not been carried out so far. In this work, a three-dimensional single-phase DMFC model has been used; the genetic algorithm (GA), coupled with sequential quadratic programming optimization method, is applied to find the global optimum design.

5.2 DMFC model

A three-dimensional DMFC model consisting of the anode side, the cathode side and the membrane is shown in Fig.5-1. The methanol and water were considered in the anode side while air was considered in the cathode side. The flow channel is designed for

parallel flow. Both the anode side and the cathode side can be sub-divided into the gas/liquid channel, the diffusion layer as well as the catalyst layer. In Fig.1, x_{sc} and x_{land} represent the length of semi-channel and land in the X direction, respectively, y_c represents the length of the channel in the Y direction and z_c, z_d, z_{ca} and z_m represent the width of channel, the thickness of the diffusion layer, the catalyst layer and the thickness of membrane in the Z direction, respectively. All the reactants enter the channels from the surface at y = 0. All the geometry parameters stated above, catalysts loading as well as methanol flow rate and methanol concentration are incorporated in the optimization problem as design parameters.

The design vector of the optimization problem is:

$$\vec{X} = \begin{Bmatrix} x_1 \\ x_2 \\ x_3 \\ x_4 \\ x_5 \\ x_6 \\ x_7 \\ x_8 \\ x_9 \\ x_{10} \end{Bmatrix} = \begin{Bmatrix} x_{sc} \\ x_{land} \\ z_c \\ z_d \\ z_{ca} \\ z_m \\ l_{c,a} \\ l_{c,c} \\ f_a \\ c_w \end{Bmatrix} \tag{5.1}$$

where x_{sc} is the semi-channel length width in the x direction (mm);

x_{land} is the land depth in channel layer (mm);

z_c is the channel region thickness in z direction (mm);

z_d is the diffusive region thickness (mm);

z_{ca} is the catalyst layer thickness (mm);

z_m is the thickness of membrane for both anode and cathode (mm);

$l_{c,a}$ is the catalyst loading of anode (mg/cm^2);

$l_{c,c}$ is the catalyst loading of cathode (mg/cm^2);

f_a is the methanol volumetric flow rate (cm^3/min);

c_w is the methanol concentration by weight;

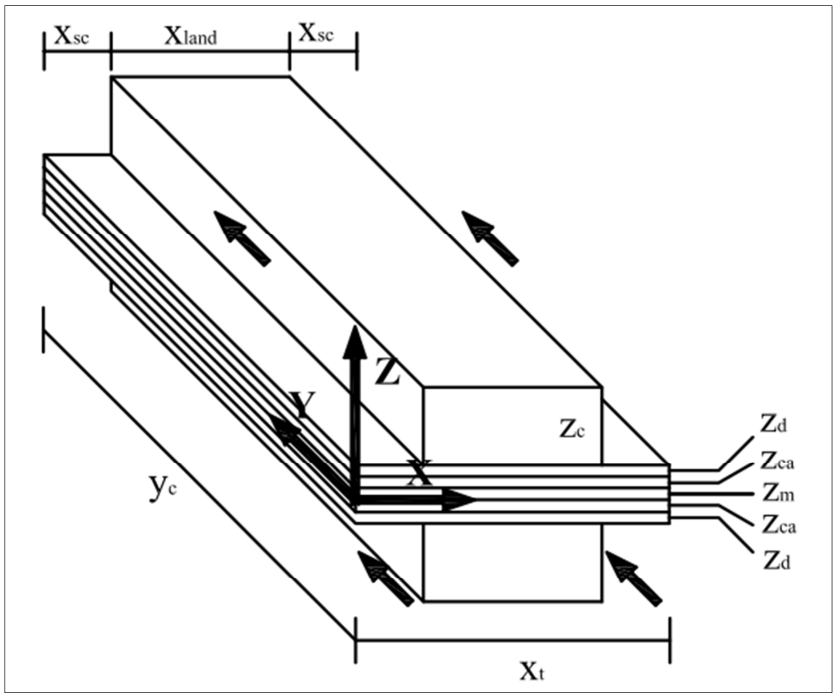

Figure 5-1 Schematic of the modeling domain

5.2.1 Assumptions made

In order to reduce the complexity while still capturing the basic process characteristics of the numerical model, the following assumptions were employed:

1) All the fluids are incompressible and the flows are laminar;
2) All the processes are steady state and isothermal;
3) The effect of carbon dioxide generated in the anode side is negligible;
4) The methanol crossed over from the anode to the cathode is completely oxidized at the interface between the membrane and the cathode catalyst layer;
5) The membrane is fully hydrated and is impermeable to gases;

6) No limitation on mass transport in the cathode side.

5.2.2 Governing equations

The governing equations used in the numerical study include continuity equation (Eq. 5.2) momentum equations (Eq. 5.3) and species equations (Eq. 5.4). The continuity equation is valid for all components of the fuel cell; mainly, the reactants' distribution channels, the diffuser and the catalyst layers (Zhou and Liu: 2001).

$$\nabla \cdot \vec{V} = 0 \tag{5.2}$$

The momentum equation reduces to the Navier-Stokes equation in the channels. However, when applied to the diffuser and the catalyst layers, their porosities need to be considered as well as reactants' permeability and the membrane's hydraulic and electro-kinetic permeabilities. This leads to

$$\rho\vec{V} \cdot \Delta\vec{V} = -\nabla P + r_{\varepsilon}\mu\nabla^2\vec{V} + \rho S_i \tag{5.3}$$

The source term in the species equation accounts for the consumption and the creation of reactants by electrochemistry, k represents methanol or water in the anode side, and oxygen, nitrogen, or water vapor in the cathode side, X_k denotes the mole fraction of species k, D_k^{eff} indicates the effective diffusion coefficient of the k^{th} component and S_k indicates the mass generation rate for species k per unit volume.

$$\rho\vec{V} \cdot \nabla X_k = \rho D_k^{eff}\nabla^2 X_k + S_k \tag{5.4}$$

$$\text{with} \quad \sum_k X_k = 1 \tag{5.5}$$

$$D_k^{eff} = D_k\epsilon^{1.5} \tag{5.6}$$

More details can be found in Zhou and Liu (2001) and Ge and Liu (2006).

5.2.3 Electrochemical kinetics

The anodic and the catholic reaction rates per unit volume can be determined by using the Tafel equations(O'Hayre et al., 2006)

$$j_a = (ai^{ref})_a(\frac{X_{CH}}{X_{CH}^{ref}})^{\gamma_a}\exp(\frac{\alpha_a F}{R_c T}\eta_a) \tag{5.7}$$

$$j_c + j_{\text{cross}} = (ai^{ref})_c(\frac{X_O}{X_O^{ref}})^{\gamma_c}\exp(-\frac{\alpha_c F}{R_c T}\eta_c) \tag{5.8}$$

where the specific reaction surface area (a) is a function of catalyst loading (m_{Pt}) and thickness (δ) as well as catalyst surface area per unit mass of catalyst (A_o) (Marr and Li: 1999)

$$a = \frac{m_{\text{Pt}} A_o}{\delta} \tag{5.9}$$

The value of A_o, in Eq. (5.9), depends on percent weight of the platinum in the catalyst mixture (Marr and Li, 1999; Secanell et al., 2008).

The pseudo-current associated with methanol crossover rate (j_{cross}) per unit volume can be calculated by

$$j_{cross} = \frac{6F\, N_{CH}^m}{\delta} \tag{5.10}$$

where N_{CH}^m is methanol crossover flux and it is caused by diffusion and electro-osmotic drag as shown in the following equation

$$N_{CH}^m = \frac{\lambda_{CH} I}{F} - \varepsilon_m^{1.5} D_{CH}^m \frac{dC_{CH}^m}{dz} \tag{5.11}$$

in which, D_{CH}^m is the diffusion coefficient of methanol in the membrane and λ_{CH} is the electro-osmotic drag coefficient for methanol and it is defined as the number of methanol molecules dragged by each proton conducted through the membrane.

$$\lambda_{CH} = X_{CH}|_{ac/m}\lambda_w \tag{5.12}$$

$$D_{CH}^{m} = 4.012 \times 10^{-13} \exp(0.024312 \times T) \quad (5.13)$$

The average current density $(I)$of the fuel cell is given by

$$I = \int_0^{\delta} j_a dz \quad (5.14)$$

The cell voltage is determined by:

$$\mathrm{E}_{cell} = E_0 - \eta_a + \eta_c - IR_m \quad (5.15)$$

where the membrane resistance (R_m) is defined by

$$R_m = \int_0^{t_m} \frac{1}{\sigma_m} dz = \frac{t_m}{\sigma_m} \quad (5.16)$$

for a fully hydrated membrane with the ionic conductivity (σ_m) given by

$$\sigma_m(T) = \sigma_m^{ref} exp\left[1268\left(\frac{1}{303} - \frac{1}{T}\right)\right] \quad (5.17)$$

where T is the operating temperature of the fuel cell, assumed to be 343 K in this work.

5.2.4 Solution procedure

1. Determine the velocity of methanol at anode side and the velocity of oxygen (or air);

2. Assume an over-potential in the anode side and solve for the corresponding species concentration and the average current density;

3. Calculate the flux of methanol crossover and the pseudo current density due to methanol crossover;

4. Solve the over-potential in the cathode side and the cell voltage iteratively until convergence;

5. Repeat steps 2-5 by assuming another over-potential in the anode side until the entire polarization curve is obtained.

5.2.5 Cost model

The total cost of DMFC, C_{total}, can be separated into three components, cost of the materials, cost of machining and cost of fuel:

$$C_{total} = C_{material} + C_{mechining} + C_{fuel} \tag{5.18}$$

1. Cost of material

The cost of material for DMFC can be separated into two parts—cost of the membrane electrode assembly and cost of the stack—as:

$$C_{material} = C_{MEA} + C_{stack} \tag{5.19}$$

where C_{MEA} is the cost of the membrane electrode assembly, C_{stack} is the cost of the stack.

$$C_{MEA} = C_{catalyst} + C_{membrane} + C_{electrode} \tag{5.20}$$

$$C_{catalyst} = (U_{PtRu} \cdot \rho_{PtRu} \cdot x(7) \cdot x(5) \cdot Ar_a + U_{Pt} \cdot \rho_{Pt} \cdot x(8) \cdot x(5) \cdot Ar_a) \cdot 1.2 +$$

$$(U_{NS} \cdot Ar_a \cdot (\rho_{PtRu} \cdot x(7) \cdot x(5) + \rho_{Pt} \cdot x(8) \cdot x(5))) \cdot 15 \tag{5.21}$$

where A_r is the active area the fuel cell, U_{PtRu} and U_{Pt} are the unit prices of Pt/Ru and Pt respectively, ρ_{PtRu} and ρ_{Pt} are the densities of the Pt/Ru and the Pt, respectively.

$$C_{membrane} = (-9.1686(x(6))^2 + 3.3828x(6) + 0.0549) \cdot A_r \cdot 1.5 \tag{5.22}$$

where the quadric term $(-9.1686(x(6))^2 + 3.3828x(6) + 0.0549)$ is the unit price of Nafion. This cost model is generated based on the price and the thickness of membrane (Alfa, 2010). The size of the membrane is assumed to be 50% more the active area.

$$C_{electrode} = 2 \cdot U_{El} \cdot A_r \tag{5.23}$$

where the U_{El} is the cost of carbon paper.

$$C_{stack} = 2 \cdot (U_G \cdot 1.5A_r) + 2 \cdot (U_{st} \cdot 1.5A_r) + 2 \cdot (U_{cc} \cdot 3 \cdot A_r) \tag{5.24}$$

where U_G is the cost of gasket, U_{st} is the cost of the frame and C_{cc} is the cost of the current collector.

2. Cost of machining

The cost of machining depends on the geometry parameters of the fuel cell. Since the magnitudes of the parameters are very small, the manufacturing cost is relatively expensive since smaller dimensions cost more. Therefore, the cost of machining is assumed as:

$$C_{machining} = k_1/x(1) + k_2/x(2) + k_3/x(3) + k_4/x(4) + k_5/x(5) \qquad (5.25)$$

3. Cost of fuel (methanol)

The cost of fuel (methanol) for a specified running time can be formulated as

$$C_{methanol} = (x(9)/60) \cdot x(10) \cdot 32.04/\rho \cdot U_{methanol} \cdot H \qquad (5.26)$$

where 32.04 (g/mol) is the molar mass of methanol, and ρ is the density of the methanol, $U_{methanol}$ is the price of methanol and H is the operating time (hours) of the fuel cell.

5.3 Optimization problem

In general, the optimal design problem can be stated in the general form:

$$\text{Minimize } f(\vec{X}) \qquad (5.27)$$

$$\text{subject to} \quad g_j(\vec{X}) \leq 0;\ j = 1,2,\ldots m \qquad (5.28)$$

$$h_k(\vec{X}) = 0;\ k = 1,2,\ldots n \qquad (5.29)$$

$$a_i \leq x_i \leq b_i;\ i = 1,2,\ldots l \qquad (5.30)$$

where f is objective function, g_j is the j^{th} inequality constraint function, h_k is the k^{th} equality constraint function, x_i is the i^{th} component of the design vector $\vec{X}$, and a_i and b_i are the lower and upper bounds on the design variable x_i, respectively.

5.3.1 Optimization method

Traditional optimization techniques become inefficient in finding a global optimum point for the DMFC model since it is a three-dimensional, multi-component CFD based model. The genetic algorithm (GA) method is suited for solving such a problem. Compared to the classical gradient-based algorithms, which strongly depend on the initial configuration (design) and generally stall in a locate minimum close to the starting point, the non-gradient based genetic algorithm (GA) method, which does not require an initial point and can locate the global optimum point, has aroused significant interests in engineering and industrial applications. In this work, a two-step hybrid method has been utilized to determine the optimum solution of DMFC. First, the GA method explores in the entire design space and locates the global optimum region. Based on the result of the first step, a graduate-based method, the sequential quadratic programming (SQP) method, is employed to reach the optimum point accurately. The MATLAB optimization toolbox can implement the hybrid method by using the following syntax:

$$opt = gaoptimset('HybridFcn', @fmincon) \tag{5.31}$$

$$x = ga(fitnessfcn, nvars, A, b, Aeq, beq, LB, UB, nonlcon, options) \tag{5.32}$$

where fitnessfcn denotes the objective function corresponding to a multi-dimensional design vector x, nvars indicates the number of design variables, A, b, Aeq and beq are the linear inequality and equality constraints, LB and UB are lower and upper bounds of the design variables and nonlcon is the set of non-linear constraints.

5.3.2 Maximization of the power output

In this section, the objective function is aimed at finding the maximum power density. The maximum power of the DMFC is given by:

$$P_{max} = max\{[(E_0 - \eta_a + \eta_c - IR_m) - (I_{cross}R_m)]\, I\} \tag{5.33}$$

and the objective function for minimization is taken as:

$$f_1 = -P_{max} \tag{5.34}$$

All of the design variables are assumed to have some reasonable upper and lower bounds:

$$x_i^{min} \leq x_1 \leq x_i^{max} \text{ , i = 1, 2, … , 10} \tag{5.35}$$

5.3.3 Maximization of power output with a minimum operating voltage constraint

A typical fuel cell produces a voltage from 0.7~0.8 V at open circuit stage which decreases with the increase of the current density due to the activation loss, the ohmic loss as well as the mass transport loss. For a typical power density curve, the power density usually increases with an increase of current density until a particular value and then starts to fall down dramatically to zero. Sometimes, the result of optimum voltage corresponding to the particular value of current density may be too low, which leads to an unexpected low efficiency of the fuel cell system. As a result, in this optimization problem, besides all the side constraints, an additional behavior constraint on the operating voltage (a lower bound of 0.3) is considered. Thus the problem becomes

Minimize $$f_2 = -P_{max} \tag{5.36}$$

subject to:

$$x_i^{min} \leq x_1 \leq x_i^{max} \text{ , i = 1, 2, … , 10} \tag{5.37}$$

$$V \geq 0.3 \tag{5.38}$$

5.3.4 Minimization of cost

The power density of the DMFC has been maximized in the formulation of the last two sections. However, maximization of the performance may result in a relatively high cost, which can make DMFCs less competitive. Therefore another important objective function—minimization of the cost— is introduced in this section. The objective function (cost) is given in Eq. (5.18). In addition to all the constraints considered in the minimizing of f_2, the following additional constraints are considered while minimizing f_3. The maximum power output of the DMFC should be at least 80% of the optimum value found in the case of the problem described in section 5.3.2. The optimization problem can be stated as:

$$f_3 = C_{total} \tag{5.39}$$

subject to

$$x_i^{min} \leq x_1 \leq x_i^{max} \text{ , i = 1, 2, … , 10} \tag{5.40}$$

$$V \geq 0.3 \tag{5.41}$$

$$P \geq 80\% \times P_{opt2} \tag{5.42}$$

5.4 Numerical Results

Three numerical examples are considered to illustrate optimization problems of DMFC in this section. The physical parameters and basic operating conditions are tabulated in Table 5-1.

Table 5-1 Physical parameters and basic operation conditions

Physical parameters and basic operation conditions	Value
Cell temperature (K)	343
Water density (kg/m^3)	1000
Air viscosity (kg/(m·s))	2.05×10^{-5}
Gas constant (J/(mol·K))	8.314
Inlet oxygen mole fraction	0.21
Methanol reference concentration (mol/m^3)	2000 (Ge and Liu, 2006)
Oxygen reference concentration (mol/m^3)	0.472 (Shukla et al., 1999)
Diffusion coefficient of oxygen in air (m^2/s)	1.22×10^{-10} (Ge and Liu, 2006)
Diffusion coefficient of methanol in water (m^2/s)	2.80×10^{-9} (Scottel et al., 1999)
Porosity of diffusion layer	0.6 (Ge and Liu, 2006)
Porosity of catalyst layer	0.4 (Ge and Liu, 2006)
Porosity of membrane	0.28 (Bernardy and Verbrugge, 1992)
Permeability to air in the gas diffuser (m^2)	1.76×10^{-11} (Ge and Liu, 2006)
Permeability to water in the gas diffuser (m^2)	1.00×10^{-11} (Ge and Liu, 2006)
Electrokinetic permeability of the membrane (m^2)	7.18×10^{-20} (Bernardy and Verbrugge, 1992)
Anode reaction order	1.0 (Shukla et al., 1999)
Cathode reaction order	1.0 (Shukla et al., 1999)
Electro-osmotic drag coefficient of water	2.5 (Baxter et al., 1999)
Charge of fixed (sulfonate) sites	-1.0 (Ge and Liu, 2006)

The following upper and lower constraints of design variables are assumed:

$k_1 = 200$; $k_2 = 400$; $k_3 = 400$; $k_4 = 20$; $k_5 = 5$; $A_r = 50$ cm^2; $x_1^{min} = 0.25$; $x_1^{max} = 1.00$;

$x_2^{min} = 0.50$; $x_2^{max} = 2.00$; $x_3^{min} = 0.50$; $x_3^{max} = 2.00$; $x_4^{min} = 0.1$; $x_4^{max} = 0.2$;

$x_5^{min} = 0.01$; $x_5^{max} = 0.05$; $x_6^{min} = 0.08$; $x_6^{max} = 0.20$; $x_7^{min} = 0.5$; $x_7^{max} = 2.0$;

$x_8^{min} = 0.5$; $x_8^{max} = 6.0$; $x_9^{min} = 5.0$; $x_9^{max} = 25.0$; $x_{10}^{min} = 0.5$; $x_{10}^{max} = 8.0$; $H = 5000$

The cost parameter used in this work is summarized in Table 5-2.

Table 5-2 Cost parameters

Parameter	Value	Unit
Cost of methanol	12	USD/L
Cost of Pt/Ru	73	USD/g
Cost of Pt	56	USD/g
Cost of Nafion solution	1	USD/ml
Cost of Electrode	417	USD/m^2
Cost of gasket	150	USD/m^2
Cost of graphite plate	800	USD/m^2
Cost of End plate	75	USD/m^2

The results of three optimization problems are summarized in Table 5-3. It can be seen that the difference in the cost of material of three different optimization problems is very similar and the difference in the cost of machining is relatively larger. However, the costs of fuel corresponding to different optimization problems are completely different. The cost of fuel corresponding to the minimization of f_1 is \$9760 while the cost of fuel corresponding to the minimization of f_2 reduces by 40% to \$5938 and the cost of fuel corresponding to the minimization of f_3 further reduces to \$2811, which is only 28.80% of the corresponding result of the minimization of f_1.

By comparing the total cost and the power density corresponding to the minimizations of f_1 and f_2, the following observation can be made. Although the value of maximum power density corresponding to minimization of f_3 is 0.0682 W/cm^2, which is 65% and 80% of the values obtained in the minimizations of f_1 and f_2, (0.1064 and 0.0852 W/cm^2), respectively, the total cost is only \$4131. This cost is only 35.5% and 53.8% of the total costs associated with the minimizations of f_1 and f_2, respectively. Hence, the price per unit energy has been reduced by 45% and 33% compared to the first and second problems, respectively, when the third optimization problem is solved.

Table 5-3 Results of optimization

Design variable / Outputs	Unit	Minimization of f_1, (Minimization of the negative value of the performance without any voltage constraint)	Minimization of f_2, (Minimization of the negative value of the performance with an operating voltage constraint)	Minimization of f_3 (Minimizing the cost)
x_1	mm	0.6692	0.9798	0.5230
x_2	mm	0.5842	0.5201	2.0000
x_3	mm	1.1620	1.7884	2.0000
x_4	mm	0.1198	0.1178	0.1174
x_5	mm	0.5000	0.5000	0.5000
x_6	mm	0.1002	0.1226	0.1335
x_7	mg/cm^2	6.0000	5.5800	4.1625
x_8	mg/cm^2	1.9985	1.9553	1.6650
x_9	cm^3/min	17.0056	14.3904	11.9875
x_{10}	mol/l	3.9409	2.8332	1.6103
Cost of material	$	274	274	267
Cost of machining	$	1595	1467	1053
Cost of fuel	$	9760	5938	2811
Total Cost	$	11629	7679	4131
power density	W/cm^2	0.1064	0.0852	0.0682
corresponding voltage of optimum power	V	0.1846	0.2999	0.3335

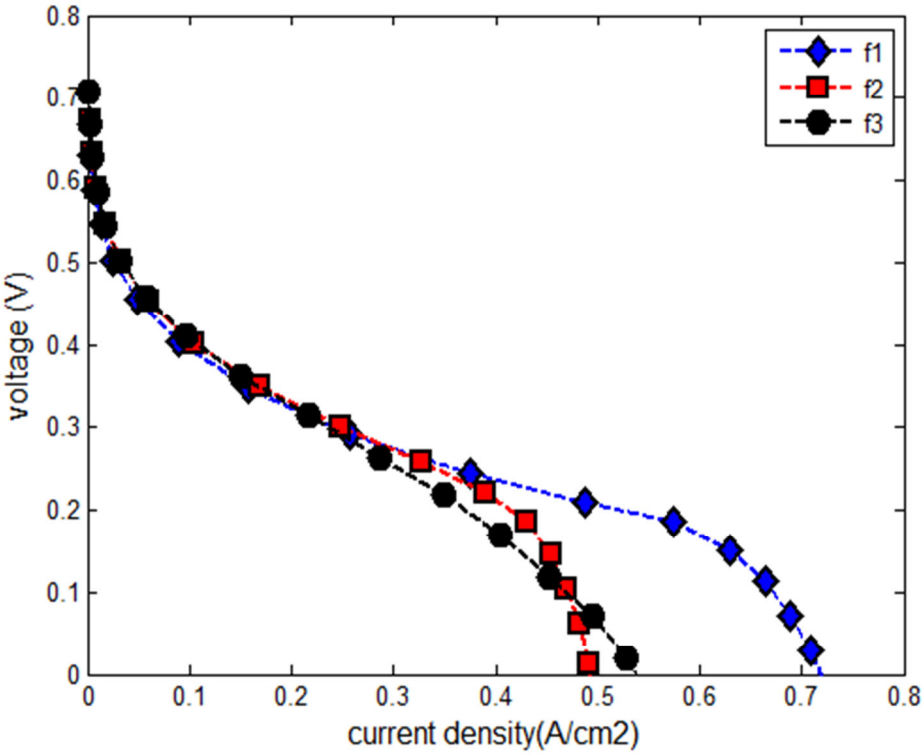

Figure 5-2 Polarization curves for the optimum designs

Figure 5-2 shows the polarization curves for the three different optimization problems. In the activation loss area (with current density less than 0.15 A/cm^2), the curve corresponding to the minimization of f_1 is slightly lower than the other two curves, but the difference is very small. Since the methanol concentration corresponding to the minimization of f_1 is relatively high, a large amount of methanol is expected to crossover from the anode to cathode, and as a result, the corresponding curve with the minimization of f_1 is expected to be much lower than the other two in the activation loss region. However, a relatively higher methanol flow rate (17.0056 cm^3/min), coupled with a relatively higher catalyst loading (6.0 mg/cm^2), can still guarantee enough amount of methanol to be electro-oxidized, which results in shifting the curve back to a similar level as the other curves. In contrast, the corresponding values of the methanol flow rate (11.9875 cm^3/min) and the catalyst loading (4.1625 mg/cm^2) are relatively lower when f_3

is minimized, which means the total amount of methanol that can be electro-oxidized is not as much as in the other two cases. However, the value of methanol concentration is also low which results in a relatively lower methanol crossover. Therefore, the actual amount of electro-oxidized methanol is still remains at a high level and hence the curve corresponding to the minimization of f_3 also remains at a high level in the activation loss area.

The curves in the ohmic loss region are dominated by one design variable, namely, the thickness of membrane. At thicker membrane results in a higher value of resistance and therefore the slope of the curve in this region is sharper (Cai et al., 2005). As indicated in Table 5-2, the values of thickness of membrane, design variable x_6, for the minimization of f_1, f_2 and f_3 are 0.1002, 0.1226 and 0.1335 mm, respectively. Since the thickness of membrane corresponding to the minimization of f_1 is relatively lower, a curve with relatively lower slope is expected. Similarly, since the thickness of the membrane corresponding to the minimization of f_3 is relatively higher, a curve with a relatively higher slope is expected. All the curves have sharp reductions in the mass transport region because there is not enough fuel to participate in the electro-chemical reaction. Since the value of catalyst loading, methanol flow rate and methanol concentration is relatively higher in the minimization of f_1, there is still enough amount of methanol that can be electro-oxidized even in a high current density such as 0.6 A/cm^2. In contrast, the value of catalyst loading, methanol flow rate and methanol concentration are relatively lower in the minimizations of f_2 and f_3; therefore the curves starts to drop dramatically when the current density is larger than 0.4 A/cm^2.

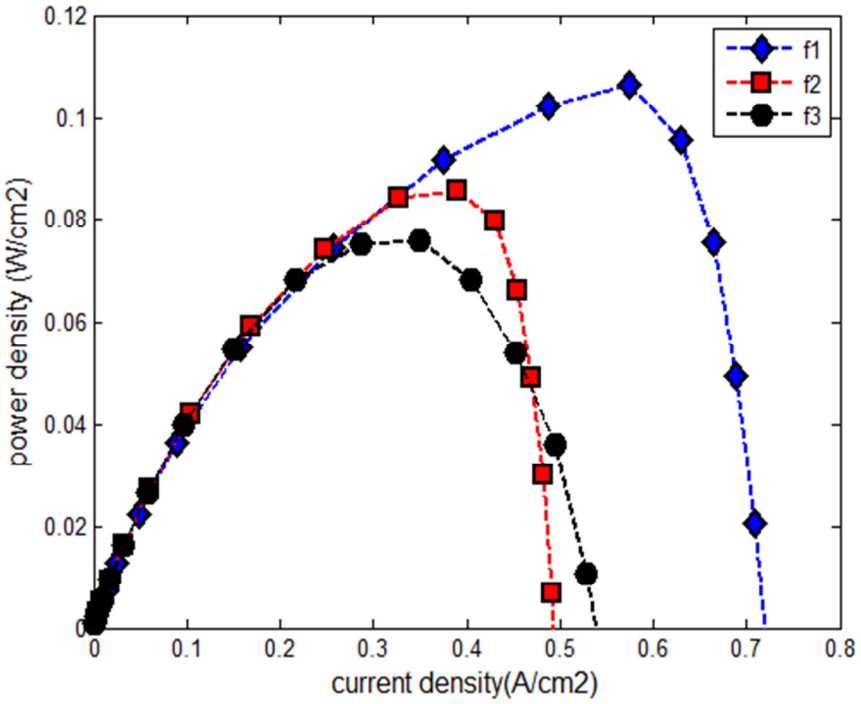

Figure 5-3 Power density vs. current density curves of the optimum designs

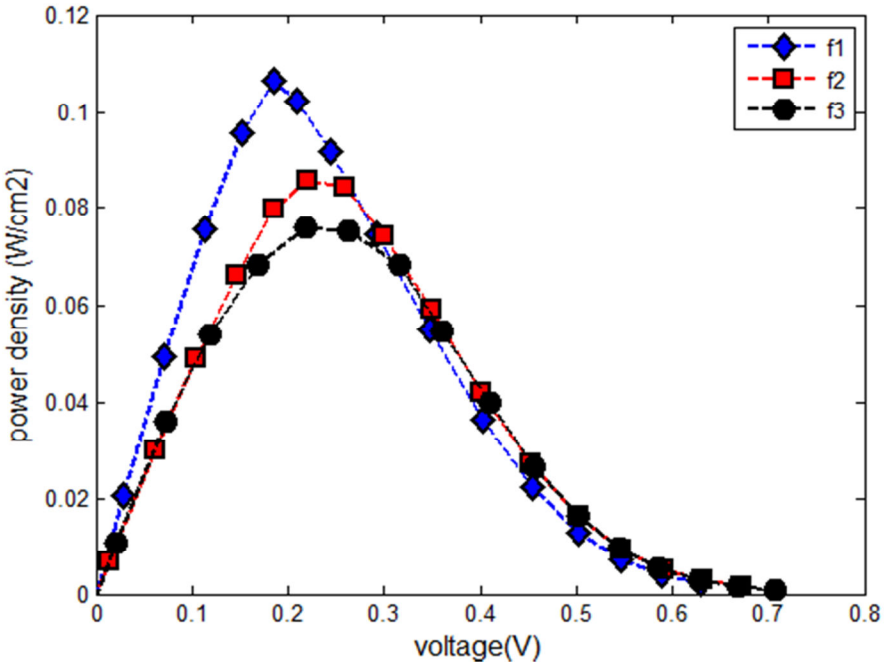

Figure 5-4 Power destiny vs. voltage curves for the optimum designs

Figures 5-3 presents the relationship between current density and power density for three different optimization problems while Fig. 5-4 demonstrates the relationship between voltage and power density. In Fig. 5-3, as current density increases from 0 to 0.3 A/cm^2, all of the curves appear to be identical until the power density increases from 0 to 0.075 W/cm^2. As the current density increases from 0.3 to 0.8 A/cm^2 continuously, the three curves exhibit different behaviors. The curve corresponding to the minimization of f_1 keeps increasing to a peak value at 0.11 W/cm^2 until the current density reaches 0.6 A/cm^2 and then it drops to zero dramatically. The curve corresponding to the minimization of f_2 continuously increases until the current density reaches 0.4 A/cm^2 and then drops to zero dramatically. The curve corresponding to the minimization of f_3 reaches its peak value when the current density is around 0.3 A/cm^2 and afterwards it decreases to zero. Figure 5-4 indicates that the highest values of power density for the three different optimization problems are 0.1064, 0.0852 and 0.0682 W/cm^2, respectively. It appears that the optimization of f_1 results in a highest power density; however, the corresponding value of voltage is very low—only 0.18 V—which is unpractical and inefficient in most engineering applications. For most practical voltage values ($V \geq 0.3$), the power density corresponding to the minimization of f_1 appears to be even lower than in the case of minimizations of f_2 and f_3.

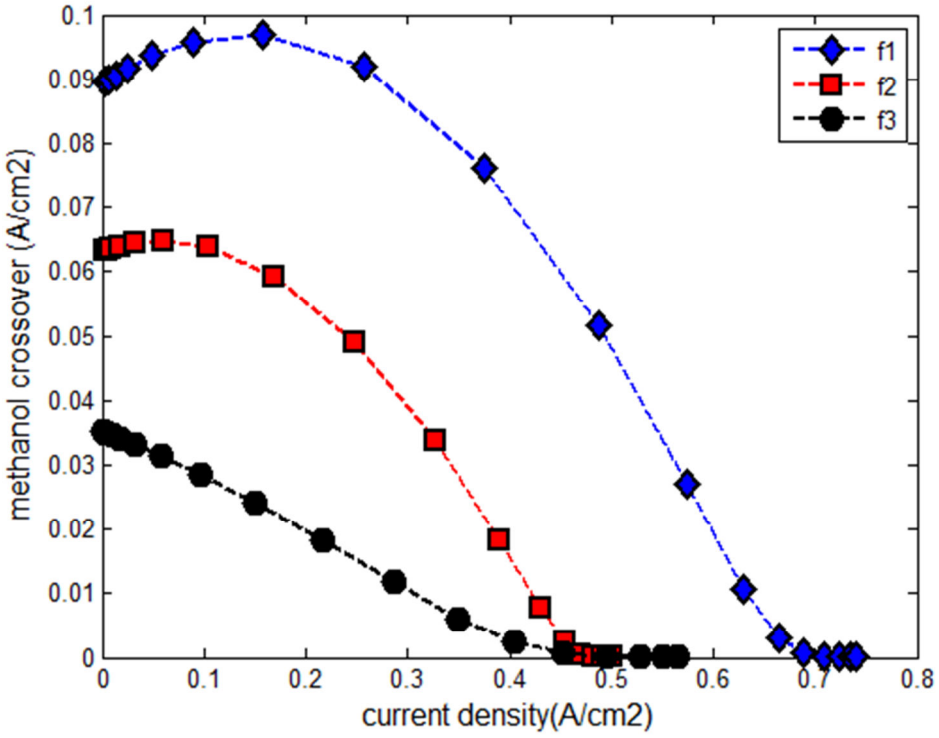

Figure 5-5 Methanol crossover vs. current density curves for the optimum designs

The relationship between methanol crossover and current density is presented in Fig. 5-5. At zero current density (open circuit voltage), the curve corresponding to the minimization of f_1 has a relatively high value of methanol crossover while the curve corresponding to the minimization of f_3 has a relatively low value. The reason for this phenomenon can be primarily explained by the corresponding values of methanol concentration—3.9409, 2.8332, 1.6103—in the first, second and third optimization problems, respectively. A relatively larger methanol concentration results in a relatively larger value of methanol crossover at the open circuit voltage and vice versa. With an increase of the current density, more and more of methanol is involved in the electro-chemical reaction and the gradient of methanol concentration reduces, which results in a reduction in the value of methanol crossover. Since the value of methanol concentration corresponding to the minimization of f_1 is relatively higher, the value of methanol

crossover remains at a higher level when the current density increases from 0 to 0.3 A/cm^2. When the value of methanol concentration reduces to 2.8332, which is the optimum result corresponding to the minimization of f_2, the value of methanol crossover remains stable only when the current density is less than 0.2 A/cm^2. When the value of methanol concentration reduces further to 1.6103, which is the optimum result corresponding to the minimization of f_3, the value of methanol crossover decreases immediately after the zero current density. With an increase in the current density, the value of methanol crossover of any of these curves eventually becomes zero because the whole amount of methanol is involved in the electro-chemical reaction and there would be no more methanol that can cross the membrane from the anode to cathode.

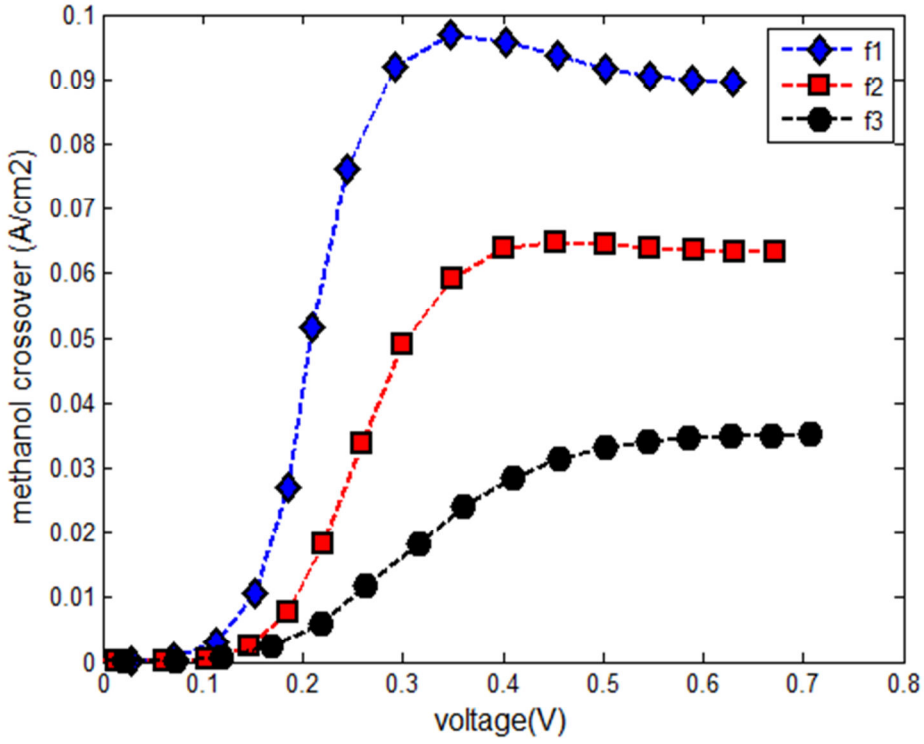

Figure 5-6 Methanol crossover vs. voltage curves for optimum designs

Figure 5-6 demonstrates the relationship between methanol crossover and voltage. At low voltage, the value of methanol crossover corresponding to each optimization problem is

almost zero. As the operating voltage increases to more practical values, the value of methanol crossover corresponding to the minimization of f_1 is much higher than the value corresponding to the minimization of f_2. The value of methanol crossover corresponding to the minimization of f_2 is also much higher than the value corresponding to the minimization of f_3. These results show that large amounts of methanol are wasted instead of being involved in the electro-chemical reactions in the minimizations of f_1 and f_2.

5.5 Conclusions

A three-dimensional, single-phase, multi-component mathematical model has been used for a liquid-fed direct methanol fuel cell (DMFC). The continuity, momentum, and species conservation equations coupled with electrochemical kinetics, are treated as the governing equations in both the anode and cathode catalyst layers. A finite-volume-based CFD technique is applied to develop the numerical program of DMFC. The genetic algorithm coupled with sequential quadratic programming optimization technique is applied for seeking the global optimization point. Optimization problems with ten design variables, three objective functions and a couple of constraints are formulated and solved subsequently. The maximization of the power density is considered as the first objective function and the solution resulted in a very high power density. However, the operating voltage corresponding to the optimum power density is too low. Therefore, in the second optimization problem, a minimum operating voltage is set as an additional constraint while the maximization of the power density is considered as the objective function. The result shows that the maximum power density is higher than first optimization problem. The minimization of the cost is considered as the third objective function. Although the

value of the maximum power density corresponding to minimization of f_3 is only 65% and 80% of the corresponding results solved in the minimizations of f_1 and f_2, respectively, the total cost is only 35.5% and 53.8% of the total costs associated with the minimizations of f_1 and f_2, respectively. The polarization, power density and methanol crossover curves are presented and explained to help designers better understand the performance of optimization of different objective functions.

CHAPTER 6

Conclusions and Future Work

6.1 Conclusions

The present work is aiming at helping renewable energy system designers to seek optimum designs in order to improve the performance and reduce the cost. Different optimization techniques including sequential quadratic programming, game theory methodology, genetic algorithm method and robust design methods, namely, Taguchi method and its extensions, are implemented in different renewable energy systems including solar, wind and hydrogen fuel cell systems under deterministic and probabilistic approaches.

In the optimum design of flat plate solar collector system, a multi-objective optimum design is presented with a consideration of solar radiation with shading effect. Three objectives, namely, the maximization of the annual average incident solar energy, the maximization of the lowest month incident solar energy and minimization of the cost, are considered. Most of the design variables and the altitude, solar constant and typical day of each month are treated as random variables following normal distribution. Game theory methodology with probabilistic uncertainty is used for the solution of the three objective constrained optimization problems to find a balanced solution. The solution represents the best compromise based on the terms of the super-criterion selected. Numerical results are obtained at a specific location (Miami, USA). The sensitivity

analysis based on the results of deterministic approach is conducted at the optimum solution. Since the design parameters of the solar collector are subject to manufacturing and installation errors, a sensitivity study was conducted to find the influence of the design variables, as they change by ±20% about their respective optimal values, on the three objective functions as well as the supercriterion. It was observed that the construction parameters—height, length and number of rows—have more influence than the installation factors—tilt angle and distance between two adjacent panels—on the objective functions. The standard deviation of each of the random parameters is varied from 1% to 5% of the respective mean values to find the influence of uncertainty on different objective functions. The numerical results are given to show the influence of the level of probability of constraint satisfaction and the coefficient of variation of the random variables. It is observed that the absolute value of each objective function is decreased with an increase in either the probability of constraint satisfaction or the coefficient of variation of the random variables. Better objective function values can be obtained with a lower value of probability of constraint satisfaction, but it might not be suitable (safe) for practical applications. A relatively higher constraint satisfaction (like 99.9997%) would result in worse objective function values. The results of the present study help designers in producing optimum solar collectors based on customer requirements. As seen from the present results, there is a trade-off between the absolute values of the various objectives and the probability of constraint satisfaction. From practical point of view, an increase in the overall objective implies improvement in a combination of annual energy output, winter energy output and cost of manufacture. With

a higher probability of constraint satisfaction, the manufacture has to sacrifice the energy values as well as the profit if the costs of raw and processed materials are relatively large.

Similar to the optimum design of flat plate solar collectors, compound parabolic concentrator solar collectors system, which is one alternative solar system of flat plate solar collector system, has been optimized by using the same optimization technique under both determinist and probabilistic uncertainty. The optimum results of two types of solar collectors are compared. Since the price of reflector is much cheaper compared to the solar cell, the primary objective of the CPC solar panel system design is to reduce the area of solar cell by increasing the area of reflectors. Sensitivity analyses are presented with respect to the total energy expectation ratio (compared to flat plate solar collectors) and different land price. It is found that the cost per unit energy can be significantly reduced by 10% to 23% depending on different land prices if the total energy output can be sacrificed by 15% or more compared to the flat-plate solar collector system.

In the optimum design of wind energy system, horizontal axis wind turbine (HAWT) was optimized by using the traditional Taguchi method and its extensions. It provides a simple way of designing robust horizontal axis wind turbine systems by considering multiple design parameters (variables), multiple objectives, and multiple constraints simultaneously. The robust design of HAWT, including both parameter design and tolerance design, is presented. The performance of these turbines is predicted using the axial momentum theory and the blade element momentum theory. In the parameter design stage, the energy output of the turbine is maximized by using the Taguchi method and the wind energy output is improved by 52.7%. However, in a practical point of view,

the design of HAWT needs to involve some behavior constraints. In this work, two constraints, namely, minimum requirement of power coefficient and maximum limit of stress induces or permissible fractional fatigue damage, are considered. A novel extended penalty-based Taguchi method is demonstrated in the numerical example and the energy output is improved by 33.0%. Although the result is less in the latter example, all of the imposed constraints are satisfied. Based on the results of parameter design, an appropriate set of tolerance setting of the parameters is formulated so as to yield an economical design while ensuring a minimal variability of performance of the wind turbine. The resulting objective function is formulated as a multi-objective function and solved by traditional Taguchi method.

In the optimum design of fuel cell, a three-dimensional, single-phase, multi-component mathematical model has been developed for a liquid-fed direct methanol fuel cell (DMFC). The continuity, momentum, and species conservation equations coupled with electrochemical kinetics, are treated as the governing equations in both the anode and cathode catalyst layer. A finite-volume-based CFD technique is applied to develop the numerical program of DMFC. The genetic algorithm coupled with sequential quadratic programming optimization technique is applied based on the numerical code for seeking global optimization point. Optimization problems with ten design variables, three objective functions and a couple of constraints are generated and solved subsequently. Maximization of the power density is implemented in the first objective function and a very high power density is achieved. However, the operating voltage corresponding to the optimum power density is too low. Therefore, in the second optimization problem, a minimum operating voltage is set as an additional constraint while the maximization of

the power density is still the objective function. The result shows that the maximum power density is higher than the result solved in first optimization problem under most practical operating voltages. Minimization of the cost is considered as the third objective function. Although the value of maximum power density corresponding to minimization of f_3 is only 65% and 80% of the corresponding results solved in minimization of f_1 and f_2, respectively, however, the total cost is only 35.5% and 53.8% of the total costs of minimization of f_1 and f_2, respectively. Besides, the polarization power density and methanol crossover curves are presented and explained to help designers better understand the phenomenon of optimum design behind the optimization results.

6.2 Future work

Optimum design on renewable energy system is a hot and wide topic. The contribution of this work to the renewable energy industry is limited due to time sensitiveness.
Suggestion for future work can be summarized as following:

1. In this dissertation, two solar collector systems, a wind turbine system and a fuel cell system have been optimized. However, there are still numerous types of renewable energy systems need to be optimized. For example, other types of solar, wind and fuel cell systems like parabolic trough collectors system, cylindrical trough collectors system, parabolic dish reflectors system, vertical-axis wind turbine system, phosphoric acid fuel cell system, alkaline fuel cell system and solid oxide fuel cell system can be optimized. Besides, other types of renewable energy systems including geothermal, ocean wave, and biomass resources can be optimally designed.

2. In most engineering applications, functions of many variables have a large number of local optimum points. However, it is more valuable to find the global optimum point though it is more challenging. Besides the genetic algorithm optimization technique, which is applied in this work, there is also some other global optimization methods like particle swarm optimization technique and ant colony optimization method. In the future, researcher or designer can apply these methods or develop new global optimization methods to renewable energy systems.

3. Unexpected weather conditions like a passing cloud, fog or hurricane is a big challenge for the renewable energy systems. In order to provide a more stable energy system, energy storage devices can be incorporated, besides, different types of renewable energy systems can be combined as a hybrid clean energy system, furthermore, renewable energy can also be combined with traditional energy system. Real time energy management can be proposed to integrated renewable energy system to satisfy different energy demands.

References

Abdul-Jabbar, N.K. and Salman, S.A., 1998, Effect of two-axis sun tracking on the performance of compound parabolic concentrators, *Energy Conversion and Management*, **39** (10), 1073–1079.

Alfa, 2010, www.alfa.com.

Al-Hassan, A. Y. and Hill, D. R., 1986, Islamic Technology: An illustrated history, Cambridge University Press, 1st edition.

Alotto, P., Guarnieri, M. and Moro, F., 2009, Optimal design of micro direct methanol fuel cells for low-power applications, *IEEE Transactions on Magnetics*, **45**(3), 1570-1573.

Ang. S.M.C., Brett, D.J.L. and Fraga, E.S, 2010, A multi-objective optimization model for a general polymer electrolyte membrane fuel cell system, *Journal of Power Sources*, **195**(9), 2754-2763.

Appelbaum, J. and Bany, J., 1979, Shadow effect of adjacent solar collectors in large scale systems. *Solar Energy*, **23**, 497-507.

Archer, C. L. and Jacobson, M. Z., 2005, Evaluation of global wind power, *Journal of Geophysical Research*, **110**, D12110 (1-20).

Bany, J. and Appelbaum, J., 1987, The effect of shading on the design of a field of solar Collectors, *Solar Cells*, **20**, 201–228.

Basri, S., Kamarudin, S.K., Daud, W.R.W. and Ahmad, 2010, Non-linear optimization of passive direct methanol fuel cell (DMFC), *Hydrogen Energy*, **35**, 1759-1768.

Baxter, S. F., Battaglia, V. S. and White, R. E, 1999, Methanol fuel cell model: anode, *Journal of Electrochemistry Society*, **146** (2), 437-447.

Benini, E. and Toffolo, A., 2002, Optimal design of horizontal-axis wind turbines using blade-element theory and evolutionary computation, *ASME , Journal of Solar Energy*, **124**, pp. 357-363.

Bernardy, D. M. and Verbrugge, M. W., 1992, Mathematical model of the solid-polymer-electrolyte fuel cell, *Journal of Electrochemical Society*, **139**(9), 2477-2491.

Bhadra, S.N., Kastha, D. and Banerjee, S., 2005, *Wind electrical systems*, Oxford University Press, New Delhi.

Buhl, M.L., 2004, *WT_Perf User's Guide*, National Wind Technology Center, National Renewable Energy Laboratory, Golden, Colorado.

Buhl, M.L., 2005, A new empirical relationship between thrust coefficient and induction factor for the turbulent windmill state, Technical report NREL/TP-500-36834.

Cai, K., Yin, G., Zhang, J., Liu, P. and Wang, Z., 2005, Effect of different types of Nafion membranes on direct dimethyl ether fuel cell, *Electrochemistry communications*, **7**, 1385-1388.

Carlsson, P., Cider, L. and Lindgren, B., 1998, Yield losses due to shading in a building-integrated PV installation: evaluation, simulation and suggestion for improvement, *2nd World Conference and Exhibition on Photovoltaic Solar Energy Conversion, Vienna,* 2666–2670.

Carvalho, J. Collares-Pereira, M. and Gordon,J.M., 1987. Economic optimization of stationary non evacuated CPC solar collectors. *Trans. ASME, J. Solar Energy*, **109** (1), 40-45.

Chen, K.I., Winnick, J. and Manousiouthakis, V.I., 2006, Global optimization of a simple mathematical model for a proton exchange membrane fuel cell, *Computers and Chemical Engineering*, **30**, 1226-1234.

Chiang, K. T., 2005, Optimization of the design parameters of Parallel-Plain Fin heat sink module cooling phenomenon based on the Taguchi method, *International Communication in Heat and Mass Transfer*, **32**, 1193-1201.

Conti, S. and Raiti, S., 2007, Probabilistic load flow using Monte Carlo techniques for distribution networks with photovoltaic generators, *Solar Energy*, **81**, 1473-1481.

Crawford R. H. and Rao S. S., 1989, Probabilistic analysis of function generating mechanisms, *Journal of Mechanisms, Transmissions and Automation in Design*, **111**, 479-481.

Datskov, I.V., Ostrovsky., G.M., Achenie., L.E.K. Achenie and Volin, Y.M., 2005, An approach to multicriteria optimization under uncertainty, *Chemical Engineering Science*, **61**, 2379-2393.

Derrick, G.H., Bassett, I.M. and Mills, D.R., 1986, Comparsion of reflector design for stationary tubular solar collector, *Solar energy*, **37**(3), 195-203.

Di Barba, P., 2008, Strategies of game theory for the automated optimal design in electromechanics, *International Journal of Applied Electromagnetics and Mechanics,* **27**(4), 275-295.

Drela, M., 2001, *XFOIL 6.94 User Guide*, MIT Aero and Astro Harold Youngren, Aerocraft, Inc.

Duquette, M.M and Visser,K.D., 2003, Numerical implications of solidity and blade number on rotor performance of horizontal-axis wind turbine, *ASME, Journal Solar Energy*, **125**(4), 425-432.

Enel, R. B., 2007, *World Geothermal Generation in 2007*, Renewable energy business development, Rome, Italy.

Fraidenraich, N., Tiba, C., Brandão, B. B. and Vilela, O.C., 2008. Analytic solutions for the geometric and optical properties of stationary compound parabolic concentrators with fully illuminated inverted V receiver. *Solar Energy*, **82**(2), 132-143.

Frohlich, C., 2006, Solar irradiance variability since 1978. Revision of the PMOD composite during solar cycle 21, *Space Science Reviews*, **125**(1-4), 53-65.

Ge, J. and Liu, H., 2006, A three-dimensional mathematical model for liquid-fed direct methanol fuel cells, *Journal of Power Source*, **160**, 412-421.

Ge , J. and Liu, H., 2007, A three-dimensional two-phase flow model for a liquid-fed direct methanol fuel cell, *Journal of Power Source*, **163**, 907-915.

Glauert, H., 1935, *Airplane Propellers, In Division L of Aerodynamic Theory*, W.F. Durand, Springer Verlag, Berlin, Germany.

Gong, X.Y. and Kulkarni, M., 2005, Design Optimization of a large scale rooftop photovoltaic system, *Solar Energy*, **78**(3), pp. 362-374.

Gopinathan, K., 1991, Optimization of the angle of solar collectors for maximum irradiation on sloping surfaces, *International Journal of Solar Energy*, **10**, 51–61.

Groumpos, P. P. and Kouzam, K. Y., 1987, A generic approach to the shadow effect in large solar power systems, *Solar Cells*, **22**, 29–46.

Grove, W.R., 1839, On voltaic series and the combination of gases by platinum, *London and Edinburgh Philosophical Magazine and Journal of Science*, **3**(14), 127-130.

Grujicic, M. and Chittajallu, K.M., 2003, Design and optimization of polymer electrolyte membrane (PEM) fuel cells, *Applied Surface Science*, **227**, 56-72.

Gur, O. and Rosen, A., 2008, Optimal design of horizontal axis wind turbine blades, *Proceedings of the 9th Biennial ASME conference on engineering systems design and analysis*, Jaifa, Israel, 99-109.

Guter, W., Schöne, J., Philipps, S. P., Steiner, M., Siefer, G., Wekkeli, A., Welser, E., Oliva, E., Bett, A.W., and Dimroth, F., 2009, Current-matched triple-junction solar cell reaching 41.1% conversion efficiency under concentrated sunlight, *Applied Physics Letters*, **94**, 223504(1-3).

Hati, S.K. and Rao, S.S., 2001, Game theory approach for the design of an optimal air pollution control system for thermal power plants. *International Journal of Environment and Pollution*, **15**(5), 505-516.

Hill, D.R., 1991, Mechanical engineering in the medieval near east, *Scientific American*, 64-69.

Hottel, H.C., 1976, Simple model for estimating the transmittance of direct solar radiation through clear atmospheres, *Solar Energy*, **18**(2), 129-134.

Hu, Y. and Rao, S. S., 2009, Game-theory approach for multi-objective optimal design of stationary flat-plate solar collectors, Engineering *Optimization*, **41**(11), 1017 – 1035.

Iqbal, M., 1983, *An introduction to solar radiation, academic*, Toronto.

Johnson, G.L., 1985, *Wind Energy Systems*, 1st Edition. Prentice-Hall, New Jersey.

Jung, B., Jang, K., Min, B., Lee, S. and Seok, J. 2009, Parameter optimization for finishing hard materials with magnetorheological fluid using the penalized multi-response Taguchi method, *Proceedings of the Institution of Mechanical Engineers, Part B: Journal of Engineering Manufacture*, **223**, 955-968.

Jureczko, M., Pawlak M. and Mężyk, A., 2005, Optimisation of wind turbine blades. *Journal of materials processing technology,* **167**, 463-471.

Justus, C.G., 1978, *Winds and Wind System Performance*, Franklin Institute Press, Philadelphia, PA.

Kackar, R., 1985, Off-line quality control, parameter design, and the Taguchi method, *Journal of Quality Technology*, **17**(4), 176-188.

Kalogirou, S.A., 2003, The potential of solar industrial process heat applications, *Applied Energy*, **76**, 337-361.

Kalogirou, S.A., 2004, Solar thermal collectors and applications, *Progress in Energy and Combustion Science*, **30**, 231-295.

Kaushika, N.D., Gautam, N. K. and Kaushik, K., 2005, Simulation model for sizing of stand-alone solar PV system with interconnected array, *Solar Energy Materials & Solar Cells*, **85**, 499-519

Kim, J.H., Sin, H.C., Kang., B.J. and Kim, N.W., 2006, Characteristic study of bushing compliance in consideration of stresses in a vehicle suspension system by the Taguchi method, Proceedings of the Institution of Mechanical Engineers, Part D: *Journal of Automobile Engineering*, **220**, 1383-1399.

Kim, Y., Han, G. and Seo, T., 2008, An evaluation on thermal performance of CPC solar collector. *International Communications in Heat and Mass Transfer*, **35**(4), 446-457.

Klein, S.A., 1977, Calculation of monthly average insolation on tilted surfaces, Solar Energy, **19**, 325.

Ko, D., Lee, M., Jang, W.H. and Krewer, U., 2008, Non-isothermal dynamic modeling and optimization of a direct methanol fuel cell, *Journal of Power Sources*, **180**, 71-83.

Ku, K., Rao, S.S. and Li, C., 1998, Taguchi-aided search method for design optimization of engineering systems, *Engineering Optimization*, **30**, 1-23.

Kulkarni, G. N., Kedare, S. B. and Bandyopadhyay, S., 2007, Determination of design space and optimization of solar water heating systems, Solar Energy, **81**, 958-968.

Lanzafame, R. and Messina, M., 2007, Fluid dynamic wind turbine design: critical analysis, optimization and application of BEM theory, *Renewable energy*, **32**, 2291-2305.

Lanzafame, R. and Messina, M., 2009, Optimal wind turbine design to maximize energy production, *Proceedings of the Institution of Mechanical Engineers, Part A: Journal of Power and Energy*, **223**(2), 93-101.

Lawrence, D., 1991, *Handbook of Genetic Algorithms*, Van Nostrand Reinhold, New York.

Liu, B.Y.H. and Jordan, R.C., 1960, Interrelationship and characteristic distribution of direct, diffuse and total solar radiation, *Solar Energy,* **4**(3), 1-19.

Liu W. and Wang, C., 2007, Three-dimensional simulations of liquid feed direct methanol fuel cells, *Journal of Electrochemical Society*, **154**(3), B352-B361.

Lorenzen, T, and Anderson, V., 1993, *Design of Experiments: A No-Name Approach*, Marcel Dekkel, New York.

Lu, S.M., Li, Y.C.M. and Tang, J.C., 2003, Optimum design of natural-circulation solar-water-heater by the Taguchi method, *Energy*, **28**, 741-750.

Lyon, C.A., Broeren, A.P., Giguère, P., Gopalarathnam, A., and Selig, M.S., 1998, *Summary of Low-Speed Airfoil Data*, Vol. 3, SoarTech Publications, Virginia Beach, VA.

Lysen, E.H., *Introdcution to Wind Energy*, CWD Publication CWD 82-1, The Netherlands.

Maalawi, K.Y. and Badawy, M.T.S, 2001, A direct method for evaluating performance of horizontal axis wind turbines, *Renewable and Sustainable Energy Review*, **5**, 175–190.

Maalawi, K.Y. and Badr, M.A., 2003, A practical approach for selecting optimum wind rotor, Renew Energy, **28**, 803-822.

Mallick, T.K., Eames, P.C., Hyde, T.J. and Norton, B., 2004, The design and experimental characterization of an asymmetric compound parabolic photovoltaic concentrator for building façade integration in the UK, *Solar Energy*, **77**, 319-327.

Marr, C. and Li, X., 1999, Composition and performance modeling of catalyst layer in a proton exchange membrane fuel cell, *Journal of Power Sources*, **77**(1), 17-27.

Marston, Matthew C., 2000, Game based design: a game theory approach to engineering design, PhD thesis, Georiga Institute of Technology.

Martin, K., 2006, Site specific optimization of rotor/generator sizing of wind turbines, M.S. thesis, Georgia Institute of Technology.

Mallick, T.K., Eames, P.C. and Norton, B., 2007, Using air flow to alleviate temperature elecation in solar cells within asymmetric compound parabolic concentrator, *Solar Energy*, **81**, 173-184.

Mills, D.R. and Giutronich, J.E., 1977, Asymmetrical non-imaging cylindrical solar concentrators, *Solar Energy*, **20**, 45-55.

Miyamoto, T., Noguchi, S. and Yamashita, H., 2008, Selection of an optimal solution for multi-objective electromagnetic apparatus design based on game theory. *IEEE Transaction on magnetic,* **44**(6), 1026-1029.

Nash, J., 1953, The bargaining problem. *Ecomertrica*, **18**, 155-162.

Negm, H. M. and Maalawi, K.Y., 2000, Structural design optimization of wind turbine towers, Computers & Structures, **74**(6), 649-666.

O'Gallagher, J.J., 2008, Nonimaging optics in solar energy, Synthesis lectures on energy and the environment: technology, science, and society, Morgan & Claypool Publishers.

O'Hayre, R., Cha, S.W., Colella, W. and Prinz, F. B., 2006, *Fuel Cell Fundamentals,* 1st ed., John Wiley & Sons, Hoboken, NJ.

Patel, M.R., 2006, *Wind and Solar Power Systems*, 2nd edition, CRC Press, Taylor & Francis Group, Boca Raton, Florida.

Rabl, A., 1976, Optical and thermal properties of compound parabolic concentrators, *Solar Energy*, **18**, 497–511.

Rao, S.S., 2009, *Engineering Optimization: Theory and Practice*, 4th ed., Wiley, Hoboken, NJ.

Rao, S.S. and Freiheit, T.I., 1991, A modified game theory approach to multi-objective optimization. *ASME, Journal of Mechanical Design*, **113**, 286-291.

Rao, S.S. and Hati, S.K., 1979, Game theory approach in multi-criteria optimization of function generating mechanism. *ASME, Journal of Mechanical Design*, **101**(3), 398-406.

Rao, S.S. and Hati, S.K., 1986, Pareto optimal solution in two-criteria beam design problems. *Engineering Optimization*, **10**, 41-50.

Rao, S.S. and Hu, Y., 2010, Multi-objective optimal design of stationary flat-plate solar collectors under probabilistic uncertainty, *ASME, Journal of Mechanical Design*, 132 (9), 094501 (6 pages).

Reise, C. and Kovach, A., 1995. PV Shading analysis in complex building geometries, *13th European Photovoltaic Solar Energy Conference, Nice, France,* 2157–2160.

REN21, 2007, *Renewables 2007 Global Status Report*.

REN21, 2009, *Renewables Global Status Report: 2009 Update*.

REN21, 2010, *Renewables 2010 Global Status Report*.

Righter R.W., 1996, *Wind Energy in America: A history*, University of Oklahoma Press.

Ross, P.J., 1988, *Taguchi Techniques for Quality Engineering*, McGraw-Hill Book Company, New York.

Scott, K., Argyropouos, P. and Sundmacher, K., 1999, A model for the liquid feed direct methanol fuel cell, *Journal of Electroanalytical Chemistry*, **477**, 97-110.

Secanell, M., Carnes, B., Suleman, A. and Djilali, N., 2006, Numerical optimization of proton exchange membrane fuel cell cathodes, *Electrochimica Acta*, **52**, 2668-2682.

Secanell, M., Karan, K., Suleman A., and Djilali, N., 2008, Optimal design of ultralow-platinum PEMFC anode electrodes, *Journal of Electrochemistry Society*, **155**, B125–B134.

Selig, M.S., Guglielmo, J.J., Broeren, A.P., and Giguère, P., 1995, *Summary of Low-Speed Airfoil Data*, Vol. 1, SoarTech Publications, Virginia Beach, VA.

Selig, M.S., Lyon, C.A., Giguère, P., Ninham, C.N., and Guglielmo, J.J., 1996, *Summary of Low-Speed Airfoil Data*, Vol. 2, SoarTech Publications, Virginia Beach, VA.

Selig, M.S. and McGranahan, B.D., 2004, *Wind Tunnel Aerodynamic Tests of Six Airfoils for Use on Small Wind Turbines*, National Renewable Energy Laboratory, NREL/SR-500-34515.

Shukla, A.K., Jackson, K., Scott, K. and Murgia, G, 2002, A solid-polymer electrolyte direct methanol fuel cell with a mixed reactant and air anode, *Journal of Power Sources*, **111**, 42-51.

Sovacool, B.K., 2010, A critical evaluation of nuclear power and renewable electricity in Asia, *Journal of Contemporary Asia*, 369-400.

Suzuki, A. and Kobayashi. S.,1995. Yearly distributed insolation model and optimum design of a two dimensional compound parabolic concentrator, *Solar energy*, **54**(5), 327-331.

Thumthae, C. and Chitsomboon, T., 2009, Optimal angle of attack for untwisted blade wind turbine, *Renewable Energy*, **34**(5), pp. 1279-1284.

Tripanagnostopoulos Y. and Yianoulis, P., CPC solar collectors with multichannel absorber, *Solar Energy*, **58**, 49–61.

Tripanagnostopoulos, Y., Yianoulis,P, Papaefthimiou, S and Zafeiratos, S., 2000, CPC collectors with flat bifacial absorbers. Solar Energy, **69**, 191–203.

Trupanagnostopolos, Y. and Souliotis, M., 2004, ICS solar systems with horizontal cylindrical storage tank and reflector of CPC or involute geometry, Renewable Energy, **29**, 13-38.

Von Neumann, J. and Morgenstern, O., 1947, *Theory of Games and Economic Behavior,* Princeton University Press: Princeton, New Jersey.

Wang Z. H, and Wang, C., Y., 2003, Mathematical modeling of liquid-feed direct methanol fuel cell, *Journal of Electrochemical Society*, **150**(4), A508-A519.

Wei, S.X., Li, M., Zhou, X.Z., 2007, A theoretical study on area compensation for non-directly-south-facing solar collectors, Applied Thermal Engineering, **27**(2-3), 442-449.

Weinstock, D. and Appelbaum, J., 2004, Optimal solar field design of stationary collectors. *ASME, Journal of Solar Energy Engineering*, **126**, 898-905.

Weinstock, D. and Appelbaum, J., 2007, Optimization of economic solar field design of stationary thermal collectors, *ASME, Journal of Solar Energy Engineering*, **129**, 363-370.

Whillier, A., 1953, Solar heat collection and its utilization for house heating, ScD Thesis in Mechanical Engineering, MIT, 1953.

Winston. R. and Hinterbergerb, H., 1975. Principles of cylindrical concentrators for solar energy, *Solar Energy*, **17**(4), 255-258.

Wilson, R. and Lissaman, P., 1974, *Applied aerodynamics of wind power of wind power machines*, National Science Foundation. Under Grant No. GI-41840, Oregon State University.

World Wind Energy Association (WWEA), 2009, *World wind energy report 2008*, WWEA head office, Bonn, Germany.

Wu, H.W. and Gu, H.W., 2009, Analysis of operating parameters considering flow orientation for the performance of a PEM fuel cell using the Taguchi method*, Journal of Power Sources*, **195**(11), 3621-3650

Xu, C., Follmann, P.M., Biegler, L.T. and Jhon, M.S., 2005, Numerical simulation and optimization of a direct methanol fuel cell, *Computers and Chemical Engineering*, **29**, 1849-1860.

Yeh, T.K. and Chen, C.H., 2008, Modeling and optimizing the performance of a passive direct methanol fuel cell, *Journal of Power Sources*, **175**, 353-362.

Zhao, M. Chen, Z. and Blaabjerg, F. 2006, Probabilistic capacity of a grid connected wind farm based on optimization method. *Renewable Energy,* **31**, 2171–2187.

Zhou T., and Liu, H., 2001, A general three-dimensional model for proton exchange membrane fuel cells, *International Journal of Transport Phenomenon*, **3**, 177-198.